INFORMATION TO USERS

This manuscript has been reproduced from the microfilm master. UMI films the text directly from the original or copy submitted. Thus, some thesis and dissertation copies are in typewriter face, while others may be from any type of computer printer.

The quality of this reproduction is dependent upon the quality of the copy submitted. Broken or indistinct print, colored or poor quality illustrations and photographs, print bleedthrough, substandard margins, and improper alignment can adversely affect reproduction.

In the unlikely event that the author did not send UMI a complete manuscript and there are missing pages, these will be noted. Also, if unauthorized copyright material had to be removed, a note will indicate the deletion.

Oversize materials (e.g., maps, drawings, charts) are reproduced by sectioning the original, beginning at the upper left-hand corner and continuing from left to right in equal sections with small overlaps.

Photographs included in the original manuscript have been reproduced xerographically in this copy. Higher quality 6" x 9" black and white photographic prints are available for any photographs or illustrations appearing in this copy for an additional charge. Contact UMI directly to order.

Bell & Howell Information and Learning
300 North Zeeb Road, Ann Arbor, MI 48106-1346 USA
800-521-0600

Université d'Ottawa · University of Ottawa

Methylmercury Disassembles Microtubules and Induces Apoptosis in P19 Embryonal Carcinoma Cells

By
Allison M. Hunter

A thesis submitted to the School of Graduate Studies and Research, University of Ottawa, in partial fulfillment of the requirements for the degree of Master of Science, Ottawa-Carleton Institute of Biology

January, 1999

For Me

ACKNOWLEDGEMENTS

First of all, I would like to thank my supervisor, Dr. David L. Brown, who suggested what became an interesting and challenging project. I appreciate all that I have learned under his supervision.

I would also like to thank the members of my advisory committee, Dr. Doug Johnson, Dr. Jim Cheetham, Dr. John Bell and Dr. Roy Walker for their input. I extend a special thanks to Dr. Roy Walker for the invaluable discussions on apoptosis. I thank all of the people who graciously took me into their labs so that I could learn new techniques; Christine Carson at the NRC, and Shelley Maves and Sean Cregan at AECL.

I appreciate all of the support and friendship from the members of Dr. Brown's lab, all of whom made my work more enjoyable; Jason Broome, Andrew Vaillant, Joseé Dufresne, and Bea Valentine. I would like to extend a special thanks to Jason, firstly, for always being there for me, and secondly, for the many hours of computer tutoring. I also thank Jeannine Pratte, our honourary lab member, for her concern and kindness.

Finally, I thank my friends Ingeborg Stensrud, John Francis, Jacqui Whiteway, Christine Morgan, Dorothy McColl, and Terri Faulkner who were supportive through the difficult times and lastly, Miguel for his patience.

TABLE OF CONTENTS

ABBREVIATIONS

α-MEM	alpha-modified Eagle's minimal essential medium
ASK1	apoptosis signal-regulating kinase
ATP	adenine triphosphate
BES	N, N- bis(2-Hydroxyethyl)-2-aminoethanesulfonic acid
BSA	bovine serum albumin
bp	base pair
CCD	charge-coupled device
CED	cell death abnormal
cs	coverslip
CY2	carboxymethylindocarbocyanine
CY3	indocarbocyanine
DAPI	4'-6-diamidino-2-phenylindole
DCF	2,7-dichlorofluorescein
ddH_2O	double distilled water
DNA	deoxyribonucleic acid
dpi	dots per inch
DTT	dithiothreitol
EC	embryonal carcinoma
ECL	enhanced chemiluminescence
EDTA	ethylenediaminetetraacetic acid disodium salt

EGTA	ethylene glycol-bis (β-aminoethyl ether) N,N,N'-N'-tetraacetic acid
EM	electron microscopy
FCS	fetal calf serum
FITC	fluorescein isothiocyanate
GDP	guanidine diphosphate
GFP	green fluorescent protein
GSH	glutathione
GTP	guanidine triphosphate
HMW	high molecular weight
HRP	horse radish peroxidase
ICE	interleukin-1β-converting enzyme
JNK	c-JUN N-terminal kinases
kb	kilobase
kDa	kilodalton
LB	Luria Bertani
LMP	low melting point
LMW	low molecular weight
mAb	monoclonal antibody
MAP	microtubule-associated protein
MDB	microtubule destabilizing buffer
MeHg	methylmercury
MES	4-morpholine ethanesulfonic acid

mRNA	messenger RNA
MSB	microtubule stabilizing buffer
MTOC	microtubule organizing center
Mt	microtubule
NC	nitrocellulose
NEM	N-ethylmaleimide
pAb	polyclonal antibody
PARP	poly (ADP ribose) polymerase
PBS	phosphate buffered saline
PC	phosphocellulose
PEFA	p-aminoethylbenzenesulfonyl fluoride
PFGE	pulsed field gel electrophoresis
PIPES	piperazine-N,N'-bis-2-ethanesulfonic acid
RA	retinoic acid
RNAse	ribonuclease
ROS	reactive oxygen species
SAPKs	stress-activated protein kinases
SDS-PAGE	sodium dodecyl sulfate polyacrylamide gel electrophoresis
TBE	Tris/Boric acid/EDTA
T-broth	terrific broth
TdT	Terminal deoxynucleotidyl transferase
TE	Tris/EDTA

TIFF	tagged image file format
TUNEL	Terminal deoxynucleotidyl transferase-mediated dUTP-biotin Nick End Labelling

LIST OF FIGURES

ABSTRACT

The relationship between the sensitivity of microtubules (Mts) to MeHg-induced disassembly and the extent apoptosis was examined in undifferentiated and neuronally differentiated P19 cells. The extent of Mt disassembly was examined qualitatively by immunofluorescence microscopy and quantitatively by polymer and soluble protein extractions, followed by dot blotting or by SDS-PAGE and western blotting. In both undifferentiated and neuronally differentiated P19 cells MeHg treatments disassembled Mts in a time- and dose- dependent manner, as assessed by immunofluorescence microscopy. However, when the extent of Mt disassembly was assessed by quantitative dot blotting or by SDS-PAGE followed by western blotting there was no change observed in the amount of tubulin in the polymer and soluble fractions between control and MeHg-treated samples. These data suggest that MeHg treatments disassemble Mts into a form which is not extractable as soluble protein.

MeHg-induced apoptosis was assessed using a combination of assays including single cell gel electrophoresis (Comet assay), TUNEL, conventional agarose gel electrophoresis, and pulsed field gel electrophoresis. It was observed that sensitivity to MeHg-induced apoptosis changed during neuronal differentiation. In undifferentiated P19 cells a 12 hr, 4μM MeHg treatment resulted in complete loss of Mts, as assessed by immunofluorescence microscopy, and induced apoptosis in 98% of the cells as determined by the Comet assay. In neuronally differentiated P19 cells the same MeHg concentration resulted in less Mt disassembly and induced apoptosis in only 5% after

12hr and 25% of the cells after a 24 hr treatment. The TUNEL assay showed that 18% of undifferentiated cells were TUNEL positive following an 18 hr, 4 μM treatment, with the same proportion of the cells exhibiting condensed DNA morphology. Conventional gel electrophoresis showed that this treatment also resulted in DNA laddering, indicative of DNA fragmentation at the oligonucleosomal level. Pulsed field gel electrophoresis showed that high molecular weight DNA fragmentation occurred, resulting in DNA fragments approximately 50 kb in size, in both undifferentiated and differentiated cells. The correlation between the extent of Mt disassembly and apoptosis was observed to be time- and dose- dependent with a variety of MeHg treatments. These data establish that MeHg induces apoptosis in both undifferentiated and differentiated P19 cells and suggests that the induction of apoptosis results from the known Mt disrupting activity of this toxicant.

FORWARD

The cytoskeleton consists of a network of protein filaments that extend throughout the cytoplasm. The three types of protein filaments are: microfilaments, intermediate filaments and Mts. These cytoskeletal filaments interact to perform several cellular functions including mitosis, cell movement and axonal transport. Since the cytoskeletal network is essential in many cellular functions, the cell is vulnerable to toxic agents which target components of the cytoskeleton. A wide range of environmental toxicants, including heavy metals, have been shown to alter cytoskeletal components both *in vivo* and *in vitro* (reviewed by Graff and Reuhl, 1996).

Depending on the toxicant, one or all of the cytoskeletal components may be damaged upon exposure. Typically, when the cytoskeleton is damaged the organization of the filamentous network is altered. This reorganization may result from the assembly or disassembly of the cytoskeletal protein filaments (reviewed by Graff and Reuhl, 1996). If sufficient cytoskeletal damage occurs it is conceivable that signal transduction or signal effector systems, prompted by the loss of cytoskeletal integrity (reviewed by Graff and Reuhl, 1996), may induce pathways leading to a type of cell death known as apoptosis.

Apoptosis is a process of cell death with characteristic morphological and biochemical features distinguishable from those associated with necrosis, or accidental cell death (Kerr *et al.*, 1972). During apoptosis cells shrink, chromatin condenses and DNA is cleaved into oligonucleosomal sized fragments. Also characteristic of

apoptotic cells is blebbing of the plasma membrane followed by compartmentalization of the cytoplasm and nucleus into membrane bound "apoptotic bodies" (reviewed by Johnson *et al.*, 1995). Apoptosis can be induced by withdrawal of trophic factors, exposure to adverse conditions of such as ionizing radiation or ischemia, treatments with Mt-targetting agents including taxol or colchicine, as well as by exposure to chemical toxicants (reviewed by Wertz and Hanley, 1996).

In Chapter I of this thesis the effects of MeHg on Mts are examined. It has been shown previously that of the three filamentous cytoskeletal components, Mts were the primary target for MeHg-induced damage in both undifferentiated and neuronally differentiated P19 embryonal carcinoma cells. In this study it was shown that Mts were depolymerized in a time- and dose- dependent fashion and that Mts in neuronally differentiated cells were less sensitive to MeHg than those in undifferentiated cells.

The Mt-damaging effects of MeHg in both the adult and the developing brain have been well documented. During development MeHg inhibits both mitosis and neuronal migration such that certain regions of the brain are underdeveloped. It has also been suggested that MeHg may affect neuronal development in the fetus through the induction of apoptosis (Kunimoto and Suzuki, 1997). Apoptosis has been shown to be induced due to loss of Mt integrity in non-neuronal cell lines which have been treated with the Mt-damaging agents taxol and colchicine. Chapter II examines whether MeHg induces apoptosis in undifferentiated and differentiated cells as a result of its effects on Mts.

Chapter I

A. INTRODUCTION

A. 1 Methylmercury Toxicity

Methylmercury (MeHg) is a ubiquitous environmental pollutant which has a wide range of deleterious effects on mammalian systems. For example, it has been observed that MeHg exposure leads to lipid peroxidation and loss of cell membrane integrity (Sarafian and Verity, 1991). Peripheral blood lymphocytes from exposed humans show significant increases in the number of chromosome breaks and abnormal chromosome segregation during mitosis (Skerfving *et al.*, 1974;Verschaeve *et al.*, 1976). Neuropathological data of fetal Minimata disease suggests that neuronal migration, one of the essential processes of brain development, is affected by MeHg (Choi *et al.*, 1978).

During brain development, cell proliferation occurs in spatially and temporally defined patterns which are highly regulated (reviewed by Sager and Syversen, 1986). Regions of the brain active in cell proliferation were shown to be particularly sensitive to MeHg due to the antimitotic effect of this toxicant (Sager *et al*,1982; Rodier *et al.*, 1984; Sager, 1988). To study the effects of MeHg-induced mitotic arrest on brain development neonatal mice were exposed to MeHg and the external granular layer of the cerebellum was examined (Sager *et al.*, 1982). When the total number of mitotic cells was counted in selected regions of the external granular layer the overall number of mitotic cells increased because they were unable to exit mitosis (Sager *et al.*, 1982; Rodier *et al.*, 1984; Sager, 1988).

A. 2 Methylmercury and the Cytoskeleton

Cell proliferation, neuronal migration, and axonal transport are some of the cellular functions which are affected by MeHg (Abe *et al.*,1975; Sager *et al.*, 1982; Rodier *et al.*, 1984; Cadrin *et al.*, 1988; Wasteneys *et al.*, 1988; Kunimoto and Suzuki, 1997). All of these functions are in some way dependent on the cytoskeleton.

The cytoskeleton consists of a network of protein filaments that extends throughout the cytoplasm. The types of protein filaments include: **1)** microfilaments, which are filamentous actin polymers 3-5 nm in diameter; **2)** intermediate filaments consisting of a family of polypeptides which are approximately 10 nm in diameter; and, **3)** Mts , the largest diameter cytoskeletal component, assembled from heterodimers of α-and β-tubulin subunits, each with a molecular weight (MW) of 55 kilodaltons (kDa). When tubulin heterodimers assemble into Mts they form linear protofilaments with the β-tubulin subunit of one heterodimer in contact with the α-tubulin subunit of the next. A total of 13 protofilaments interact laterally to form a cylinder 24 nm in diameter (**Figure 1A**). Mts are organized radially in interphase cells and originate at the microtubule organizing center (MTOC) located at the periphery of the nucleus (**Figure 1B**).

Of the three cytoskeletal components, Mts are most sensitive to the effects of MeHg. Immunofluorescence studies on EC, PtK2 and HeLa S3 cells show that low MeHg doses, which cause moderate Mt damage, have no effect on the other cytoskeletal components (Wasteneys *et al.*, 1988; Sager, 1988). Rearrangements of intermediate filaments and microfilaments are observed, but only after complete Mt disassembly (Wasteneys *et al.*, 1988; Sager, 1988). When mouse glioma cells were

Figure 1: Arrangement of tubulin subunits in an assembled Mt **(A)** the organization of microtubules at the MTOC in an interphase cell **(B)**. From Vaillant, 1997.

A

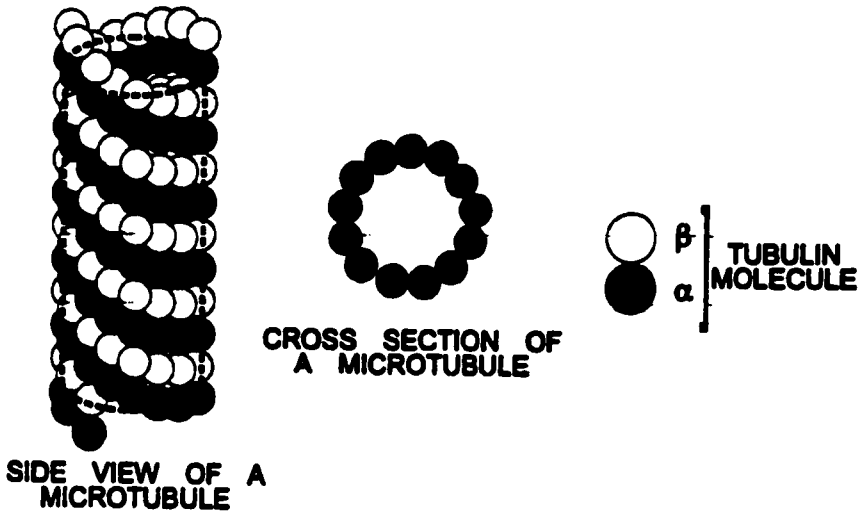
SIDE VIEW OF A MICROTUBULE
CROSS SECTION OF A MICROTUBULE
β
α
TUBULIN MOLECULE

B

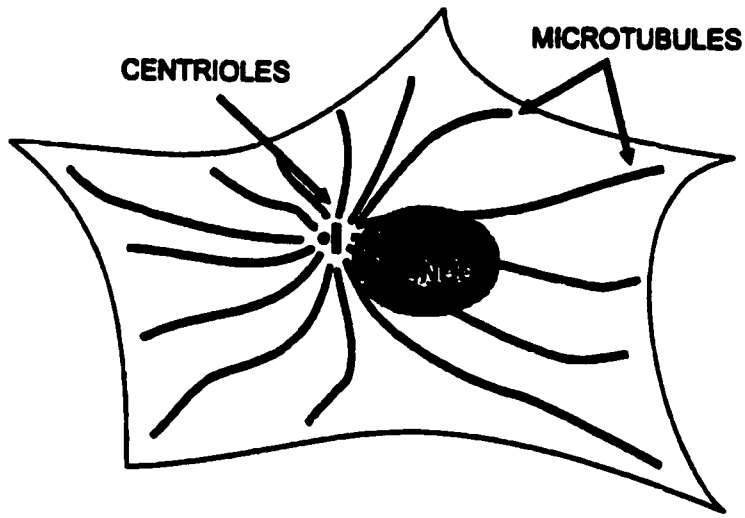
CENTRIOLES
MICROTUBULES

examined by electron microscopy (EM) the disruption of Mts by MeHg was observed before any cellular organelles showed morphological changes, further demonstrating the extreme sensitivity of Mts to the effects of MeHg (Imura *et al.*, 1980).

The mechanism for Mt disruption, or inhibition of polymerization by MeHg, is believed to be through an interaction of MeHg with tubulin sulfhydryl groups. Kuriyama and Sakai (1974) showed that when organic sulfhydryl blocking agents such as N-ethylmaleimide (NEM) were applied during assembly of Mts from purified porcine brain tubulin, tubulin polymerization was inhibited. Kuriyama and Sakai (1974) also showed that there were 15 free sulfhydryl groups on one tubulin dimer and blocking 2 of these was enough to completely inhibit Mt polymerization. When the effects of inorganic cations on tubulin polymerization were examined, it was found that they also bound to tubulin and prevented Mt assembly (Wallin *et al.*, 1977). Of several inorganic cations, the mercuric ion (Hg^{2+}) was found to be the most potent inhibitor of *in vitro* Mt polymerization, followed by Cu^{2+} and Cd^{2+} (Wallin *et al.*, 1977).

In vitro studies show that MeHg disrupts Mts and directly inhibits Mt polymerization in a time and dose-dependent manner (Sager *et al.*, 1983; Miura *et al.*, 1984; Vogel *et al.*, 1985). Mt protein was prepared from both newborn mouse brain and porcine brain by successive cycles of assembly and disassembly. Polymerization of brain extracts with and without specified concentrations of MeHg was measured by changes in absorbance at 320 nm. For both sources of Mt proteins, it was found that slight inhibition of assembly began with 10-12 μM of MeHg and 75%

inhibition occurred with 50-60 μM of MeHg (Keates and Yott, 1983; Sager *et al.*, 1983). Total inhibition of Mt assembly occurred at approximately equimolar concentrations of MeHg and tubulin (Imura *et al.*, 1980; Sager *et al.*, 1983; Keates and Yott, 1983; Miura *et al.*, 1984). When these MeHg-treated samples were examined by EM it was observed that at low doses (< 15 μM) Mts still formed, but at intermediate MeHg concentrations (15-100 μM) Mt assembly was depressed (Imura *et al.*, 1980; Keates and Yott, 1983; Sager *et al.*, 1983; Miura *et al.*, 1984). At concentrations higher than 100 μM, it was observed that nonmicrotubule aggregates formed (Sager and Syversen, 1986).

In vivo studies using immunofluorescence microscopy also demonstrated the time- and dose-dependent effects of MeHg on a variety of cell lines (Sager *et al.*, 1983; Miura *et al.*, 1984; Cadrin *et al.*, 1988; Wasteneys *et al.*, 1988; Brown *et al.*, 1988; Sager, 1988; Graff *et al.*, 1997). When human fibroblasts were treated for 1 hr with 10 μM MeHg, immunolabelling with anti-tubulin antibodies showed a significant loss of cytoplasmic microtubules, accompanied by rounding up of the cells (Sager *et al.*, 1983). Wasteneys *et al.* (1988) established that not all Mts within the cell are equally sensitive to the effects of MeHg. When mitotic and interphase cells were examined within the same sample following a 1 μM, 2 hr MeHg treatment, it was found that the spindle Mts were severely damaged, while the interphase Mts appeared only slightly affected. Severe damage of interphase Mts was evident only after treating cells with higher MeHg doses (3-10 μM) for 1-2 hr. With these same treatments it was also

observed that a majority of the cells became blocked at prometaphase and metaphase and were prevented from progressing through to the final stages of mitosis

It has also been established that there is a significant difference in MeHg sensitivity between Mts in interphase cells and Mts in neuronal cells (Cadrin *et al.*, 1988; Graff *et al.*, 1997). Immunofluorescence microscopy, using anti-tubulin antibodies showed that MeHg treatments that disrupted Mts in undifferentiated P19 cells had no effect on Mts in neurites of RA-induced neurons. During neuronal development Mts became increasingly resistant to MeHg-induced disassembly, most likely due to the mechanisms which normally reduce Mt dynamics during neuronal development (reviewed by Falconer *et al.*, 1994).

A. 3 Microtubule Dynamics

Within the cell, Mts are in a state of continuous assembly and disassembly. This dynamic behaviour of Mts is best described by the "dynamic instability model". In this model individual Mts undergo phases of elongation and shortening by the addition or loss of subunits from the filament ends (Mitchison and Kirschner, 1984a). The transitions between elongation and shortening are abrupt and random, giving an asynchronous array of Mts.

Each α- and β-tubulin subunit binds one GTP molecule. However, only the β-tubulin subunit is able to hydrolyze the bound GTP to GDP. GTP hydrolysis is believed to cause a conformational change in the β-tubulin subunit. GDP-tubulin dissociates from the Mt lattice more readily than GTP-tubulin and an accumulation of

GDP-tubulin results in an unstable Mt which rapidly depolymerizes. If GTP- bound tubulin accumulates at the growing end, the Mt remains stable and assembly may continue. Therefore, if more GTP-bound tubulin is available it will continue to add to the growing end of the Mt before the GTP on the previous subunits has been hydrolyzed. In this way, assembly and disassembly is dependent on both the concentration of free tubulin in the cytosol and on the rate of GTP hydrolysis on the polymerized Mt.

A. 4 Microtubule Stability in Neurons

Neuronal Mts are organized into bundles and are present throughout the length of the axon. These bundled Mts are not associated with a centrosomal MTOC, but are free in the cytoplasm (**Figure 2**). Neuronal Mts differ from interphase Mts not only in organization, but also in their rate of turnover, or dynamics. The interphase Mts of proliferating or cycling cells have a turnover rate of only minutes (Schulze and Kirschner, 1987). However, during neurogenesis Mt dynamics change resulting in Mt populations in neurites which persist for hours (Li and Black, 1996). These alterations in Mt dynamics are a reflection of the changes in Mt stability during neuronal development.

In studies using P19 EC cells it was observed that during neuronal differentiation there was an increased resistance to the known Mt-depolymerizing drug, colchicine (Falconer *et al.*, 1992; Laferrière and Brown, 1996) as well as to MeHg (Cadrin *et al.*, 1988;; Graff *et al.*, 1997). This resistance may be due to changes in

Figure 2: Changes in Mt organization folllowing neurogenesis. From Vaillant, 1997.

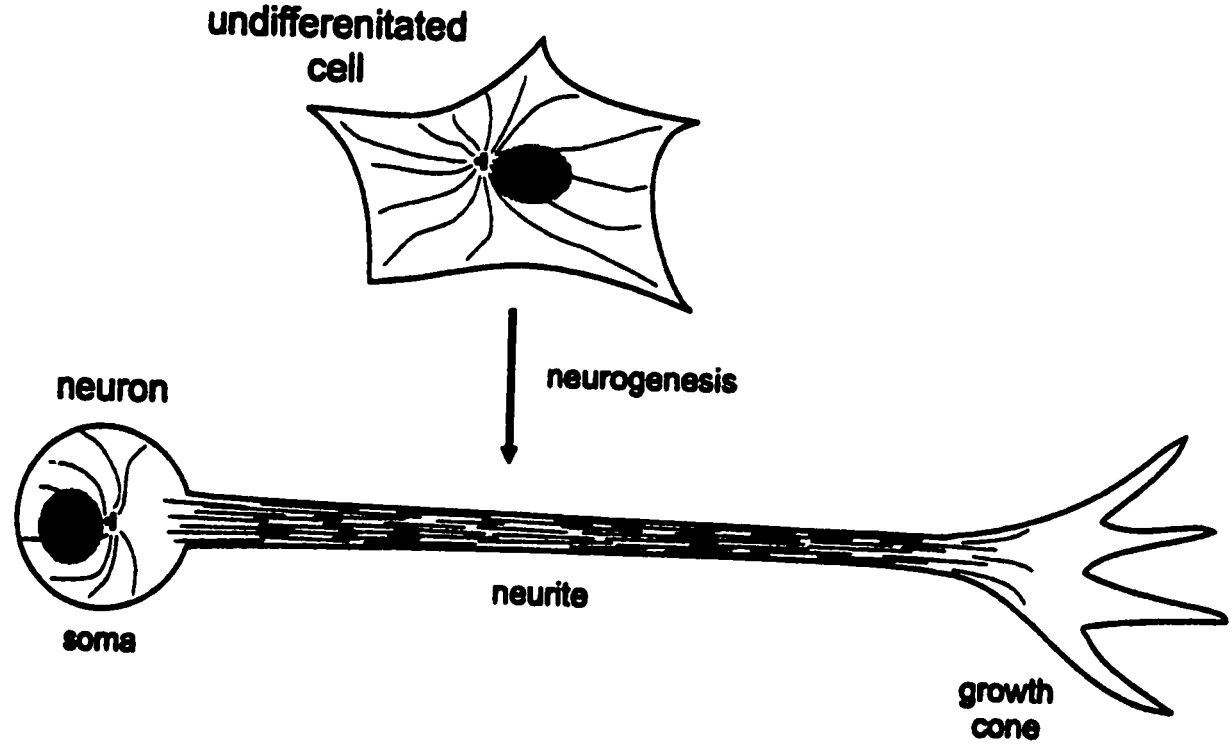
undifferenitated
cell
neurogenesis
neuron
neurite
soma
growth
cone

tubulin isotype composition, the expression of posttranslationally modified α- and β-tubulin, and the expression of microtubule-associated proteins (MAPs). These are all developmentally regulated and contribute to Mt stability.

A. 4. 1 *Tubulin Isotypes*

In mammals, five α- and six β-tubulin isotypes have been identified (Lopata and Cleveland, 1987). The β-tubulin isotypes are encoded by a highly conserved, multigene family which produces distinct polypeptide isotypes that differ mainly in the carboxyl-terminal region of the protein (Sullivan and Cleveland, 1986). There is evidence that both the α- and β-tubulin isotypes are expressed in a tissue-specific manner (reviewed by Sullivan, 1988). As well as the α- and β- tubulin families the γ-tubulin family, has been identified. γ-tubulin is located in the MTOC and is likely involved in Mt nucleation (Moritz *et al.*, 1995).

It has been suggested that the dynamic properties of Mts may be related to their tubulin isotype composition. Several α- and β-tubulin isotypes are coexpressed in variable quantities in many cell types (reviewed by Sullivan, 1988). However, there is evidence that cells may be able to distinguish and selectively incorporate specific isotypes into assembled Mts. Joshi and Cleveland (1989) found that in neurons two tubulin isotypes, βI and βII, were preferentially incorporated into polymerized Mts, regardless of the quantity of other isotypes available in the soluble tubulin pool. Using

neuronally differentiated P19 cells, Falconer *et al.* (1992) showed that β-tubulin isotypes are sorted into colchicine stable and colchicine labile Mts.

The reasons for preferential incorporation of certain tubulin isotypes over other isotypes into assembled Mts are not clear. However, *in vitro* Mt assembly studies using phosphocellulose purified β-tubulin isotypes demonstrated that Mt isotype composition can influence Mt dynamics. In these studies, it was observed that Mts assembled from purified αβIII tubulin are more dynamic than Mts assembled from αβII or αβIV tubulin or Mts assembled from tubulin containing all brain-specific isotypes (Panda *et al.*, 1994). When Mts were assembled from a mixture of αβII and αβIII tubulins, in which there was 80% αβII and only 20% αβIII present, the Mts were less dynamic than when assembled from αβIII alone (Panda *et al.*, 1994).

Further evidence that Mt isotype composition may affect Mt dynamics comes from studies which show that βIII tubulin, a neuron-specific isotype, may increase Mt stability in neurons. Laferrière and Brown (1996) showed that in differentiating P19 neurons, as βIII tubulin became incorporated into Mts, there was a concomitant increase in Mt stability. These data suggest that tubulin isotype composition and interactions between isotypes may influence Mt dynamics. The preferential sorting of certain tubulin isotypes into neuronal Mts may explain the decrease in Mt sensitivity to toxicants such as MeHg during later stages of neuronal development.

A. 4. 2 *Posttranslational Modifications*

Posttranslational modifications of tubulin generate diversity within Mt populations and possibly influence Mt function. Both α- and β-tubulins are posttranslationally modified. These modifications include acetylation, detyrosination / tyrosination, polyglutamylation and phosphorylation.

Acetylation is the addition of an acetyl group to the lysine 40 residue of α-tubulin (LeDizet and Piperno, 1986). Although the function of acetylation is unknown, acetylated α-tubulin is found in increasing proportions in more stable Mts (Piperno *et al.*, 1987). These stable, acetylated Mts are resistant to depolymerizing agents such as colchicine and MeHg (Falconer *et al.*, 1989; Graff and Reuhl, 1997). It has been suggested that acetylation may be a marker for stability rather than a cause.

Detyrosination involves the removal of a tyrosine residue located at the carboxy-terminal end of α-tubulin by a tubulin carboxypeptidase. Removal of this tyrosine results in a carboxy-terminal glutamic acid to which a tyrosine may be added back with a tubulin tyrosine ligase (reviewed by Bulinski and Gundersen, 1991). Detyrosination occurs preferentially on polymerized Mts and is a marker for Mt stability, whereas, tyrosination occurs preferentially on soluble tubulin (Gundersen *et al.*, 1984). Stable or less dynamic Mts, such as those found in proximal regions of neurites, are detyrosinated ; whereas, the more dynamic Mts at the growth cone are heavily tyrosinated (reviewed by Bulinski and Gundersen, 1991). Although detyrosination occurs on stable Mts, this modification is thought to be a consequence rather than the cause of stabilization (Khawaja *et al.*, 1988).

Glutamylation of both α- and β- tubulin occurs on a glutamic acid residue in the carboxy terminus. This modification involves the addition of 1-6 glutamyl residues and occurs preferentially on polymerized Mts (Audebert *et al.*, 1993). High levels of glutamylated α-tubulin are present, and remain constant, throughout neuronal differentiation. At the early stages of differentiation low levels of glutamylated β-tubulin are present which steadily increase with neuronal development (Audebert *et al.*, 1993). There is evidence that posttranslational modifications of tubulin, such as glutamylation, can affect MAP binding. For example it has been shown that polyglutamylated tubulin, has an affinity for binding to the MAP, tau (Boucher *et al.*, 1994).

Of the six β-tubulin isotypes, only βIII tubulin has been shown to be phosphorylated (Khan and Ludueña, 1996). The role of βIII phosphorylation is unknown, but there is some evidence that it may be involved in regulating both Mt assembly and Mt stability (Gard and Kirschner, 1985; Khan and Ludueña, 1996; Laferrière and Brown, 1996). Khan and Ludueña (1996) showed that when the phosphate group is enzymatically removed from βIII *in vitro*, the ability for Mts to assemble is reduced. Studies also showed that the amount of phosphorylated βIII increases concomitantly with Mt stability during neuronal development (Laferrière and Brown, 1996).

A. 4. 3 *Microtubule Associated Proteins (MAPs)*

MAPs are a diverse group of proteins which associate with Mts and promote Mt assembly (reviewed by Matus, 1990). There are two main groups of MAPS: motor MAPs and structural MAPs. Motor MAPs include the dynein and kinesin families of proteins and are involved in chromosome movement during mitosis, intracellular transport, and flagellar based motility (reviewed by Vale, 1990). The structural MAPS, which have been classified based on MW, function, and expression during development include: MAP1, MAP2, MAP3, MAP4 and tau. The best studied structural MAPs are MAP1, MAP2 and tau (reviewed by Matus, 1988). It has been suggested that structural MAPs may be involved in determining neuronal shape and in regulating the balance between rigidity and plasticity in neuronal processes (reviewed by Matus, 1988).

MAP1 consists of two structurally related proteins: MAP1a and MAP1b. MAP1a is the largest MAP found in brain (MW of 350 kDa) and is expressed at high levels in adult neurons (reviewed by Schoenfeld and Obar, 1994). MAP1b has a MW of 320 kDa and is expressed at high levels in the developing brain (Matus, 1991). In neurons, both MAP1a and MAP1b are localized to the cell body, axons and dendrites

There are four isoforms of MAP2 which are generated by alternative splicing of a primary transcript (Lewis *et al.*, 1989). There are two high molecular weight (HMW) MAP2 isoforms, MAP2a and MAP2b, with a molecular weight of approximately 280 kD (Matus, 1991). These isoforms are expressed at low levels during development and expression increases to high levels in adult brain. HMW

MAP2 isoforms are localized to the dendrites of neuronal cells (reviewed by Schoenfeld and Obar, 1994). There are two LMW isoforms of MAP2, designated MAP2c and MAP2d, which are approximately 70-75 kDa in size (Olesen,1994). MAP2c is present in both the axon and the dendrite of neuronal cells. This MAP is sometimes called a juvenile MAP due to its high levels of expression during brain development and low levels in the adult brain (Tucker *et al.*,1988). MAP2d is found only in glial cells at late stages of brain development (Doll *et al.*, 1993).

Tau proteins, like MAP2, are also present as different isoforms, generated by alternative splicing of a primary mRNA transcript, during neuronal development (Lee *et al.*, 1988). This alternative splicing is developmentally regulated giving rise to juvenile and adult isoforms (Tucker *et al.*,1988). The tau family of proteins can range in size from 50-65 kDa and are found in most axons (reviewed by Matus, 1988).

A. 5 Microtubule and MAP Interactions

Structural MAPs consist of two regions, a projection domain and a highly basic MT binding domain. It is thought that the projection domain permits MAPs to form lateral extensions or cross-bridges between adjacent Mts (**Figure 3**). This interaction may contribute to the density and stability of Mt arrays. Tubulin isotype composition and posttranslationally modified tubulin subunits may affect the interactions between MAPs and Mts. Examples of MAP-Mt interaction were observed using synthetic peptides, defined by carboxy terminal tubulin sequences of α-and β-tubulin, which

demonstrated that MAP2 and tau bind to both tubulin subunits (Serrano *et al.*, 1985; Littauer *et al.*, 1986; Cross *et al.*, 1991).

A. 6 P19 EC Cells As An Experimental Model

P19 EC cells were isolated by McBurney and Rogers (1982) from a teratocarcinoma which was generated by grafting a 7 day mouse embryo to the testes of an adult mouse. From this, a clonal cell line was derived which can be maintained undifferentiated in culture. With the addition of 10^{-6} M RA, P19 cells differentiate into a culture which is composed of neurons, glial and fibroblast-like cells (Jones-Villeneuve *et al.*, 1982).

The organization and dynamics of MT arrays and the expression of developmentally regulated proteins, including MAP1a, HMW MAP2, MAP2c and tau have been characterized in P19 cells and have been shown to have the same pattern of expression observed in developing brain (Falconer *et al.*, 1992; Falconer *et al.*, 1994) **(Figure 4)**. Genetic manipulation by transfection is also possible with this cell line (MacPherson and McBurney, 1995). This provides an appropriate system to investigate the function of specific proteins which are expressed during neuronal development.

A. 7 Rationale for Experiments

In undifferentiated P19 cells, Mts appear to be sensitive to MeHg-induced disassembly. However, as P19 cells differentiate into neurons Mts become less

Figure 3: A model showing the association of MAPs with Mts. From Vaillant, 1997.

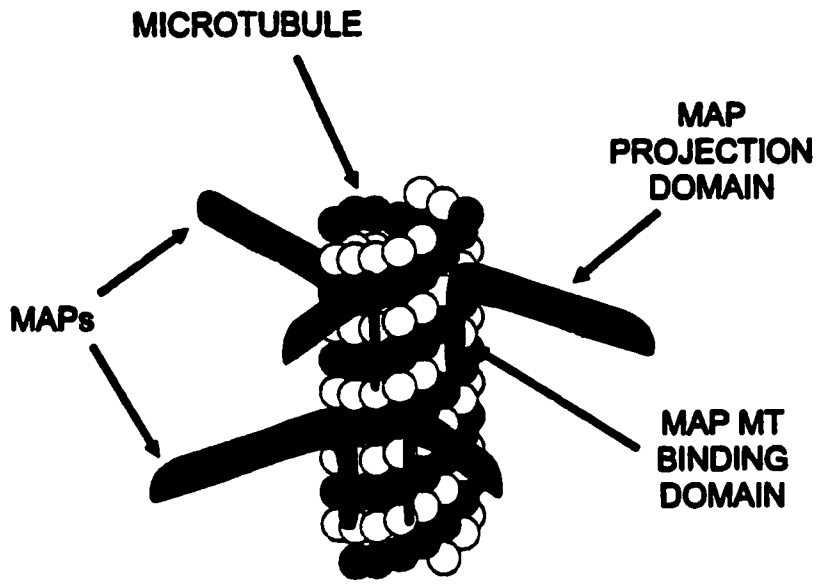
MICROTUBULE
MAP
PROJECTION
DOMAIN
MAPs
MAP MT
BINDING
DOMAIN

sensitive to depolymerizing agents, such as colchicine and nocodazole (Falconer *et al.*, 1994). Therefore, the first goal in this study was to determine whether **Mts in undifferentiated cells and neuronally differentiated cells differ in sensitivity to MeHg-induced depolymerization.**

Previous studies have shown that stable Mt bundles, similar to those found in neuronal processes, are formed when MAPs such as the juvenile isoform of MAP2 and tau are expressed in non-neuronal cells by transient transfections (Lewis *et al.*, 1989; Takemura *et al.*, 1992). As well as alterations in Mt organization in MAP-transfected cells, changes in sensitivity to the Mt depolymerizing agents, colchicine and nocodazole, were observed (Lewis *et al.*, 1989; Baas *et al.*, 1994). The second goal in this study was to examine whether **MAP expression alters Mt-sensitivity to MeHg in undifferentiated P19 cells.**

Figure 4: Developmentally regulated expression of Mt proteins in P19 EC cells during RA-induced neuronal differentiation. From Falconer *et al.* (1994).

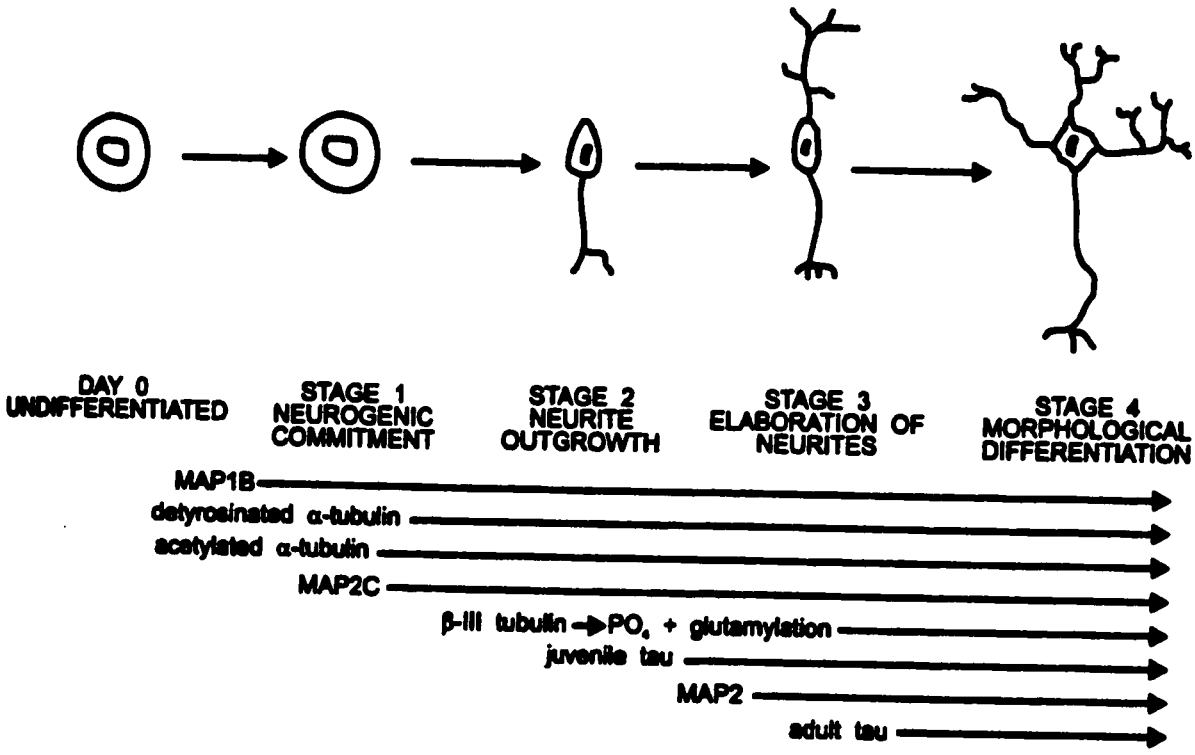
DAY 0
UNDIFFERENTIATED
STAGE 1
NEUROGENIC
COMMITMENT
STAGE 2
NEURITE
OUTGROWTH
STAGE 3
ELABORATION OF
NEURITES
STAGE 4
MORPHOLOGICAL
DIFFERENTIATION
MAP1B
detyrosinated α-tubulin
acetylated α-tubulin
MAP2C
β-III tubulin → PO4 + glutamylation
juvenile tau
MAP2
adult tau

B. MATERIALS AND METHODS

B. 1 Cell Culture

P19 EC cells (McBurney and Rogers, 1982) were maintained at 37°C and 5% CO_2 in α-modified Eagle's minimal essential medium (α-MEM) (GIBCO BRL), supplemented with 10% heat-inactivated fetal calf serum (FCS) (CanSera) and 1% of a 100X antibiotic-antimycotic stock (penicillin, streptomycin, and fungizone) (GIBCO BRL). All cultures were maintained in 100-mm tissue culture grade dishes (Corning) and passaged every 48 hr.

B. 2 Neuronal Differentiation

P19 EC cells were differentiated into neurons using the method of MacPherson and McBurney (1995). For immunofluorescence studies cells were plated on 22 x 22mm glass coverslips (VWR). Cells were plated on 100 mm culture dishes for protein extraction experiments. The cells remained in α-MEM containing 10% FCS and 1% antibiotics for 24 hr after plating. The medium was then changed and supplemented with 10^{-6} M retinoic acid (RA) (Sigma), diluted from a 10^{-3} M RA stock prepared in ethanol. The medium was replaced 24 hr later with a defined, serum - free, medium which inhibits cell proliferation and is enriched for neuron growth (MacPherson and McBurney, 1995). Each day, half of the medium was replaced, until the cells were ready for processing.

B. 3 Plasmid DNA Constructs (Figure 5)

The plasmid pPGK2c was previously constructed (C. Addison, University of Ottawa) by blunt-end ligation of a 1.75 kb *NotI* fragment containing the MAP2c cDNA (Kindler *et al.*, 1990) from pCMVneo2c (gift from Dr. C.C. Garner, University of Alabama, Birmingham) into the *SmaI* multicloning site of pPOP (provided by Dr. M.W. McBurney, University of Ottawa). The pPOP plasmid contains the constitutive phosphoglycerate kinase (PGK-1) promoter to drive the expression of MAP2c in undifferentiated P19 cells.

B. 4 Plasmid DNA Preparation

Bacterial transformations, plasmid DNA minipreparations and restriction digests were performed according to Sambrook *et al.*, (1989). For large scale DNA preparations, competent DH5αF' *E.coli* cells were transformed by the plasmid DNA using heat-shock. The cultures were plated on LB agar plates containing 100 mg/ml ampicillin and grown overnight at 37°C. Using aseptic technique, one colony was transferred into 3 ml Terrific (T)-broth cultures, containing 100 mg/ml ampicillin, and grown overnight at 37°C with vigorous shaking. 2 ml of the T-broth culture were used to inoculate a 250 ml LB broth culture containing 100 mg/ml ampicillin and was grown overnight with agitation at 37°C. The bacteria were then harvested by centrifugation and the plasmid DNA was isolated by alkaline-lysis using the Qiagen DNA preparation kit (Qiagen). The plasmid DNA was resuspended in distilled, deionized water (ddH_20) and the concentration and purity was determined spectrophotometrically by UV

Figure 5: Diagram of the MAP2c coding region which was cloned into an expression vector used for transient transfections of P19 EC cells. This coding region contains the PGK-1 (phosphoglycerate kinase) constitutive promoter to drive gene expression. Restriction sites for *Eco*RI (E) and *Pst*I (P) are shown. From Addison, 1997.

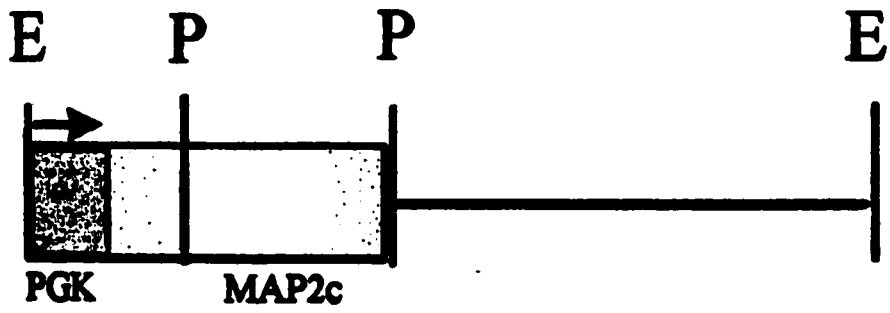

pPGK2c (5.39 kb)

absorbance at 260 and 280 nm using Genequant® spectrophotometer (Pharmacia). Agarose gel electrophoresis of 2 µl of the DNA preparation in a 0.8% agarose/Tris-acetate-EDTA gel confirmed the presence of supercoiled DNA in the preparation.

B. 5 $CaPO_4$/DNA Precipitation Transfection

Undifferentiated P19 cells were seeded on 22 x 22 mm coverslips at a density of 2 x 10^4 cells/ml or on 60 mm tissues culture dishes (Corning) at a density of 2.5 x 10^5 cells/ml. Cells were cultured overnight in α-MEM, supplemented with 10% FCS and 1% antibiotic. The next day plasmid DNA was introduced into the cells using the $CaPO_4$- precipitation method described by Chen and Okayama (1987). The $CaPO_4$-DNA mixture was prepared with 50 µl of 2.5 M $CaCl_2$, 35 µg of DNA and sterilized ddH_20 to give a final volume of 500 µl. The solution was vortexed and 500 µl of 2X BES buffered saline [50 mM BES, pH 6.86, 280 mM NaCl, 1.5 mM Na_2HPO_4] was added very slowly. The mixture was allowed to sit for 15 minutes. 500 µl of the mixture was added to each coverslip, or 1 ml was added to each 60 mm dish and incubated at 37°C under 5% CO_2 for 8 hr. The precipitate was then removed and the cells were washed twice in phosphate buffered saline (PBS) [130 mM NaCl, 5 mM Na_2HPO_4, 1.5 mM KH_2PO_4, pH 7.4] and fresh α-MEM supplemented with 5% FCS and 1% antibiotic was added.

B. 6 Methylmercury Treatments

A 4 mM stock solution of methylmercury chloride (ICN) was prepared in PBS. For treatment of undifferentiated and transfected cells, this stock was diluted in α-MEM containing 5% FCS to provide final working concentrations ranging from 0.1 μM to 4 μM. 24 hr after growing the cells on coverslips or after transfection, the culture medium was replaced with culture medium containing specified MeHg concentrations for the indicated treatment times. For treatment of neuronally differentiated cells, the MeHg stock was diluted in serum free medium to provide final working concentrations ranging from 0.4 μM to 8 μM . After 6 days of neuronal differentiation, the medium in the culture dishes was replaced with fresh medium containing MeHg. Cells were then incubated at 37°C and under 5% CO_2 for the indicated time periods.

B. 7 Polymer/Soluble Protein Extraction (Figure 6)

This method was used to determine the amount of tubulin or MAP2 present in the polymer and soluble fraction following MeHg treatment. Dishes of either undifferentiated, MAP2c transfected or neuronally - differentiated P19 cells were treated with specified concentrations of MeHg for specific time points. At the end of the treatment, the cells were rinsed briefly with 37°C pre-warmed PEM buffer [40 mM PIPES, pH 6.8, 2.5 mM EGTA, 0.5 mM $MgCl_2$ (all from Sigma)]. Cells were then incubated for 5 min at 37°C in 250-500 μl of microtubule stabilizing buffer [0.1 M MES (Boehringer Mannheim), pH 6.75, 1 mM $MgSO_4$, 2 mM EDTA (Sigma), 0.1

Figure 6: Protocol for polymer/soluble extraction. From Vaillant, 1997.

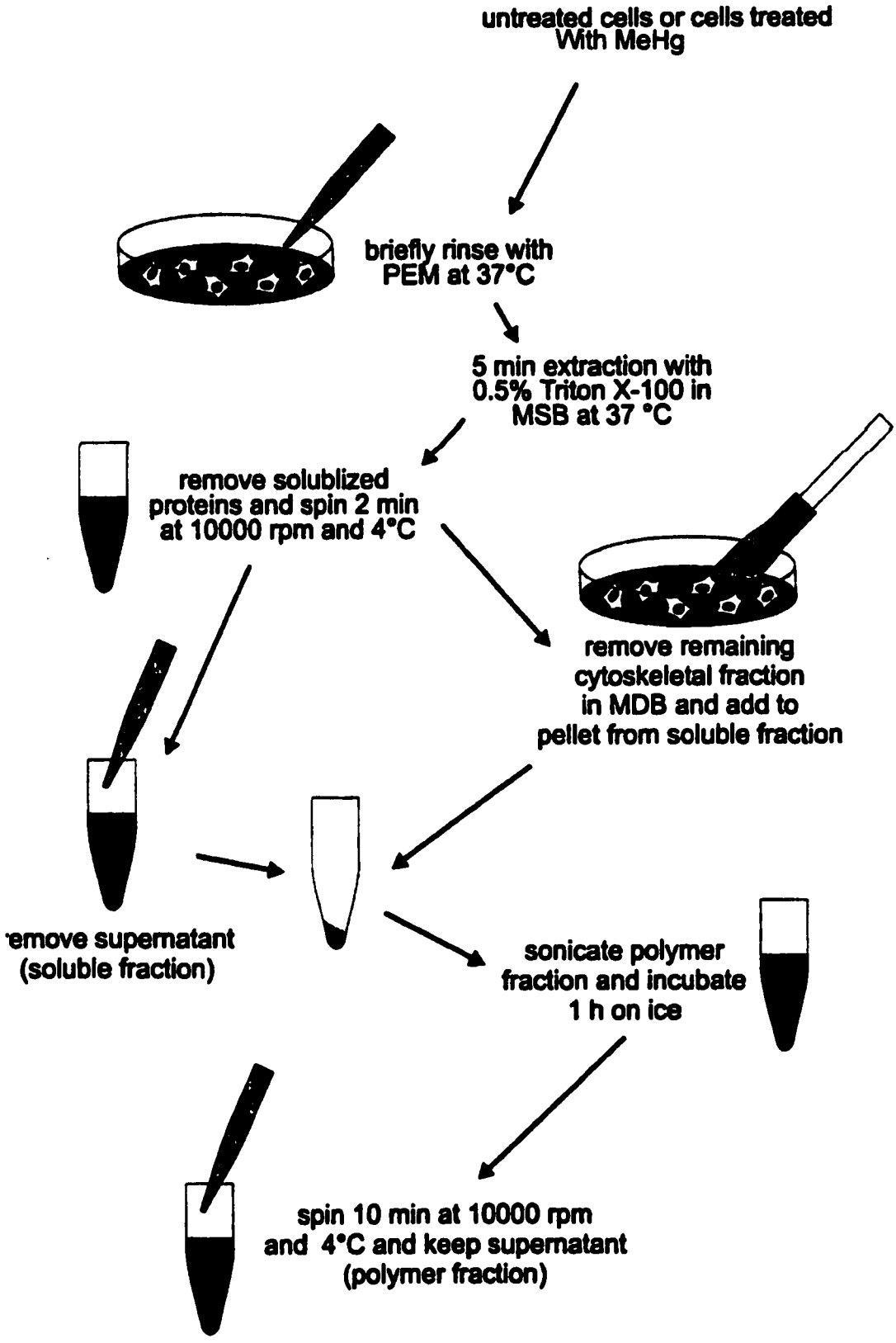
untreated cells or cells treated With MeHg
briefly rinse with PEM at 37°C
5 min extraction with 0.5% Triton X-100 in MSB at 37 °C
remove solublized proteins and spin 2 min at 10000 rpm and 4°C
remove remaining cytoskeletal fraction in MDB and add to pellet from soluble fraction
emove supernatant (soluble fraction)
sonicate polymer fraction and incubate 1 h on ice
spin 10 min at 10000 rpm and 4°C and keep supernatant (polymer fraction)

mM EGTA, 4 M glycerol (BDH), 0.5% Triton X-100 (Pierce)] (Joshi and Cleveland, 1989), including 4 mM PEFA and 40 µg/ml of aprotinin, pepstatin A and leupeptin (all from Sigma). The extraction buffer was then removed from the dish, pipetted into an eppendorf tube and was spun at 10 000 rpm for 2 min at room temperature. The supernatant was transferred to another tube and labelled as the soluble fraction. 250-500 µl of microtubule destabilizing buffer [0.1 M MES , 1 mM $MgSO_4$, 10 mM $CaCl_2$, pH 6.9, 1 mM DTT (BRL) and 5 mM GTP, type II (Sigma)] (Thrower *et al.*, 1991), also including protease inhibitors as above, was added to the dish. The buffer and cells were scraped into the eppendorf tube containing the pellet remaining from the soluble fraction. The contents in the tube were then sonicated for 15 sec at 90-95 W using a Braun sonicator, incubated on ice for 1 hr and spun at 10 000 rpm for 10 min at 4°C. The supernatant was labelled as the polymer fraction. The protein concentration of the soluble and polymer fraction was determined using the bicinchoninic acid protein assay (Pierce) with Bovine Serum Albumin (Pierce) diluted in ddH_2O as a standard. The protein samples were then stored at -80°C.

B. 8 SDS-PAGE and Western Blotting

Protein samples, diluted 1:1 in 2X sample buffer (Laemmli, 1970), and prestained broad range standards (BIORAD) were boiled for 5 min, allowed to cool and were then loaded onto 12% polyacrylamide gels and separated using the BIORAD minigel apparatus. Following separation, the proteins were electrotransferred onto nitrocellulose (NC) (Schleicher and Scheull) according to Towbin *et al.*, 1979. The

blot was rinsed in PBS and processed for western blotting. First, the blot was incubated overnight in 5% skim milk (Carnation) in PBS, at 4°C. This was followed by a 1h incubation in primary antibody, diluted in 2% skim milk in PBS. The blot was washed 3 X 5 min in 2% skim milk in PBS then incubated for 45 min in biotinylated secondary antibody diluted in 2% skim milk. Next, 3 X 5 minute washes in PBS were followed by a 30 min incubation in streptavidin-HRP (Amersham) diluted 1:5000 in PBS. Antibody binding was detected by enhanced chemiluminescence (ECL) (Amersham) using Hyperfilm-ECL (Amersham). Films were digitized at 400 dpi using a Hewlett-Packard 4c flatbed scanner. Digitized TIFF images were processed using Adobe Photoshop v4.0.

B. 9 Quantitative Dot Blotting

A 96 well Minifold apparatus (Schleicher and Scheull) was assembled with filter paper (Schleicher and Scheull) and NC, both of which were pre-wetted in PBS. Protein samples were diluted in PBS and 200 µl/well was passed through the NC using a vacuum. The wells were rinsed with an additional 400 µl of PBS. The NC was removed from the apparatus, rinsed briefly in PBS and processed for western blotting, as above. The resulting films were scanned at 400 dpi using a Hewlett-Packard 4c flatbed scanner. The chemiluminescent signal from each dot in the digitized image was quantified using SigmaGel v1.0 (Jandel Scientific). The obtained values were imported into Excel 97 (Microsoft) and Sigmaplot v4.0 (Jandel Scientific) for analysis. Standard curves for tubulin and MAP2 primary antibodies were made using phosphocellulose

(PC) purified-tubulin, and S1 isolated from bovine brain, respectively (Shelanski *et al.*, 1973). This was to ensure that sample measurements fell within the linear response for these antibodies.

B. 10. Immunofluorescence Microscopy

Cells grown on coverslips were washed in PBS and were then pre-extracted for 2 min in 0.2% Triton X-100 in PEM buffer. The cells were then simultaneously fixed and extracted in 3.7% paraformaldehyde (v/v), 0.25% glutaraldehyde (v/v) and 0.5% Triton X-100 (v/v) in PEM buffer for 10 min. Coverslips were then washed 3 X 5 min in PBS. Following fixation, cells were washed 3 X 5 min with 2 mg/ml sodium borohydride (BDH) in PBS, to reduce free aldehyde groups, and then were rinsed in PBS for 3 X 5 min.

Double immunofluorescence labelling was performed sequentially, at room temperature. All antibody incubations lasted 45 min, with 3 X 5 min washes in PBS between each application of antibody. Following the incubation of the last secondary antibody, cells were washed in PBS 3 X 5 min and were then counterstained with a 2 mg/ml stock of 4'-6-diamidino-2-phenylindole (DAPI) (Molecular Probes), diluted 1:5000, to visualize DNA. For single labelling, cells were counterstained in DAPI following the incubation with the first secondary antibody. Cells were then washed for 30 sec in PBS and mounted in 50% glycerol-PBS, pH 7.8 containing 1% (w/v) para-phenylene-diamine.

Immunolabelled samples were visualized using either a Zeiss Axiophot epifluorescence microscope or a Zeiss Universal epifluorescence microscope equipped with a 50 W mercury arc lamp. Both 40 X epifluorescence and phase optics were used. Samples visualized using the Zeiss Axiophot microscope were photographed using Ilford XP2 400 film. The film was scanned using the Polaroid Sprintscan 35mm negative scanner at 2700 dpi. Immunolabelled cells visualized using the Zeiss Universal microscope were digitally recorded with a Hamamatsu CCD camera using Metamorph v2.75 (Universal Imaging). All images were saved as TIFF images and were processed using Adobe Photoshop v4.0.

B. 11 Antibodies

Anti-α-Tubulin

5A6, a mouse monoclonal IgG specific for α-tubulin (Aitchison and Brown, 1986) (University of Ottawa) was used for single labelling at 1:10 000.

DM1A, a mouse monoclonal IgG specific for α-tubulin [clone DM1A (Amersham)] (Blose *et al.*, 1984) used at 1:200 for single immunolabelling.

YOL 1/34, a rat monoclonal IgG which recognizes α-tubulin, diluted 1:10 (Serotec) was used for double immunolabelling

Anti -β-Tubulin

DM1B, a mouse monoclonal IgG [clone DM1B (Amersham)] (Blose *et al.*, 1984) used at 1:1 000 for immunoblotting.

Anti -MAP2

HM-2, a mouse monoclonal IgG [clone HM-2 (Sigma)] (Tucker *et al.*, 1988) used 1:400 for immunofluorescence microscopy and 1:1 000 for immunoblotting.

Anti-Mouse IgG

Donkey polyclonal IgG (H+L) conjugated to indocarbocyanine (CY3) (Jackson), cross-adsorbed to rat and rabbit, used at 1:400 for immunofluorescence microscopy.

Horse polyclonal IgG, biotinylated (Vector) and used at 1:1 000 for immunoblotting.

Anti-Rat IgG

Donkey polyclonal IgG (H+L) conjugated to carboxymethyl indocarbocyanine (Cy2) (Jackson), cross-adsorbed to mouse and rabbit, used at 1:100 for immunofluorescence microscopy.

C. RESULTS

Previous studies showed that the Mt system in both undifferentiated and neuronally differentiated P19 cells responded to MeHg in a time- and dose-dependent manner (Cadrin *et al.*, 1988; Wasteneys *et al.*, 1988). Due to changes in the culture conditions of both undifferentiated and differentiated P19 cells it was necessary to redefine the treatment parameters used in these experiments. These parameters were then applied to experiments in both chapters of this thesis. In this chapter the time- and dose- dependent effects of MeHg-induced Mt damage were assessed qualitatively by immunofluorescence microscopy and an attempt was made to also assess the effects quantitatively by dot blotting and by SDS-PAGE and western blotting.

C. 1. Undifferentiated P19 cells

C. 1. 1 *MeHg-induced damage on interphase Mts*

In control samples the interphase Mt network was organized radially within the cytoplasm of the cell. The Mts originated from one region, located near the nucleus, and extended to the cell periphery (Fig. 7C). In cells treated with MeHg, the Mt organization was disrupted. The Mts were no longer intact and appeared to be less bundled and shorter in length. Figs. 8A '' and B '' show the time dependent effects of MeHg treatment. At a dose of 0.4 µM Mt damage was slight at short treatment times (2 hr) and increased with longer treatment times (10 hr). As both time and dose

Figure 7: Phase contrast (**A**) and immunofluorescence labelling of Mts in undifferentiated P19 EC cells. Cells were immunolabelled using a mouse monoclonal antibody to a-tubulin (**C**) allowing interphase Mts, organized radially within the cell, to be observed. Counterstaining with DAPI, a DNA specific dye, (**B**) allowed the nuclei to be observed. Bar = 20 µm.

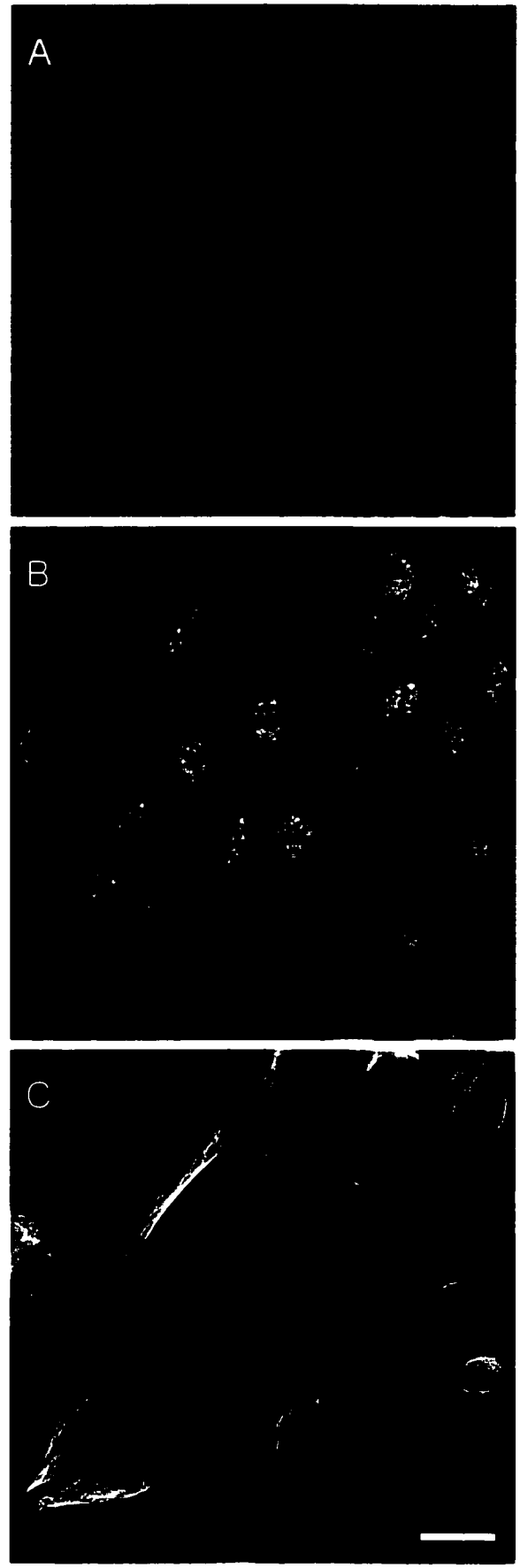
A
B
C

Figure 8: Phase contrast (**A and B**), DAPI staining of DNA (**A' and B'**) and immunofluorescence labelling of Mts using a mouse monoclonal antibody to α-tubulin (**A'' and B''**) in undifferentiated P19 EC cells treated with MeHg. Treatments with 0.4 mM MeHg for 2 hr (**A''**) and 10 hr (**B''**) showed increased Mt depolymerization with increased MeHg treatment time. Bar = 20 μm.

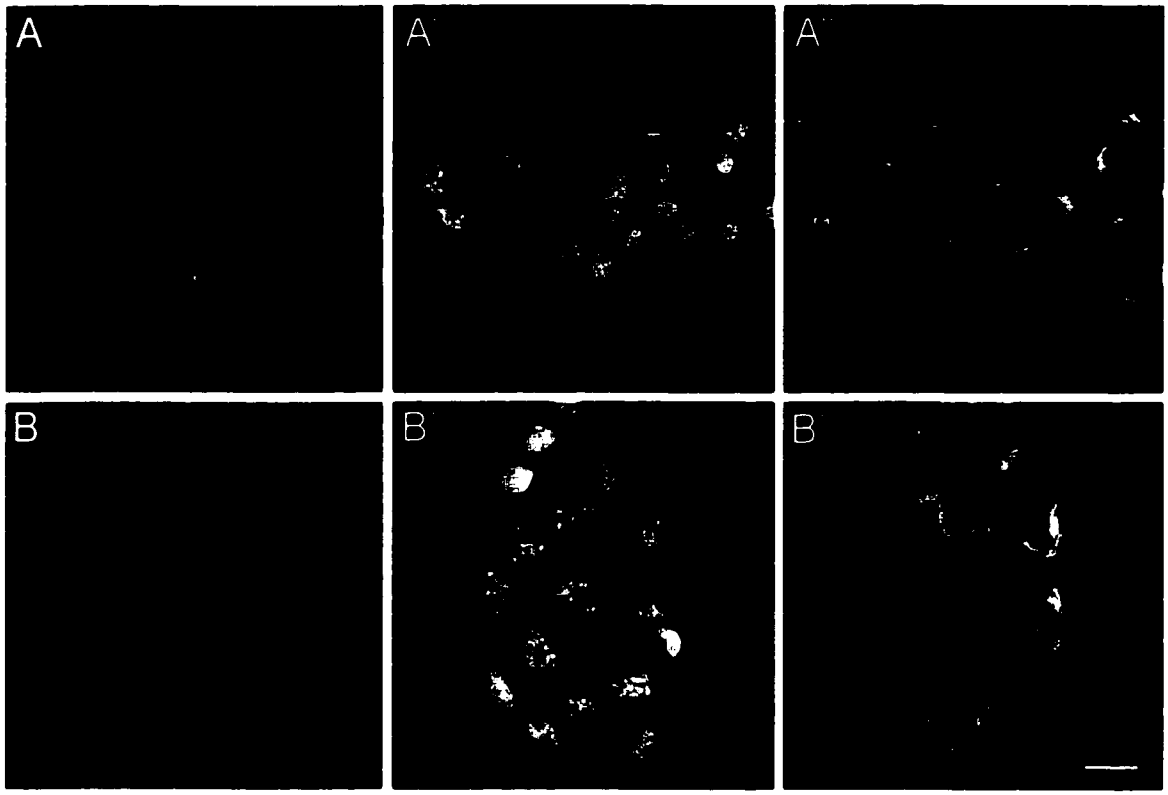
A
A
A
B
B
B

increased the effects of MeHg on interphase Mts became more severe (Fig 9). At a treatment time of 8 hr Mt damage was moderate with a 1 µM dose (9 A '') and following a 4 µM dose all the Mts had completely disassembled (9 B ''). Complete Mt disassembly was also observed following a 12 hr treatment with both 1 µM (9 C '') and 4 µM (9 D '') MeHg. Treatments which caused complete Mt disassembly resulted in diffuse tubulin immunolabelling throughout the cytoplasm.

C. 1. 2 *Effects of MeHg on the cytoplasmic pool of polymer and soluble tubulin*

In undifferentiated and neuronally differentiated samples not all of the cells are equally affected by MeHg. Therefore, a quantitative analysis would more accurately assess the extent of Mt damage occurring throughout these samples. Tubulin from control and MeHg-treated cells was extracted using a protocol in which the polymer fraction was extracted separately from the soluble fraction (see Fig. 6 Materials and Methods). This procedure has been used to monitor the disassembly of Mts caused by colchicine treatment by the observed decrease of tubulin in the polymer fraction and concomitant increase in the soluble fraction (Laferrière and Brown, 1996; Vaillant and Brown, 1998). Surprisingly, although it was clear from the immunofluorescence staining that Mts were disassembled, there was no change in the amount of tubulin in either the polymer or soluble fractions in MeHg-treated samples. This was observed by both quantitative dot blotting and SDS-PAGE followed by western blotting (Figs. 10 and 11).

Figure 9: Phase contrast (**A - D**), DAPI staining of DNA (**A' - D '**) and immunofluorescence labelling of Mts using a mouse monoclonal antibody to α-tubulin (**A'' - D ''**) in undifferentiated P19 EC cells treated with MeHg. Treatments with 1μM and 4 μM MeHg for 8 hr (**A'' and B'', respectively**) and 1μM and 4 μM MeHg for 12 hr (**C'' and D'', respectively**) show moderate to complete loss of Mts with increasing dose and time. Bar = 20 μm.

Figure 10: Levels of polymer and soluble tubulin in undifferentiated P19 cells treated with MeHg for 12 hr. Absolute tubulin levels per μg of total cellular protein in polymer and soluble fractions were determined by quantitative dot blotting with mAb DM1B, which recognizes all isotypes of β-tubulin. Phosphocellulose-purified tubulin was used as a standard. The data are the mean of three measurements taken from three separate experiments. Error bars represent the standard error from the mean.

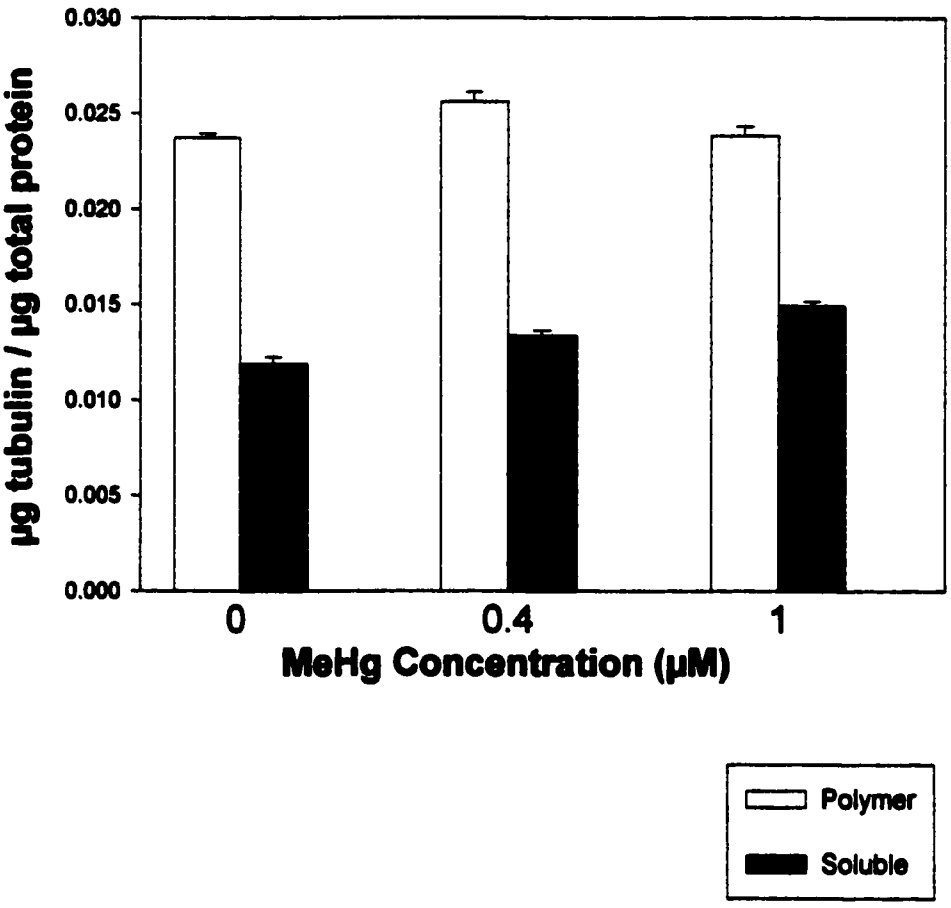
0.030
0.025
0.020
0.015
0.010
0.005
0.000
µg tubulin / µg total protein
0
0.4
1
MeHg Concentration (µM)
Polymer
Soluble

Figure 11: Detection of tubulin in MeHg-treated, undifferentiated P19 cells. 2 μg of polymer and 5 μg of soluble protein extracts taken from untreated and 12 hr, 0.4 μM and 12 hr, 1 μM MeHg-treated samples were separated by SDS-PAGE on 9% polyacrylamide gels. Tubulin was detected by western blotting using mAB DM1B. No difference was observed in the amount of polymer and soluble tubulin in MeHg-treated cells, compared to untreated cells. Molecular weight markers are in kDa.

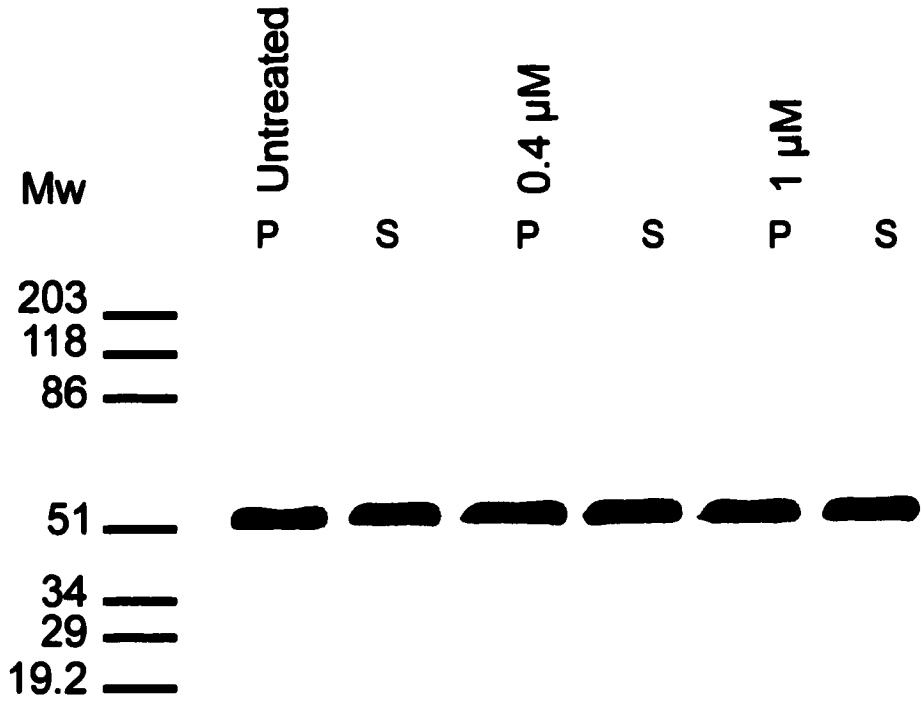
Mw
Untreated
0.4 µM
1 µM
P
S
P
S
P
S
203
118
86
51
34
29
19.2

C. 2 MAP2c-transfected P19 cells

C. 2. 1 *MAP-Mts are resistant to MeHg*

MAP2c-transfection causes bundling of Mts and increases the resistance to depolymerizing drugs such as colchicine and nocodazole (Takemura *et al.*, 1992). To determine whether the expression of MAPs confer MeHg resistance to Mts in undifferentiated cells transient transfections with pPGK2c were used to express the juvenile form of MAP2, which is not normally present in non-neuronal P19 cells. Both untransfected and MAP2c-transfected P19 cells were subjected to an 8 hr MeHg treatment at doses of 0.4 μM and 1μM. Intensely stained Mt bundles in untreated, MAP2c-transfected cells are shown in Fig. 12D. These Mt-bundles will be referred to as MAP-Mts. After an 8 hr, 0.4 μM MeHg treatment (Fig. 13C) faint staining of Mts in cells that are not transfected could be observed (compare to the control (Fig. 12C)). With an 8 hr, 1 μM MeHg treatment (Fig. 13C ') there was an almost complete absence of Mt staining, except in the transfected cells in which the MAP-Mts appeared unaffected (Figs. 13 D and D '). In experiments using the same doses, but with treatment times of 10 and 12 hr, the MAP-Mts still appeared resistant to MeHg (data not shown).

It was noted that in experiments in which MeHg-induced Mt damage was monitored by immunofluorescence microscopy with the 5A6 mAb, a diffuse anti-tubulin labelling was observed in the cytoplasm (e.g. Fig. 9). This diffuse staining was not seen when the YOL1/34 mAb was used (e.g. Fig. 13).

Figure 12: Phase contrast (**A**), DAPI staining of DNA (**B**) and double immunofluorescence labelling of Mts in P19 cells transiently transfected with pPGK2c. Cells were immunolabelled using YOL 1/34, a rat monoclonal antibody to α-tubulin (**C**), and HM-2, a mouse monoclonal antibody to MAP2 (**D**). Bundled Mts in the MAP2c-transfected cells were observed by both α-tubulin (**C**) and MAP2 labelling (**D**). Bar = 20 μm.

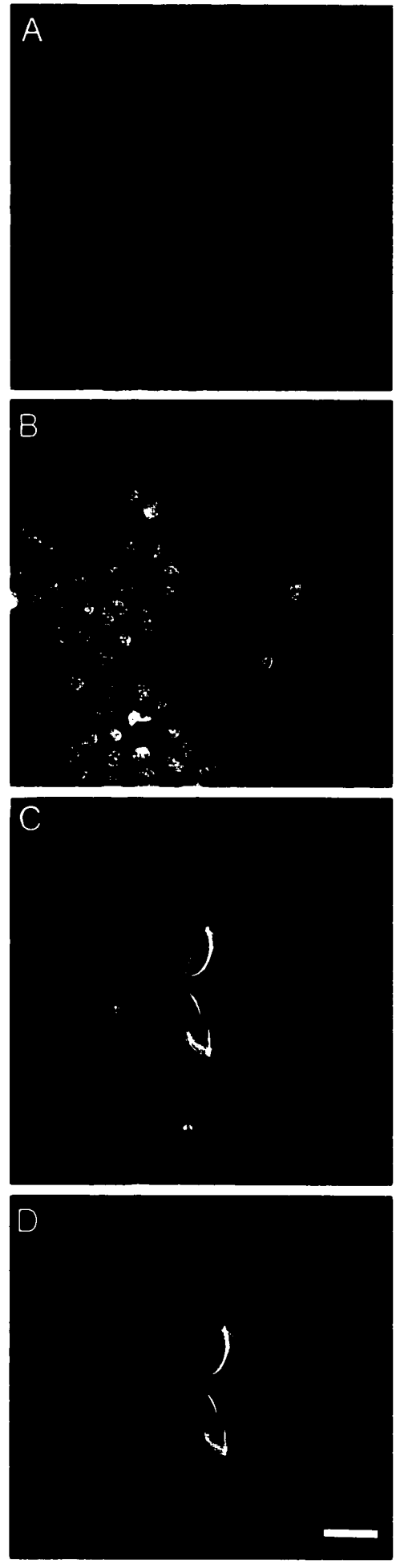
A
B
C
D

Figure 13: Phase contrast (**A - A'**), DAPI staining of DNA (**B - B'**) and double immunofluorescence labelling of Mts in MeHg-treated P19 cells transiently transfected with pPGK2c. Cells were double immunolabelled using YOL 1/34, a rat monoclonal antibody to α-tubulin (**C - C'**) and HM-2, a mouse monoclonal antibody to MAP2 (**D - D'**). Treatments with 0.4 μM MeHg for 8 hr resulted in faint Mt staining of untransfected cells (**C**), whereas MAP2c transfected cells, exhibiting bundled Mts, appeared unaffected (**C and D**). MeHg treatments of 1 μM for 8 hr resulted in complete loss of Mt staining in the untransfected cells (**C'**) and the Mt bundles in MAP2c transfected cells appeared unaffected (**C' and D'**). Bar = 20 μm.

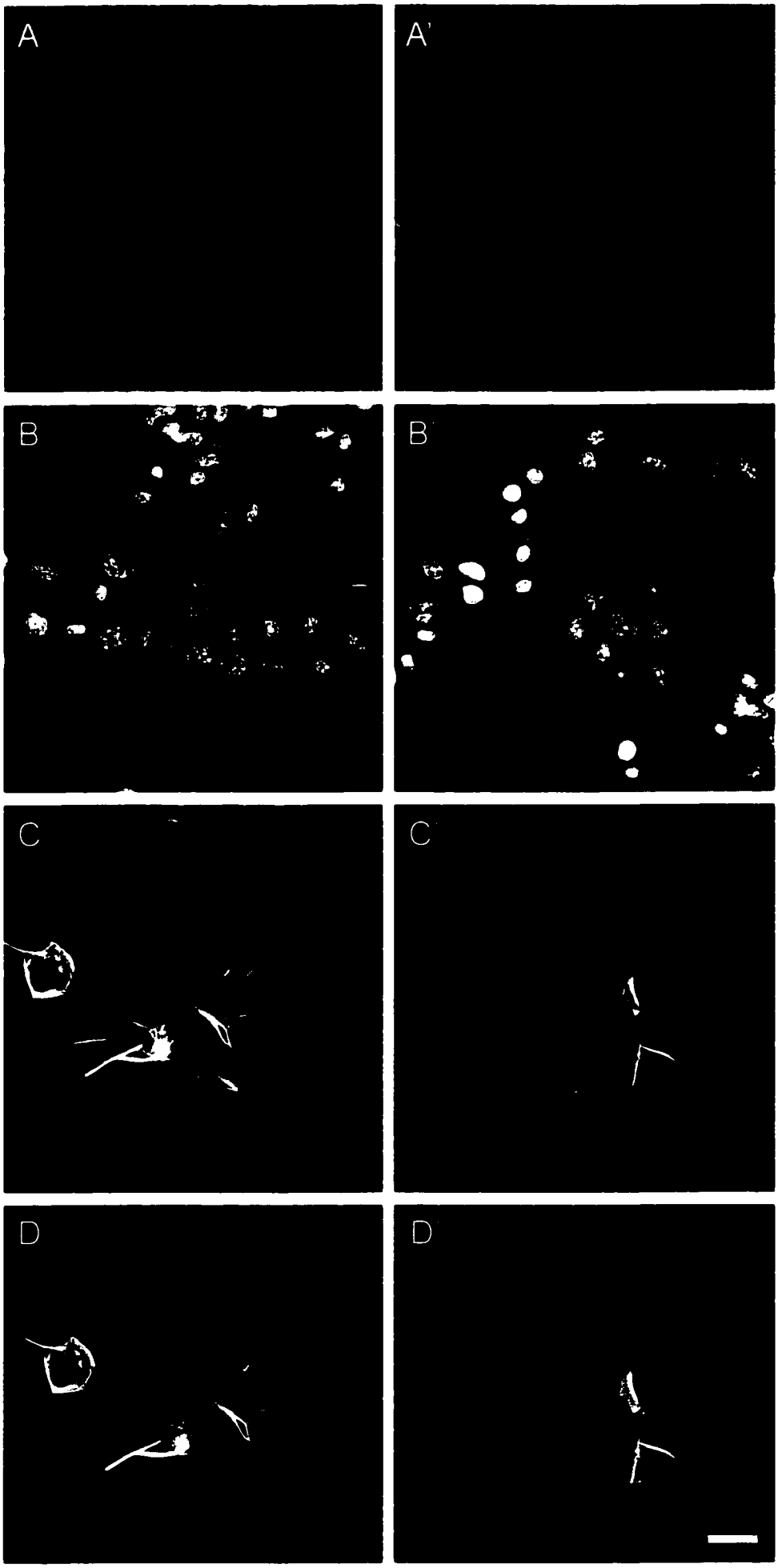
A
A'
B
B'
C
C'
D
D'

Secondary antibody controls (Fig. 14) for both tubulin and MAP2 staining of untreated and MeHg treated untransfected and transfected samples show lack of non-specific staining with secondary antibodies.

C. 2. 2 *Effects of MAP2c expression and MeHg treatment on the cytoplasmic pool of polymer and soluble tubulin*

To further assess whether MAP2c transfection conferred MeHg-resistance to Mts, quantitative dot blotting of polymer and soluble protein extractions from transfected, MeHg-treated cells was performed. As expected, MAP2c transfection resulted in an increase of the polymer tubulin fraction with a concomitant decrease in the soluble fraction (Fig. 15) compared to polymer and soluble tubulin levels found in untransfected cells (Fig. 10). In accordance with the data for untransfected cells (Fig. 10) quantitative dot blotting showed no change in the amount of tubulin in the polymer or soluble fraction in the MeHg-treated MAP2c transfected samples (Fig. 15).

C. 3 Neuronally differentiated P19 cells

C. 3. 1 *Neuronal Mts are less sensitive to MeHg damage*

As P19 cells differentiate into neurons they form cell aggregates and extend neurites which contain bundled Mts with an increased stability to colchicine (Falconer *et* al., 1992; Laferrière and Brown, 1996). The Mts in neurons also showed increased resistance to MeHg. Fig. 16 shows the effects of varying doses of MeHg on day 6

Figure 14: Secondary antibody controls of MAP2c-transfected cells. Phase contrast **(A)** and DAPI stained nuclei **(B)** are shown. The samples were incubated with secondary antibodies only. Non-specific staining was not present when samples were incubated with the secondary antibody which detects YOL 1/34 **(C)** or with the antibody which detects HM-2 **(D)**. Bar = 10 μm.

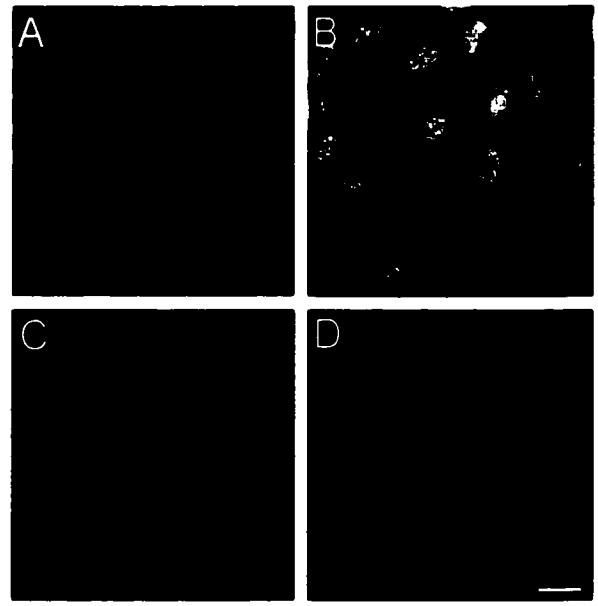
A
B
C
D

Figure 15: Levels of polymer and soluble tubulin in control and MeHg-treated undifferentiated P19 cells, transfected with pPGK2c. Absolute tubulin levels per μg of total cellular protein in polymer and soluble fractions were determined by quantitative dot blotting with mAb DM1B using phosphocellulose-purified tubulin as a standard. Extracts were taken from MAP2c-transfected cells that were treated with 0.4 μM and 1μM MeHg for 12 hr. The data are means of three measurements. Error bars represent the standard deviation from the mean.

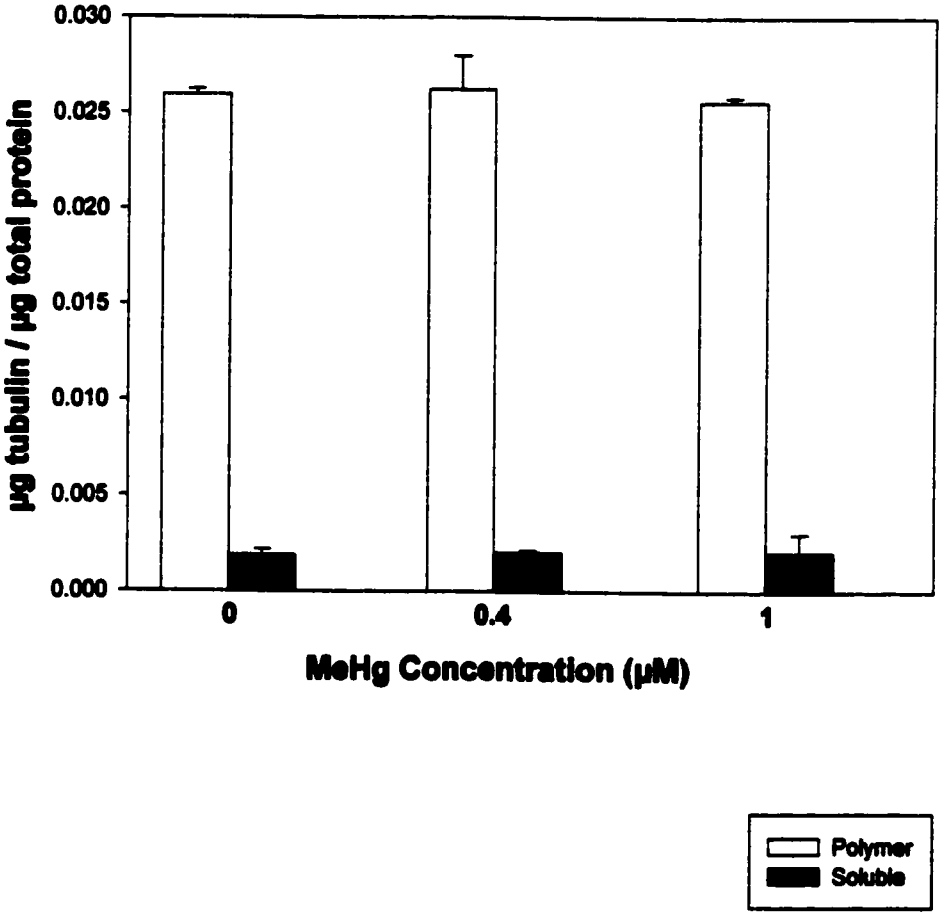
0.030
0.025
0.020
0.015
0.010
0.005
0.000
µg tubulin / µg total protein
0
0.4
1
MeHg Concentration (µM)
Polymer
Soluble

Figure 16: Phase contrast (**A - K**), DAPI staining of DNA (**A' - K '**) and immunofluorescence labelling of Mts using a rat monoclonal antibody to α-tubulin (**A'' -K ''**) in neuronally differentiated P19 treated with MeHg. (**A'' - C''**) represents an 8hr control sample and 0.4 μM and 1 μM MeHg-treated samples, respectively. (**D'' - G''**) represent 12 hr control, 0.4 μM, 1 μM and 4 μM samples, respectively. (**H '' - K''**) represent 24 hr control, 0.4 μM, 1 μM and 4 μM samples, respectively. Bar = 20 μm.

neuronally differentiated P19 cells, with treatments lasting for 8, 12 and 24 hrs. 8 hr or 12 hr treatments with 0.4 or 1 μM MeHg did not appear to have any effect on the neuronal Mts. Uniform Mt-staining was observed throughout the length of the neurite and no apparent decrease in Mt bundling was observed (Figs. 16B '' , C '' , E '' and F ''), when compared to the controls (Fig. 16A '' and D ''). However, Mt damage was evident following a 12 hr, 4μM MeHg treatment. Mt staining was no longer uniform throughout the length of the neurite and the Mt bundles became shorter and thinner (Fig. 16G ''). Following a 24 hr. 0.4 μM MeHg treatment, Mt staining appeared less uniform throughout the length of the neurites (Fig. 16I ''), compared to the control (Fig. 16H ''). and more severe effects could be observed after 24 hr with 1 μM and 4 μM doses (Figs. 16 J '' and H ''). Mts in neurites near the margins of neuronal aggregates were most affected by the MeHg treatment. In neurites within the aggregates the Mts frequently appeared undamaged.

C. 3. 2 *MeHg treatment does not alter the cytoplasmic pool of polymer and soluble tubulin in neuronally differentiated cells*

As observed with the undifferentiated and MAP2c-transfected cells there was no change in the distribution of tubulin between the polymer and soluble protein fractions of MeHg-treated neurons. The total amount of tubulin in untreated, and MeHg-treated samples remained the same in the polymer and soluble fractions following 12, 18 and 24 hr exposure with 0.4 and 1μM MeHg (Fig. 17). SDS-PAGE of these polymer and soluble extracts also showed that levels of a 55 kDa protein, detected by anti-tubulin

Figure 17: Levels of polymer and soluble tubulin in neuronally differentiated P19 cells, treated with MeHg. Absolute tubulin levels per μg of total cellular protein in polymer and soluble fractions were determined by quantitative dot blotting with mAb DM1B using phosphocellulose-purified tubulin as a standard. Extracts were taken from differentiated cells that were untreated and treated with 0.4 μM and 1μM MeHg for 12 hr **(a)** 18 hr **(b)** and 24 hr **(c)**. The data are the mean of three measurements taken from three separate experiments. Error bars represent the standard error from the mean.

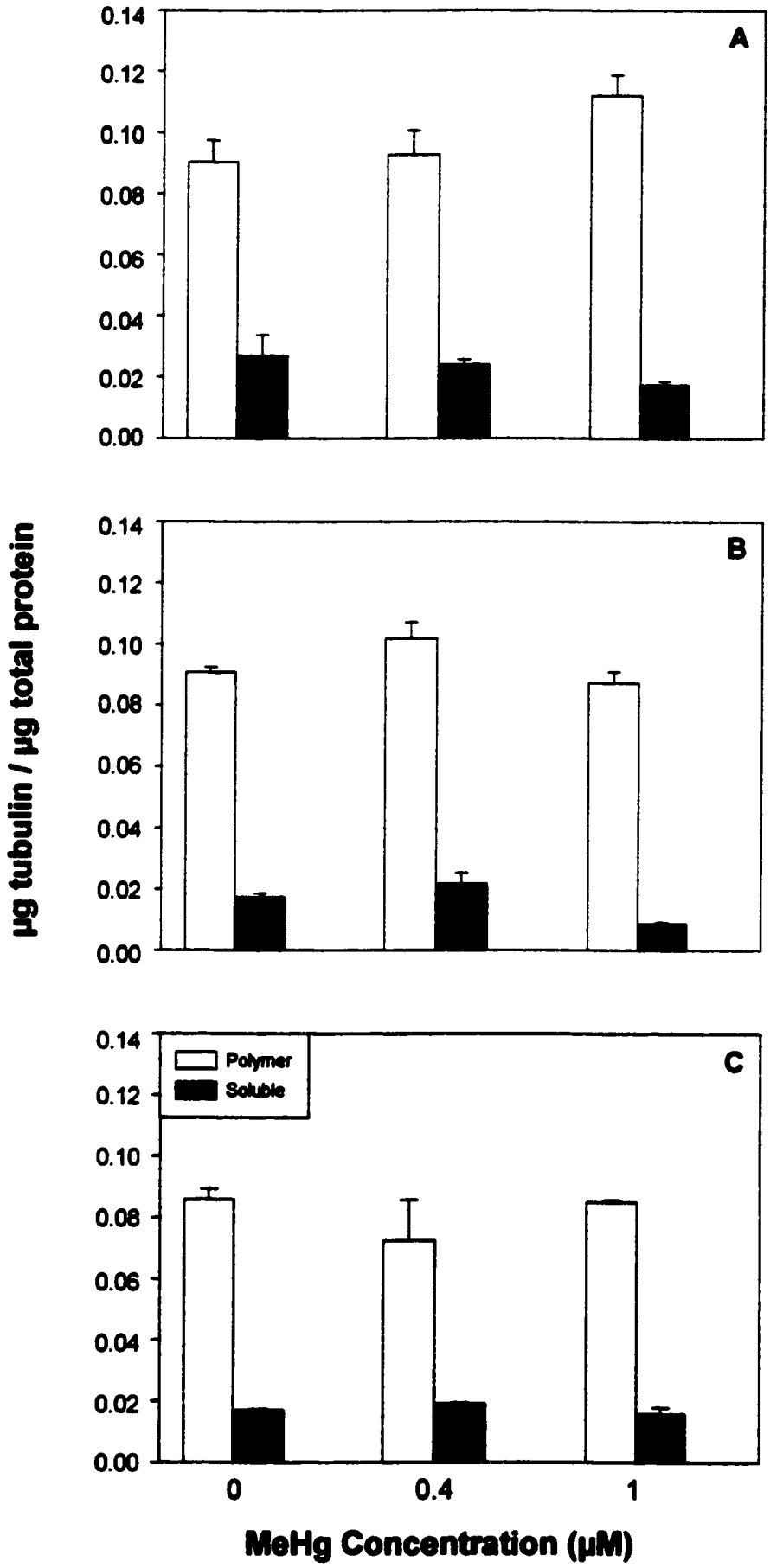
A
B
C
0.14
0.12
0.10
0.08
0.06
0.04
0.02
0.00
Polymer
Soluble
µg tubulin / µg total protein
0
0.4
1
MeHg Concentration (µM)

immunoblotting, did not change between the two fractions in untreated or MeHg-treated samples (Fig. 18).

C. 3. 3 *MAP2 is expressed in differentiated P19 cells*

At day 6 of P19 neuronal differentiation, MAP2 is expressed and can be detected immunochemically. SDS-PAGE and MAP2 immunoblotting of polymer and soluble protein extracts, taken from untreated and MeHg-treated neuronal P19 cells, showed that the HMW (280 kDa) and the LMW (75-70 kDa) forms of MAP2 are expressed (Fig.19). It was also observed that there was no loss of MAP2 from the polymer fraction to the soluble fraction in untreated and MeHg-treated samples. This was confirmed by dot blotting which showed the relative levels of MAP2 between the two fractions in untreated and MeHg-treated cells remained the same following 12, 18 and 24 hr of exposure with 0.4 and 1μM MeHg (Fig.20).

Figure 18: Detection of tubulin in MeHg-treated, neuronally differentiated P19 cells. 2 μg of polymer and 5 μg of soluble protein extracts taken from untreated and 24 hr, 0.4 μM and 24 hr, 1 μM MeHg-treated samples separated by SDS-PAGE on 9% polyacrylamide gels. Tubulin was detected by western blotting using mAB DM1B. No difference was observed in the amount of polymer and soluble tubulin in MeHg-treated cells, compared to untreated cells. Molecular weight markers are in kDa.

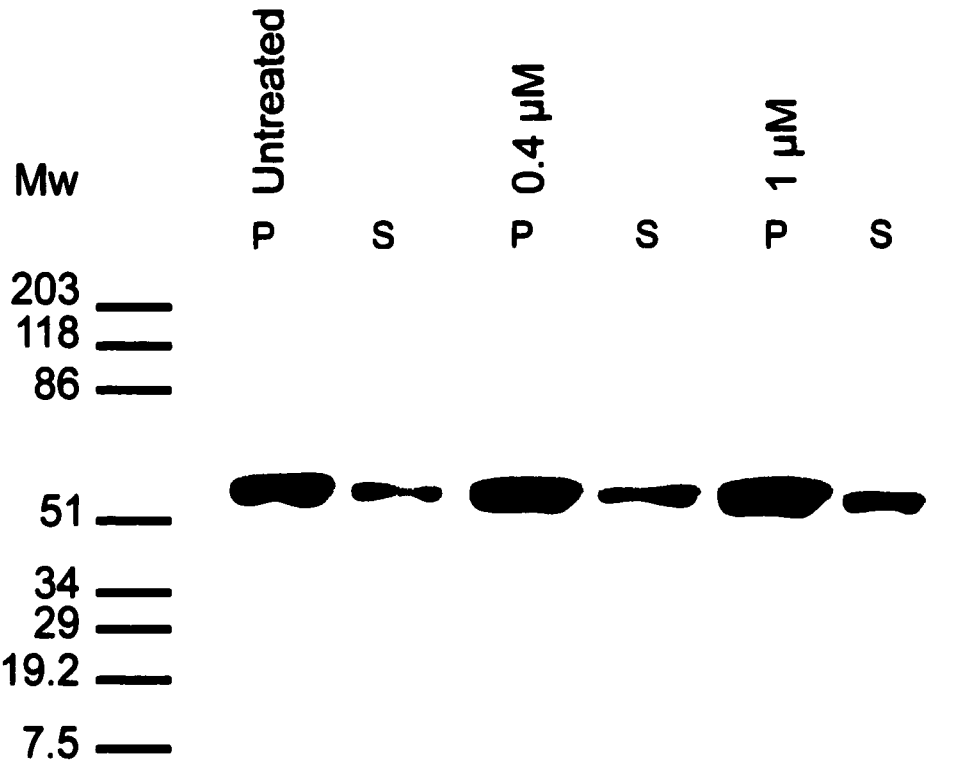
Mw
Untreated
0.4 µM
1 µM
P
S
P
S
P
S
203
118
86
51
34
29
19.2
7.5

Figure 19: Detection of MAP2 in MeHg-treated, neuronally differentiated P19 cells. 20 µg of polymer and soluble extracts were separated by SDS-PAGE on 9% polyacrylamide gels. MAP2 was detected by western blotting using mAb HM-2. No difference was observed in the amount of polymer and soluble MAP2 in cells treated with MeHg for 24 hr at 0.4 µM and 1µM, compared to untreated cells. Molecular weight markers are in kDa.

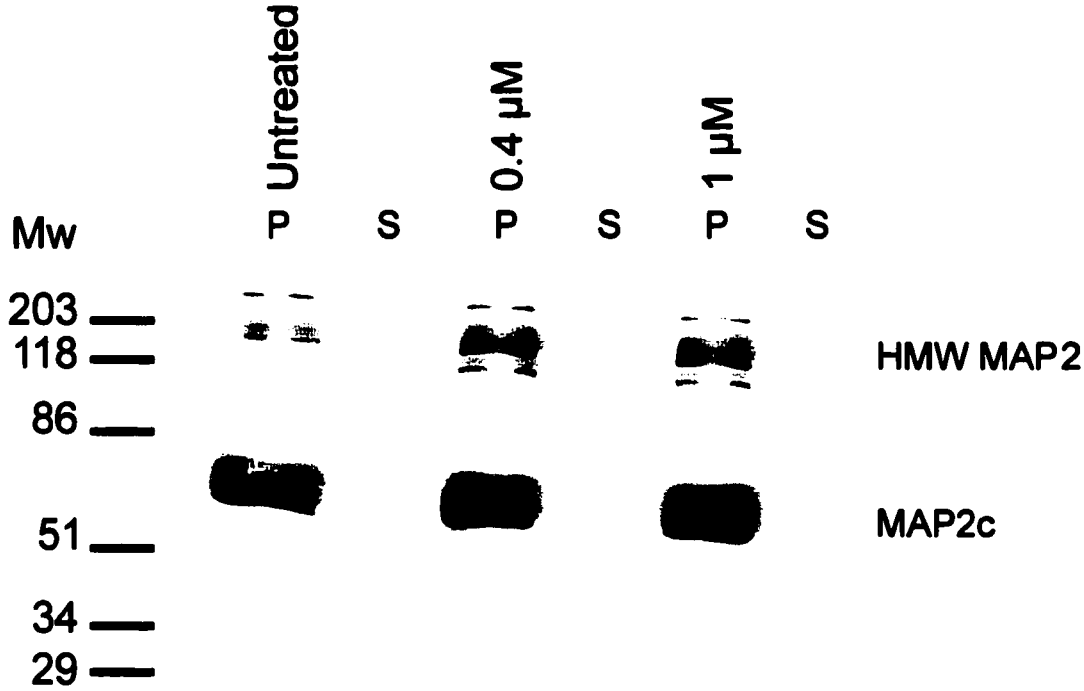
Untreated
0.4 µM
1 µM
Mw
P
S
P
S
P
S
203
118
86
51
34
29
HMW MAP2
MAP2c

Figure 20: Levels of polymer and soluble MAP2 in neuronally differentiating P19 cells, treated with MeHg. Relative levels of MAP2 per µg of total cellular protein in polymer and soluble fractions were determined by quantitative dot blotting with mAb HM-2. Extracts were taken from differentiated cells that were untreated and treated with 0.4 µM and 1µM MeHg for 12 hr **(a)** 18 hr **(b)** and 24 hr **(c)**. The data are the mean of three measurements taken from three separate experiments. Error bars represent the standard error from the mean.

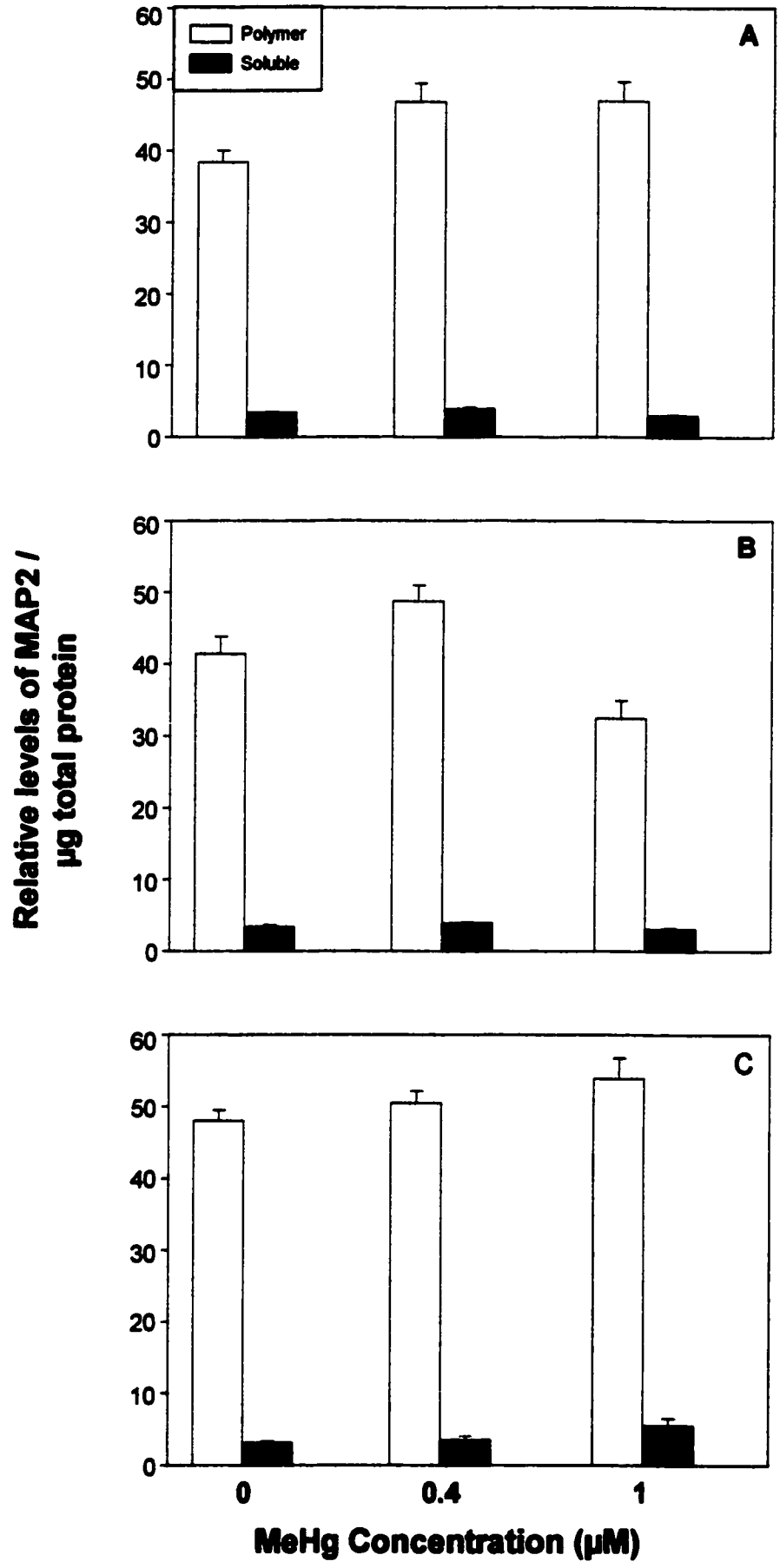
Polymer
Soluble
A
B
C
60
50
40
30
20
10
0
Relative levels of MAP2 / µg total protein
0
0.4
1
MeHg Concentration (µM)

D. DISCUSSION

The effects of MeHg on the Mt system have been well established in several cell types including primary cultures of lymphocytes, fibroblasts, glioma, neuroblastoma and P19 embryonal carcinoma cell lines (Prasad *et al.*, 1979; Sager *et al.*, 1983; Miura *et al.*, 1984; Brown *et al.*, 1988; Cadrin *et al.*, 1988; Wasteneys *et al.*, 1988; Sager *et al.*, 1988). These studies showed that the Mt component of the cell was primarily affected by MeHg and that this component was disassembled in a time- and dose- dependent manner. In this study the time- and dose- dependent effects of MeHg on Mt disassembly were examined using undifferentiated, MAP2c-transfected, and neuronally differentiated P19 cells. It was found that the interphase Mts in undifferentiated cells exhibited differential sensitivity to MeHg, compared to the Mts in both transfected and neuronally differentiated cells.

D. 1 Mt stabilizing effects of MAP2

Previous studies showed that when the HMW and juvenile MAP2 isoforms were expressed in non-neuronal cells, the stabilization and bundling of Mts occurred. As well as altering Mt organization, the expression of MAP2 stabilized Mts against depolymerizing drugs such as nocodazole (Lewis *et al.*, 1988; Takemura *et al.*, 1992). It has also been shown that the transient expression of HMW-MAP2 and MAP2c induces the formation of neuronal processes in non-neuronal cells (LeClerc *et al.*, 1996). As well, *in vitro* studies showed that the association of MAP2 with assembled

Mts results in their stabilization (reviewed by Matus, 1994). These data implicate MAP2 in a major Mt stabilizing role during neurogenesis.

In differentiating P19 cells MAP2c expression is the earliest of the Mt-stabilizing MAPs to be expressed. It can be detected by immunoblotting after 2 days of differentiation and by day 6, both the HMW and juvenile isoforms of MAP2 can be detected (Fig. 19). Although MAP 1b is expressed prior to MAP2c during neuronal differentiation, this MAP does not form stable Mt bundles which are resistant to Mt-depolymerizing agents (for review see Falconer *et al.*, 1994). For these reasons MAP2c was chosen in this study.

D.2 Response of undifferentiated, neuronally differentiated and MAP2c transfected cells to MeHg

In this study, it was shown that Mt populations in P19 neurons, differentiated to day 6, were resistant to the same MeHg treatments (Fig. 16) which caused severe Mt damage in undifferentiated cells (Figs. 8 and 9). Mt damage was not observed until the P19 neurons were subjected to high MeHg doses and/or 12 - 24 hr treatments. These observations are supported by previous studies which also showed that during neuronal differentiation of P19 cells the Mt system becomes more resistant to the depolymerizing effects of MeHg (Cadrin *et al.*, 1988; Wasteneys *et al.*, 1988; Graff and Reuhl, 1997).

Increases in Mt stability against other depolymerizing agents such as colchicine are observed during P19 differentiation (Falconer *et al.*, 1989, 1992). Concomitant

with this increase in stability is a change in the expression of tubulin isotypes, and the appearance of MAPs and of posttranslationally modified tubulin which are not present in undifferentiated P19 cells (Falconer *et al.*, 1992, 1994; Laferrière and Brown, 1996). Therefore, the increases in MeHg resistance in neuronal Mts may be as a result of several developmentally regulated neuronal proteins interacting with one another to establish a stable Mt population.

In this study it was shown that transient MAP2c expression in undifferentiated P19 cells resulted in the bundling of Mts, similar to that seen in other studies, and that these MAP-Mts withstood MeHg treatments which caused either severe damage or complete Mt disassembly in untransfected cells. These results, and the observation that MAP2c is the earliest of the Mt-stabilizing MAPs to be expressed in differentiating P19 cells, indicate that MAP2 plays a major role in the development of Mt-resistance to MeHg during early neuronal differentiation. In early brain development, the period before the appearance of MAP2c may be the temporal window in which differentiating neurons are particularly vulnerable to MeHg toxicity.

D. 3 MeHg treatments affects tubulin extractability

The extent of Mt disassembly between undifferentiated, transfected, and neuronally differentiated cells was qualitatively compared by microscopy and it was shown that there was differential sensitivity to MeHg-induced Mt disassembly among these cell types. As well, it was observed in undifferentiated cells that MeHg treatments which resulted in complete Mt disassembly also resulted in the appearance of

diffuse cytoplasmic labelling. This diffuse labelling indicates that tubulin is present in a non-extractable form which remains in the cytoplasm following MeHg treatments. The diffuse cytoplasmic labelling was observed with the anti-tubulin antibodies 5A6 and DM1A (data not shown) but not with YOL1/34. This indicates that these antibodies recognize different epitopes on α-tubulin and that the epitope for YOL1/34 is no longer recognized following MeHg treatments.

A better understanding of the diffuse labelling observed by microscopy was achieved through quantitative dot blotting experiments. With these experiments it was expected that the effects of MeHg would be similar to that of colchicine. Following colchicine treatments, when the amount of tubulin is compared between polymer and soluble fractions, the amount of polymer tubulin decreases with a concomitant increase in the soluble fraction (Falconer *et al.*, 1994). The extraction of these tubulin fractions involves Triton X-100 which has been shown to extract both soluble tubulin and MAPs following colchicine disassembly (Falconer *et al.*, 1994; Laferrière and Brown, 1996). However, following MeHg treatments there was no change in the amount of tubulin between the polymer and soluble fractions compared to untreated cells (Figs. 10, 15 and 17). The extractable fraction of soluble tubulin, equal in amount to that in untreated cells, indicates that MeHg may be depolymerizing Mts into oligomers of tubulin and MAPs that are not extractable by Triton X-100.

One way in which MeHg alters the structure of soluble tubulin was observed from *in vitro* experiments. It was shown by electron microscopy that in the presence of high MeHg concentrations large aggregates of tubulin formed from porcine brain

extracts, rather than assembled Mts (Imura *et al.*, 1990; Keates and Yott, 1983; Sager *et al.*, 1983; Miura *et al.*, 1984). If large tubulin aggregates formed *in vivo* from the soluble tubulin pool as a result of MeHg treatment a Triton X-100 soluble fraction would not be detected, as in this study. Therefore, MeHg may specifically be affecting the way in which polymer Mt proteins are disassembled and extracted from the cell. Tubulin disassembly from polymerized Mts are altered in the presence vinblastine. *In vivo* studies showed that when pre-formed Mts were treated with doses of vinblastine > 2-4 μM peeling of protofilament arrays occurred from both ends of the Mt (Wilson, 1986). Although MeHg has not been shown to induce these effects *in vivo* or *in vitro* it is possible that it may behave similarly to vinblastine by affecting the way in which polymer Mts are disassembled. Therefore, MeHg treatments in undifferentiated, MAP2c-transfected, and differentiated cells may cause the disassembly of Mts into fragments which are too large to extract by the methods used in this study.

Since it was observed that MeHg affects tubulin extraction by Triton X-100 the extractability of other proteins was examined following MeHg treatments. When MAP2 was extracted from P19 neurons and examined by quantitative dot blotting there was no observed change in the amount of MAP2 between the polymer and soluble fractions of untreated and MeHg-treated cells, as observed with tubulin. The effect of MeHg treatments on non-Mt proteins was examined in undifferentiated cells which were transfected with the expression vector for Green Fluorescent Protein (GFP). GFP is expressed in the cell as a soluble protein. Following MeHg treatment it was observed by fluorescence microscopy that GFP was extractable by Triton X-100 (data

not shown) unlike tubulin and MAP2. Therefore, MeHg affects both the extractability of Mt-proteins from the cell and the way in which polymer Mt and their associated proteins are disassembled. Further experiments testing the effects of MeHg on the extractability of other Mt and non-Mt proteins need to be performed in order to confirm that these effects are specific to Mt proteins.

Chapter II

A. INTRODUCTION

A. 1 Overview of Apoptosis

Apoptosis is a process of cell death with characteristic morphological and biochemical features distinguishable from those associated with necrosis, or accidental death (Kerr *et al.*, 1972). During apoptosis cells shrink, chromatin condenses and DNA is cleaved into oligonucleosomal sized fragments. Also characteristic of apoptotic cells is blebbing of the plasma membrane followed by compartmentalization of the cytoplasm and nucleus into membrane bound "apoptotic bodies" (reviewed by Johnson *et al.*, 1995).

The apoptotic process occurs in two physiological stages. The first stage, known as the condemned phase, varies in length depending on both the apoptotic stimulus and the cell type (Earnshaw, 1995). This phase occurs immediately after the initiation of apoptosis and is the period of time in which there is no morphological evidence for apoptosis (Earnshaw, 1995). The second stage, called the execution phase, is a rapid process and begins with the first sign of apoptosis. This involves the degradation of nuclear DNA, producing a hyperchromatic nucleus typical of apoptosis (Wyllie *et al.*, 1980). Also during the execution phase cytoplasmic condensation and the formation of blebs on the cell surface become apparent (Earnshaw, 1995). The cell may then become fragmented into a number of smaller apoptotic bodies which may contain portions of the fragmented nucleus and an array of intact organelles such as the mitochondria and lysosomes (Kerr *et al.*, 1972; Wyllie *et al.*, 1980). In the final

stages of apoptosis, the apoptotic bodies are phagocytized either by neighboring cells or macrophages and are subsequently degraded without release of cellular contents into the intercellular space.

Unlike apoptosis, necrosis usually occurs as a result of massive tissue damage (Earnshaw, 1995). This type of cell death is not biochemically regulated and involves the swelling and rupture of the cell membrane (Wyllie *et al.*, 1980; Earnshaw, 1995). Apoptosis and necrosis also differ in that apoptosis does not elicit an inflammatory immune response *in vivo* (Earnshaw, 1995).

A. 2 Biochemical Features of Apoptosis

The original biochemical hallmark of apoptosis was the production of oligonucleosomal fragments of DNA, multiples of 200 bp in size (Wyllie, 1980). It was suggested that this type of DNA degradation was produced by a Ca^{2+}/Mg^{2+}-dependent endonuclease (Wyllie, 1980; Peitsch *et al.*, 1993). This endonuclease, when activated by increases in intracellular Ca^{2+}, cleaved DNA primarily in the internucleosomal "linker region" (Wyllie, 1980; Peitsch *et al.*, 1993). However, it was observed that the extent to which DNA was degraded during apoptosis varied greatly among cell types. For example, some cell types, such as the breast cancer MCF-7 cell line, presented apoptotic morphological features even though oligonucleosomal DNA ladders could not be detected on agarose gels (Oberhammer *et al.*, 1993). The introduction of pulsed field gel electrophoresis (PFGE) demonstrated that certain cell types only produce HMW fragments 50-300 kb in size, whereas cells such as

lymphocytes and liver cells, are able to degrade their DNA extensively to produce 200 bp fragments (Walker *et al.*, 1995).

In cell types which do degrade DNA to the 200 bp level, 50-300 kb DNA fragments are formed first, before subsequent cleavage (Filipski *et al.*, 1990, Roy *et al.*, 1992; Oberhammer *et al.*, 1993a; Weaver *et al.*, 1993; Walker *et al.*, 1994). The HMW DNA fragment sizes relate to higher order structures of chromatin into which DNA is folded in the nuclei. It is also suspected that the production of HMW DNA fragmentation and internucleosomal DNA fragmentation may result from different nuclease activities. In apoptotic thymocytes internucleosomal DNA fragmentation requires Ca^{2+} and Mg^{2+} ions and can be inhibited by serine protease inhibitors and Zn^{2+} (Weaver *et al.*, 1993; Cohen *et al.*, 1994; Sun and Cohen, 1994: Walker *et al.*, 1994). However, the production of HMW DNA fragments requires primarily Mg^{2+}, and is not inhibited by serine protease inhibitors or Zn^{2+} (Filipski *et al.*, 1990; Weaver *et al.*, 1993; Cohen *et al.*, 1994; Walker *et al.*, 1994).

Arends *et al.* (1990) examined the relationship between endonuclease cleavage at internucleosomal sites and the morphological changes in chromatin during apoptosis and suggested that chromatin condensation and collapse was dependent on the generation of DNA fragments 200 bp in size. However, PFGE studies combined with microscopy showed that the presence of HMW DNA cleavage is sufficient to allow chromatin collapse and occurs even though the 200 bp DNA ladder is not present (Filipski *et al.*, 1990). HMW DNA fragments are now recognized as one of the earliest markers of apoptosis (reviewed by Walker and Sikorska, 1997).

A. 3 Regulators of Apoptosis

The first indication that specific genes may be involved in the induction of apoptosis came from studies using the soil nematode, *Caenorhabditis elegans* (reviewed by Osborne and Schwartz, 1994; Rao and White, 1997). It was observed that during embryonic development 131 somatic cells out of a total of 1090 die. A genetic map of this species identified 14 genes which are involved in cell death. These genes were referred to as cell death abnormal, or *ced* genes. It was found that two of these genes *ced-3* and *ced-4* are required for all 131 cells to die and if both of these genes were mutated, cell death would not occur. Another gene, *ced-9,* was shown to prevent cell death but if mutated, became lethal. Both the *ced-3* and *ced-9* genes show significant sequence homology to genes found in mammals (Rao and White, 1997).

A. 3. 1 *Caspases*

Interleukin-1β-converting enzyme (ICE) was identified as the first mammalian homologue of *ced-3*. It has been shown that when *ced-3* or ICE are overexpressed in cells, apoptosis is induced (reviewed by Nicholson and Thornberry, 1997; Tan and Wang, 1998). ICE is a cysteine protease which belongs to a family of caspases (reviewed by Wyllie, 1997). Caspases are synthesized as precursor forms and are activated by proteolytic cleavage induced by an apoptotic signal. This proteolytic cleavage, therefore, converts the precursors into mature functional forms (reviewed by Nicholson and Thornberry, 1997).

A variety of cellular proteins, including actin and nuclear lamins, have been identified as substrates of ICE-like caspases, or caspase 1 (reviewed by Wyllie, 1997). Other cysteine proteases such as CPP32, apopain and YAMA, which are homologous to ICE and belong to the caspase 3 family, have also been implicated in apoptosis (reviewed by Nicholson and Thornberry, 1997). The proteolysis of substrates by caspases is thought to be responsible for the morphological changes that occur during apoptosis (reviewed by Nicholson and Thornberry, 1997; Tan and Wang, 1998; Enari *et al.*, 1998).

A. 3. 2 *Bcl-2*

Bcl-2 was identified as a mammalian homologue to the anti-death gene *ced-9* and was first identified in follicular lymphoma cells (reviewed by Nuñez and Clarke, 1994; Rao and White, 1997). Several other evolutionarily conserved genes have been identified which share sequence homology with bcl-2 and constitute a family of at least 15 proteins. This family of proteins falls into two categories; inhibitors of apoptosis and accelerators of apoptosis (reviewed by Rao and White, 1997). Bcl-x_L is a bcl-2 homologue, and both are anti-apoptotic in action. Bax, also a member of the bcl-2 family, was characterized as a bcl-2 binding protein which induces apoptosis. The family of bcl-2 proteins is associated with the outer mitochondrial membrane, nuclear envelope and endoplasmic reticulum (Jacobson *et al.*, 1993).

The basis for the survival-promoting function of bcl-2 is unclear. It has been suggested that bcl-2 may contribute to oncogenesis by suppressing signals that would

typically induce apoptotic cell death (reviewed by Nuñez and Clarke, 1994; Rao and White, 1997). For example, some studies have suggested that bcl-2 inhibits apoptosis by indirectly interfering with the activation of caspases. Caspases can be activated from the mitochondrial release of cytochrome c following an apoptosis-inducing stimulus. Bcl-2 may interfere with the activation of caspases by binding to cytochrome c and preventing its release (Kluck *et al.*,1997; Yang *et al.*,1997; Rossé *et al.*, 1998) .

The pro-apoptotic homologue of bcl-2, Bax, also localized to the mitochondria, may promote apoptosis by inducing the release of cytochrome c, thereby activating caspases (Rossé *et al.*, 1998). Therefore, protein-protein interactions as well as a balance in the levels of intracellular bcl-2 and Bax may influence whether the cell lives or dies.

A. 3. 3 *p53*

p53 is a tumour suppressor gene which has been implicated in promoting apoptosis. In non-cancerous cells p53 becomes activated in response to stress signals such as DNA-damage, hypoxia, or exposure to chemotherapeutic drugs. Depending on the cell type, upregulation of p53 activates a cascade of genes resulting in cell cycle arrest or apoptosis (Debernardis *et al.*, 1997). For example, if DNA damage is induced in a cell, p53 monitors cell ploidy and prevents cells that have undergone an aberrant mitosis from passing through G1 phase into S phase (reviewed by Rudner and Murray, 1996). The involvement of p53 in monitoring cell ploidy was observed in studies which compared the effects of mitotic spindle disrupting drugs in mammalian

cells carrying a wild type or a mutant p53 gene. When cells carrying the wild type gene were treated with colchicine or nocodazole, spindle damage occurred, cell division was aborted and apoptosis was eventually induced. However, cells carrying a mutant p53 gene increased in ploidy following treatment with these same drugs. Therefore, under conditions which may lead to an aberrant mitosis, p53 appears to be involved in cell cycle checkpoints and the triggering of apoptosis (reviewed by Rudner and Murray, 1996).

A. 4 Apoptosis Initiated by Cytoskeletal Damage

There are many initiators which trigger the terminal effector pathway of apoptosis. Cytoskeletal damage as an initiator of apoptosis is of interest due to the involvement of this cytoplasmic network in some cellular functions as mitosis, cell signalling, and motility. If the cytoskeleton is damaged these processes, which are essential for cell survival, are compromised. There are several studies which emphasize the role of bcl-2 modifications and the production of reactive oxygen species in apoptosis induced by cytoskeletal damage (Haladar *et al.*, 1994; Haladar *et al.*, 1995; Jordan and Wilson, 1996; Blagosklonny *et al.*, 1997; Srivastava *et al.*, 1998).

A. 4. 1 *Microtubule Damage Induces Apoptosis*

A large number of chemically diverse compounds bind specifically to Mts. Colchicine, nocodazole and the vinca alkaloids, including vincristine and vinblastine, are a group of Mt-binding compounds which prevent Mt assembly and block

progression through the cell cycle (Sager and Syversen, 1986). These drugs may induce apoptosis by destroying the mitotic spindle (reviewed by Jordan and Wilson, 1998). Another Mt-binding drug, taxol, stabilizes Mts and prevents their depolymerization. This results in G_2-M arrest, Mt-bundling, and eventually cell death (Long and Fairchild, 1994; Trielli *et al.*, 1996; Banerjee *et al.*, 1997).

It has been suggested that G_2-M arrest induced by Mt-targetting agents may activate phosphoregulatory pathways which are involved in cell cycle control and the induction of apoptosis (Wang *et al.*, 1998). For example, the stress-activated protein kinases (SAPKs) such as c-Jun N-terminal kinases (JNK), which are involved in signal transduction pathways, have been implicated in the regulation of both the cell cycle and apoptosis (Cuvillier *et al.*, 1996; Karin *et al.*, 1997). Wang *et al.* (1998) showed that in a variety of human cells treated with taxol, vinblastine, vincristine, nocodazole, and colchicine, JNK/SAPK was activated through multiple signal transduction pathways. These signal transduction pathway involved both Ras, an oncogene which regulates adenylate kinase, and apoptosis signal-regulating kinase (ASK1) which were involved in the regulation of apoptosis as a result of Mt damage (Wang *et al.*, 1998).

The mechanism by which apoptosis is induced following Mt damage is not entirely clear. However, there is evidence which suggests, that in some cancer cell lines, apoptosis induced by Mt-targetting agents may involve the apoptotic regulator bcl-2 (Haladar *et al.*, 1994;1995; Jordan and Wilson, 1996; Blagosklonny *et al.*, 1997; Srivastava *et al.*, 1998). When human leukemia, breast cancer, and prostate cancer cells were exposed to taxol, a phosphorylated form of bcl-2 was expressed.

Phosphorylation reversed the antiapoptotic function of bcl-2 and these cells became apoptotic (Haladar *et al.*, 1994; Srivastava *et al.*, 1998). Srivastava *et al.* (1998) also showed that treatment of these cancer cells with taxol, vincristine, or vinblastine activated caspase 3. Caspase 3 activation by these drugs resulted in the degradation of poly (ADP ribose) polymerase, an enzyme involved in chromatin reorganization following DNA damage, which is one of the first proteins to be cleaved following an apoptotic stimulus. Together these data suggest that Mt-damage induced by these Mt-targetting drugs leads to apoptosis (Haladar *et al.*, 1994; Wang *et al.*, 1998; Srivastava *et al.*, 1998).

A. 5 Rationale for Experiments

As outlined in Chapter 1, MeHg is a toxicant which interacts with the Mt component of the cytoskeleton. The damaging effects of MeHg on interphase and neuronal Mts as well the induction of mitotic arrest have been determined. It has also been established that interphase Mts, Mts in the mitotic spindle, and neuronal Mts exhibit differential sensitivity to the Mt-depolymerizing effects of MeHg (Wasteneys *et al.*, 1988; Cadrin *et al.*, 1988).

In this review, the effects of other Mt-targetting drugs such as taxol, colchicine, and the vinca alkaloids on the Mt system were described. These drugs lead to the loss of Mt integrity, which results in cell cycle arrest and the induction of apoptosis. It is possible that Mt-damage, as a result of MeHg treatment, may also induce apoptosis. This section of my thesis uses the P19 EC line as an experimental model to address the

question of whether or not **MeHg induces apoptosis in undifferentiated and neuronally differentiated P19 cells.**

B. MATERIALS AND METHODS

For apoptosis assays undifferentiated P19 cells were plated on 100 mm and 60 mm dishes at cell densities of 5 x 10^5 and 2.5 x 10^5 cells/ml, respectively. For neuronally differentiated P19 cells, 100 mm dishes were plated at 2.8 x 10^5 cells/ml, and induced to differentiate as described in Chapter 1 section B.2. MeHg was added 24 hr after plating undifferentiated cells, or 6 days after plating differentiated cells. MeHg treatments ranged from 0.4 - 4 µM for 4 - 24 hr. Following the MeHg treatment, supernatant from the culture dishes was collected in a 15 ml conical tube (VWR). This was to ensure that the floating population of cells, which were likely apoptotic, were not lost and could be pooled with the adherent cell population. The cells were rinsed in PBS and the rinse was pooled with the supernatant. Trypsin (0.025% (w/v) trypsin, 1mM EDTA in PBS) was added to the cells in the dish for 3 min. The trypsinized fraction was then pooled with the supernatant and PBS. The cell suspension was centrifuged at 1100 rpm for 7 min. The supernatant was discarded and the cell pellet was resuspended in 5 ml PBS.

B. 1 Single Cell Gel Electrophoresis (Comet Assay)

Alkali comet assays were performed as described by Olive *et al.* (1993). 100 µl of cell suspension was embedded in 1.1% low melt agar (Gibco BRL) on a frosted glass microscope slide. The cells were then lysed in lysis buffer, pH 10 [1% *N*-lauryl-sarcosine (Sigma), 2.5 M NaCl, 100 mM EDTA, 10 mM Tris, pH 7.4 (BDH)] for 45 min. Next, the cells were incubated in alkaline electrophoresis buffer [300 mM NaOH, 1mM EDTA,

pH 13] for 15 min to allow for DNA unwinding. Cells were then electrophoresed in alkaline electrophoresis buffer at a constant current of 0.3 A for 10 min. Comets were stained with 1mM YoYo (a DNA specific dye) (Molecular Probes) diluted 1:100 in working solution [1:1 glycerol (BDH) and 400 mM EDTA, pH 7.4 and 0.1% 8-hydroxyquinoline (VWR)]. Apoptotic cells were detected visually and scored using a Zeiss Axiophot epifluorescence microscope equipped with a 50 W mercury arc lamp. Between 600 - 1100 individual cells were analysed for each sample. All cell counts were repeated on samples taken from four separate experiments. Images were captured using a Zeiss Universal epifluorescence microscope equipped with a 50 W mercury burner and a Hamamatsu CCD camera using Metamorph v2.75 (Universal Imaging). TIFF images were processed using Adobe Photoshop v4.0.

B. 2 ***In Situ*** **Fluorescent Labelling of DNA breaks (TUNEL assay)**

For each treatment, a cell suspension, prepared as above, was applied to poly-L-lysine coated coverslips, then fixed and permeabilized as described by Chaly *et al.* (1984). To coat the coverslips, poly-L-lysine solution [1 mg/ml (Sigma) in ddH_2O] was applied and allowed to stand for 5 min. Coverslips were then rinsed 5 times by dipping rapidly in ddH_20 and allowed to air dry before use. 500 µl of cell suspension was applied to the coverslip, allowed to stand 5 min, rinsed briefly in PBS, fixed for 5 min in 3% paraformaldehyde, rinsed twice in PBS, then permeabilized for 20 min in 0.2% Triton X-100 in PBS. Following permeabilization, DNA breaks were detected using the method of Terminal deoxynucleotidyl transferase-mediated dUTP-biotin Nick End Labelling (TUNEL)

(Gavrieli *et al.*, 1992). Samples were incubated at 37°C for 1 hr in 300 U/ml of terminal deoxynucleotidyl transferase (TDT) in TDT buffer [30 mM Tris base, 140 mM sodium cacodylate, 1 mM cobalt chloride] (Gibco BRL), containing 10 µM biotin-16-dUTP (Boehringer Mannheim). Samples were then transferred to TB buffer (300 mM NaCl, 30 mM sodium citrate) to terminate the reaction. After 3 x 4 min rinses in PBS, samples were blocked for 10 min in 2% BSA (Sigma) in PBS to block non-specific labelling, then rinsed again 3 x 4 min. The samples were incubated with streptavidin-FITC (Vector) diluted 1:200 for 30 min, rinsed 3 x 4 min in PBS, then counterstained for 1 min in 1 µg/ml of Hoescht 33258 in PBS. All samples were mounted in 50% glycerol-PBS, pH 7.8 containing 1% (w/v) para-phenylene-diamine and viewed using a Zeiss Universal epifluorescence microscope equipped with a 50 W mercury burner and a Hamamatsu CCD camera using Metamorph v2.75 (Universal Imaging). TIFF images were processed using Adobe Photoshop v4.0. Cell counts were repeated on samples taken from three separate experiments and approximately 400 cells were counter per sample.

B. 3 Agarose Gel Electrophoresis

Cell pellets from undifferentiated and neuronally differentiated P19 cells were collected as described above. The DNA was extracted from the cell pellets by the method of Ray *et al.* (1994). The cell pellet was washed 2 X with PBS and then resuspended in 50 µl lysis buffer [200 mM NaCl, 10 mM Tris-HCl (pH 8.0), 40 mM EDTA, 0.5% SDS, 400 ng RNaseI/µl (SIGMA)], transferred to an eppendorf tube and incubated for 1 hr at 37°C.

400 µl of digestion buffer [200 mM NaCl, 10 mM Tris-Hcl (pH 8.0), 0.5% SDS and 125 ng Proteinase K /µl (SIGMA)] was then added to the cell lysate and mixed by inversion before incubating at 50°C for 3 hr. An equal volume of phenol was added to the contents of the tube and mixed by inversion. The contents were then centrifuged in a microfuge at 14 000 rpm for 3 min to extract the upper aqueous phase. The aqueous phase was then transferred to a fresh eppendorf tube and an equal volume of phenol:chloroform (1:1 (v/v)) was added and the extraction was repeated. The upper aqueous phase was again removed and placed in a fresh tube. A final extraction was performed using an equal volume of chloroform. The DNA was then precipitated by the addition of 2 volumes of 100 % ice-cold ethanol and allowed to sit overnight at -20°C. The next day the DNA pellet was collected by centrifugation in a microfuge at 14 000 rpm for 5 min. The DNA pellet was washed twice in 70% ethanol and allowed to air dry. The pellet was then resuspended in a small volume of TE buffer [10 mM Tris-HCl, 1 mM EDTA] and the DNA concentration was determined using a Genequant® spectrophotometer (Pharmacia). 10 µg of DNA from each sample was loaded per lane into a 1.2% agarose gel made in TAE buffer [4 mM Tris-HCl, 40 mM sodium acetate and mM EDTA, pH 8.3]. The samples were electrophoresed for 2 hr at 50 V. The gel was then stained with ethidium bromide (0.5 µg/ml in TAE buffer) for 15 min, destained in several changes of TAE buffer for 2 hr and photographed under UV light using polaroid film 55. The negative was scanned using a Hewlett-Packard 4c flatbed scanner. Digitized images were processed using Adobe Photoshop v4.0.

B. 4 Pulsed Field Gel Electrophoresis

Undifferentiated and neuronally differentiated cells were collected as described above. The cell pellet was washed once with Nuclear Buffer (NB) [1.5 mM Tris-HCl, pH 7.4 , 60 mM KCl, 15 mM NaCl, 1 mM EGTA, 2 mM EDTA, 0.5 mM Spermidine, 0.15 mM Spermine (all from SIGMA)]. The pellet was then resuspended in 40 µl NB buffer and transferred to eppendorf tubes containing 40 µl of 1.5 % low melting point agarose made in NB buffer and 2 µl Proteinase K from a 20 mg/ml stock in ddH_20. The agarose/cell mixture was pipetted into the wells of a BIORAD casting mold and allowed to set for 10 min at 4°C. The plugs were ejected into eppendorf tubes containing TEEN buffer [10 mM Tris-HCl, pH 9.5, 25 mM EDTA, 5 mM EGTA, 10 mM NaCl], 2% (v/v) SDS and 10 µg of Proteinase K (SIGMA). The cell plugs were incubated for 1.5 hr, on a rotator, at 37°C. The plugs were then removed and washed in an eppendorf containing TE buffer [10 mM Tris-HCl, 1 mM EDTA] for 30 min at 4°C. The plugs were then loaded into a 0.8% agarose gel (GIBCO) prepared in TBE buffer [0.089 M Tris-HCl, 0.089 M boric acid, 1 mM EDTA]. The wells were sealed with 1.5% (w/v) LMP agarose and the gel was placed in a gelbox containing 0.5 X TBE buffer. PFGE was carried out using a Q-Life Autobase Electrophoresis System (Kingston, On.) as described by Weaver *et al.* (1993). The total electrophoresis run was 20.5 hr, alternating between a forward voltage of 280V for 35 sec and a reverse voltage of 90 V for 60 sec with an inversion time of 0.3 sec and 0.5 sec, between the forward and reverse voltage. After the electrophoresis run the gel was stained with 15 µg/ml ethidium bromide in dH_2O for 30 min. The gel was destained

overnight in 1L water containing 2 mg/ml RNase A (SIGMA). The gel was photographed using a Ultra-lum system equipped with a CCD camera. Tiff images were processed using Adobe Photoshop v4.0.

C. RESULTS

C. 1 DNA fragmentation detected by the comet assay

In this study, all comet assays were performed under alkaline conditions. Fig. 21A shows two control cells which have a round nucleus and retain unfragmented DNA following electrophoresis. In MeHg-treated cells extensive DNA fragmentation indicative of apoptotic cleavage was observed. This is indicated by the presence of a comet which has formed after most of the fragmented DNA has electrophoresed from the residual nucleus (the comet head) to form the comet tail (Fig. 21B). The comet morphology of extracted nuclei from control undifferentiated and differentiated cells is the same in both control and MeHg-treated cells.

In undifferentiated P19 cells treated with 1 μM MeHg for 8 hr or 12 hr approximately 60% of all cells scored exhibited apoptotic comet morphology (Fig. 22). The percentage of apoptotic cells increased to 80% following an 8hr, 4 μM MeHg treatment, (Fig. 22A) and a further increase to 98.5% was observed after a 12hr, 4 μM treatment (Fig. 22 B). Less than 2% of the cells in the control samples were apoptotic.

In neuronally differentiated P19 cells treated with 4 μM MeHg for 12 hr there was very little change in the number of apoptotic cells (Fig. 23 A). After a 24 hr treatment approximately 25% of the cells were apoptotic (Fig. 23 B). Less than 5% of the cells in the control samples were apoptotic.

Figure 21: Micrograph representing undifferentiated and neuronally differentiated P19 cells prepared by the alkali comet assay. Control cells have a round nucleus which retains the unfragmented DNA (**A**). In undifferentiated cells treated with 4 μM MeHg for 12 hr, or 24 hr for differentiated cells, most of the fragmented DNA has electrophoresed away from the residual nucleus (the comet head) to form the comet tail (**B**). Bar = 10 μm.

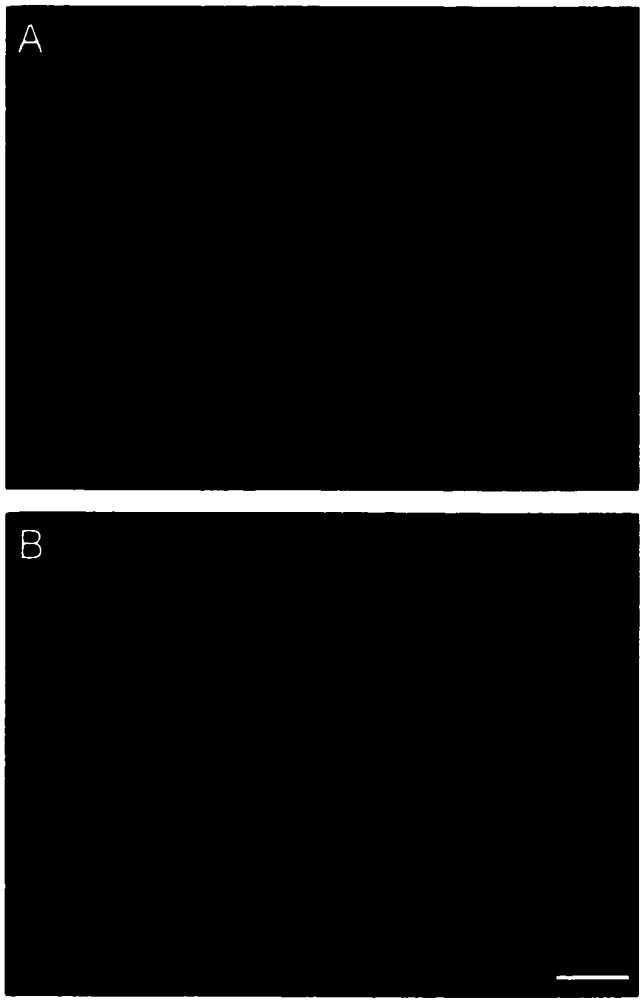
A
B

Figure 22: Histogram showing the percentage of apoptotic cells detected by the comet assay in undifferentiated control P19 cells and in cells treated with 1 μM and 4 μM MeHg for 8 hr (**A**) and 12 hr (**B**). A minimum of 900 cells were scored in each sample. The data for the 8 hr treatment are from one trial. The data for the 12 hr treatment are the means of three separate experiments. Error bars show the standard deviation from the mean.

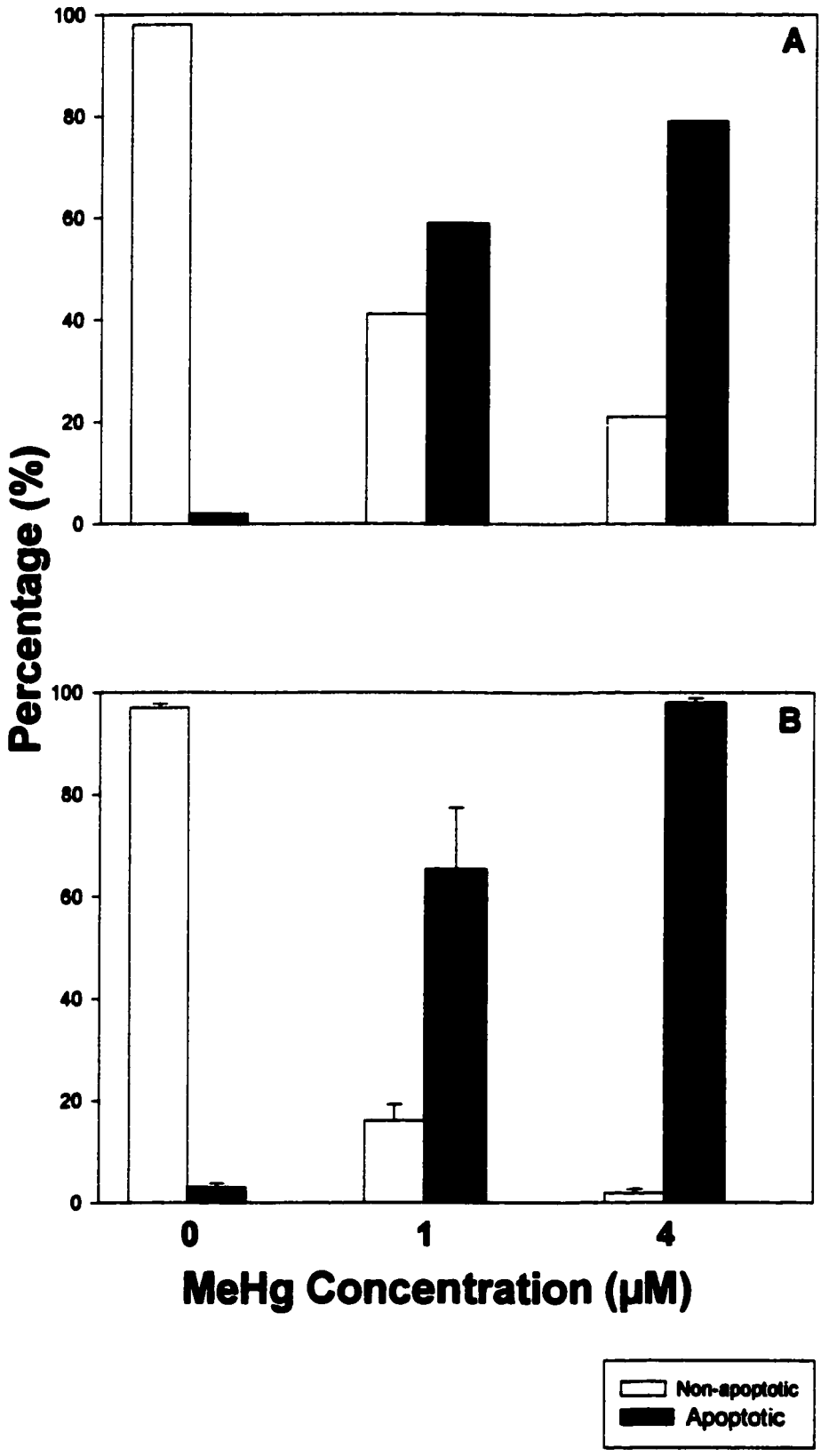
A
B
100
80
60
40
20
0
Percentage (%)
0
1
4
MeHg Concentration (μM)
Non-apoptotic
Apoptotic

Figure 23: Histogram showing the percentage of apoptotic cells detected by the comet assay in neuronally differentiated control cells and in cells treated with 4 μM MeHg for 12 hr **(A)** and 24 hr **(B)**. A minimum of 900 cells were scored in each sample. The data are the means of three separate experiments. Error bars show the standard deviation from the mean.

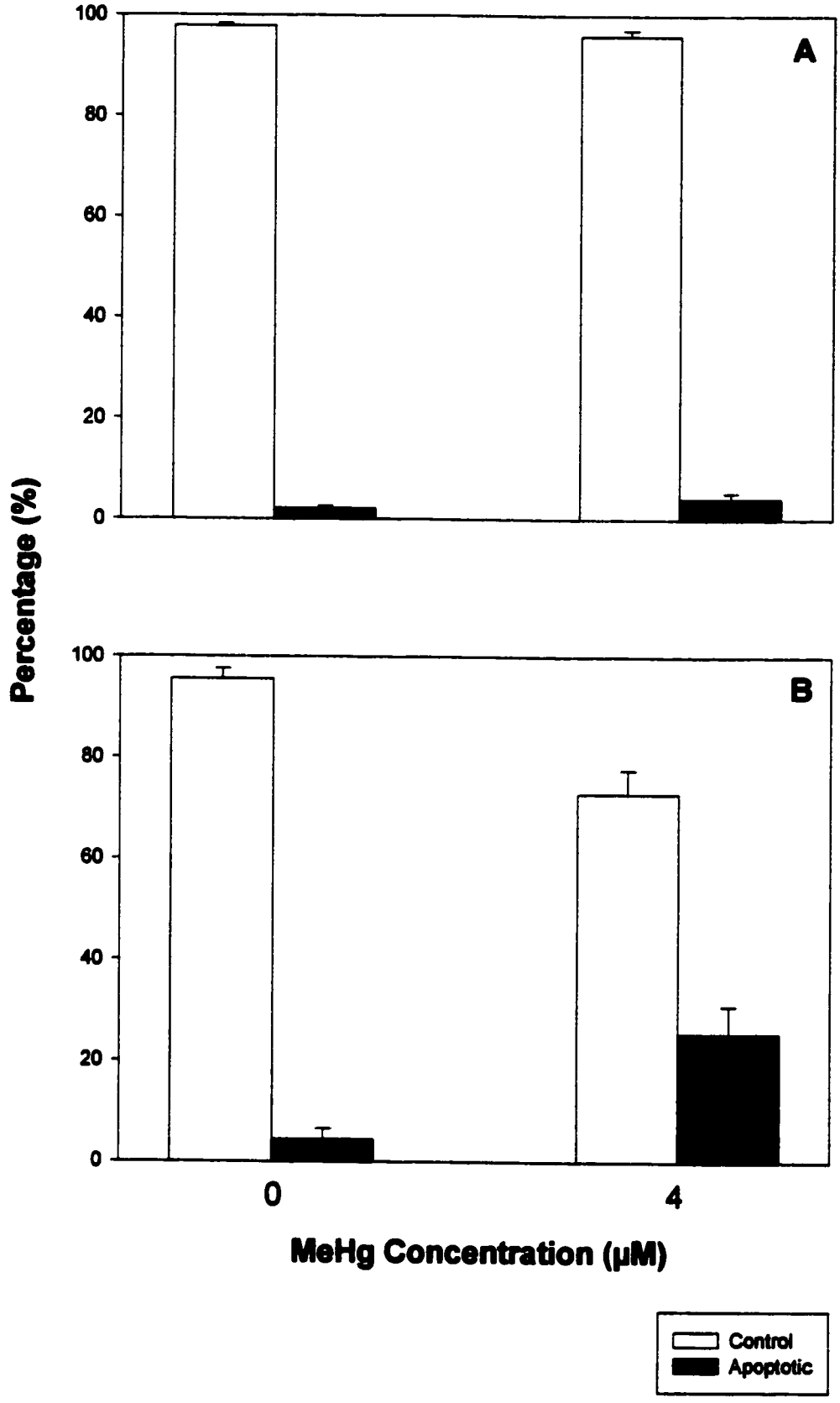
A
B
100
80
60
40
20
0
Percentage (%)
0
4
MeHg Concentration (μM)
Control
Apoptotic

C. 2 DNA fragmentation and chromatin morphology

Typically in cells undergoing apoptosis DNA fragments with 5' -P and 3' -OH ends are produced (Gavrieli *et al.*, 1992). TUNEL is a method by which DNA cleavage in apoptotic cells can be detected by enzymatically transferring biotinylated dUTP to the 3'- OH ends of DNA. The biotin-labeled ends can then be detected by fluorescence microscopy. Fig. 24 shows two DAPI stained cells which exhibit condensed DNA morphology (A and B) and are TUNEL positive (A' and B '). In undifferentiated P19 cells treated with 1μM and 4μM MeHg for 12 and 18 hr approximately 12 -18% of the cells were TUNEL positive (Fig. 25 A and B). The percentage of cells with condensed chromatin, characteristic of apoptosis, was equivalent to the proportion of TUNEL positive cells (Fig. 25).

C. 3 DNA fragmentation detected by agarose gel electrophoresis

The induction of internucleosomal DNA fragmentation, a biochemical marker of apoptosis, was examined in undifferentiated P19 cells. DNA was extracted from cells treated with 1 μM and 4 μM MeHg for 12 and 18 hr (Fig. 26). In these samples a DNA ladder, indicative of internucleosomal fragmentation was observed. It is also clear that much of the DNA did not enter the gel. This may be unfragmented DNA and/or large DNA fragments.

Figure 24: Chromatin morphology of nuclei with DNA strand breaks in MeHg-treated cells labelled with TUNEL **(A and B)** and counterstained with DAPI **(A' and B')**. Bar = 10 µm.

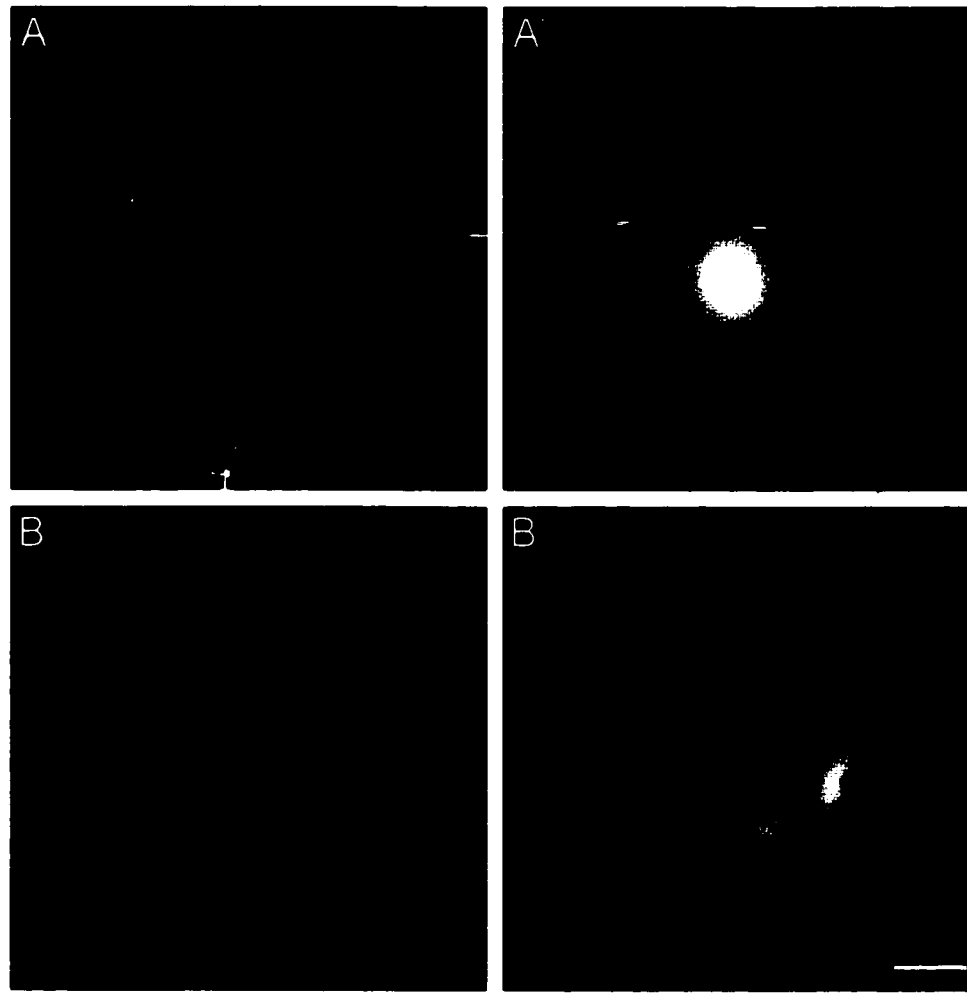
A
A'
B
B

Figure 25: Histogram showing the percentage of cells detected by TUNEL following 12 hr (**A**) and 18 hr (**B**) MeHg treatments. 600 cells were evaluated in each sample. Results are the mean of three experiments. Error bars show the standard deviation from the mean.

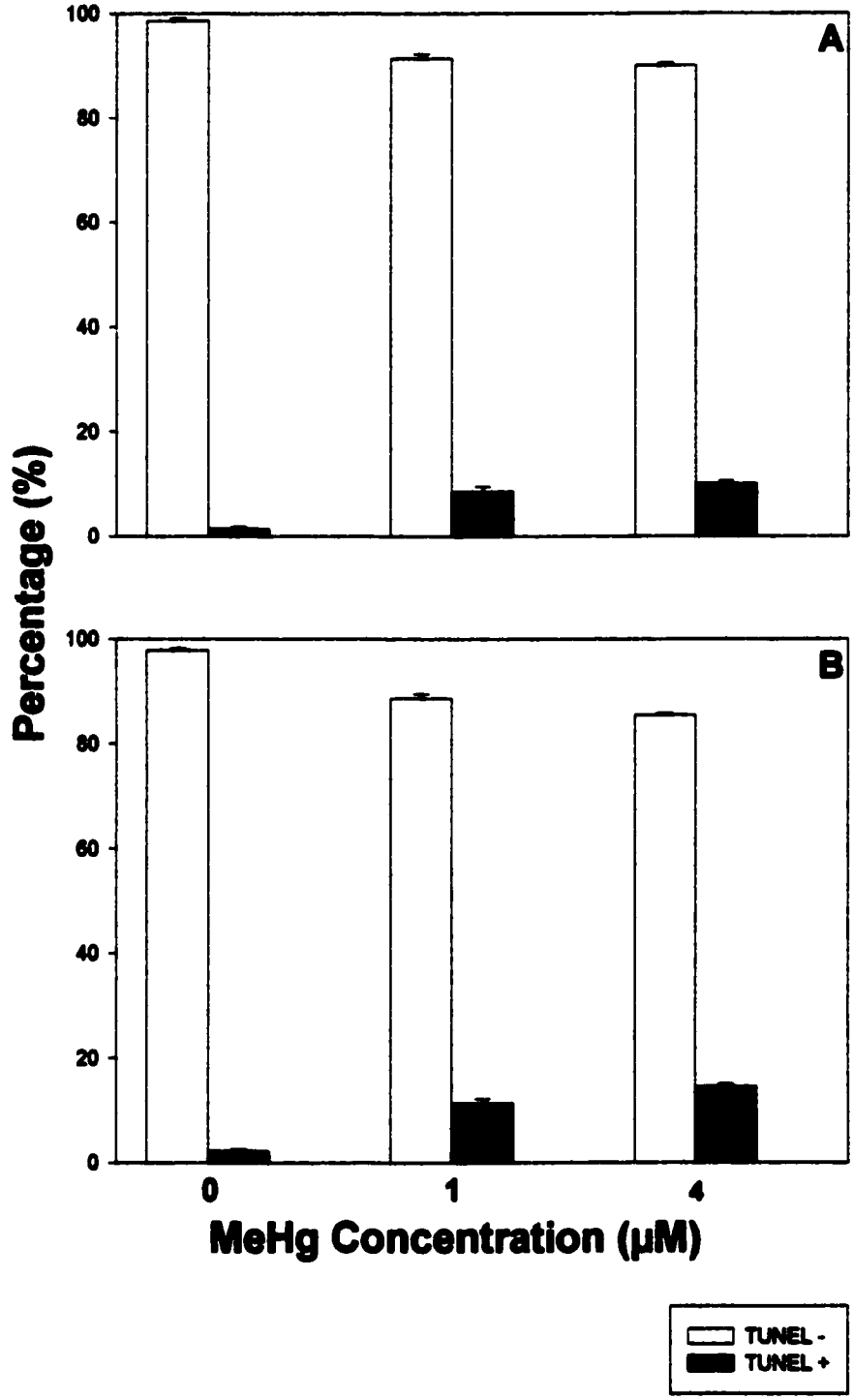
A
B
100
80
60
40
20
0
Percentage (%)
0
1
4
MeHg Concentration (μM)
TUNEL -
TUNEL +

Figure 26: Agarose gel electrophoresis of DNA extracted from undifferentiated P19 cells treated with MeHg. DNA cleavage at the oligonucleosomal level following a 4 μM MeHg treatment lasting for 12 hr or 18 hr resulted in fragments that were multiples of 200 bp. DNA was visualized by ethidium bromide.

Lambda Hind III Digest

12 hr; Control

12 hr; 1 μM

12 hr; 4 μM

100 bp Ladder

18 hr; Control

18 hr; 1 μM

18 hr; 4 μM

100 bp Ladder

C. 4 Pulsed field gel electrophoresis

PFGE was used to further characterize the pattern of DNA cleavage in undifferentiated and neuronally differentiated P19 cells treated with MeHg. In undifferentiated P19 cells treated with 1μM and 4μM MeHg for 12, 18 and 24 hr, a range of HMW DNA fragments > 50 kb in size were observed (Fig. 27). Fig. 28 shows that there was also an accumulation of HMW DNA fragments in neuronally differentiated P19 cell samples treated with 1μM and 4μM MeHg for 12, 18 and 24 hr. These fragments appeared to approximately 50 -100 kb in size. It is important to note that in both undifferentiated and differentiated samples there was intense DNA staining in the wells of the gel indicating that the majority of the DNA in all samples is either intact or contains infrequent single strand DNA breaks.

Figure 27: Pulsed field gel electrophoresis of DNA from control and MeHg-treated undifferentiated P19 cells. Position of 50 kb DNA fragments is indicated by the arrowhead.

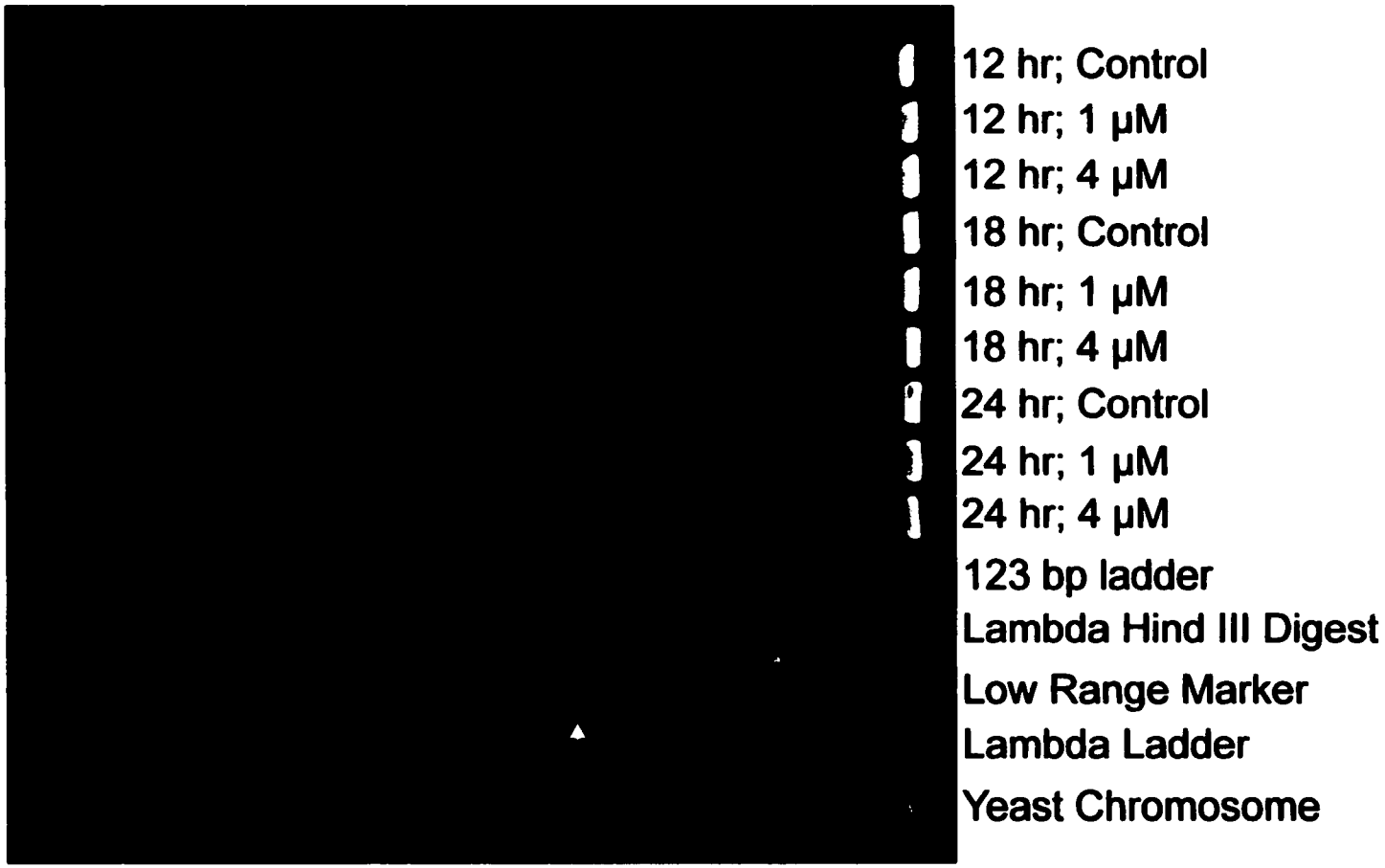
12 hr; Control
12 hr; 1 µM
12 hr; 4 µM
18 hr; Control
18 hr; 1 µM
18 hr; 4 µM
24 hr; Control
24 hr; 1 µM
24 hr; 4 µM
123 bp ladder
Lambda Hind III Digest
Low Range Marker
Lambda Ladder
Yeast Chromosome

Figure 28: Pulsed field gel electrophoresis of DNA from control and MeHg-treated neuronally differentiated P19 cells. Position of 50 kb DNA fragments is indicated by the arrowhead.

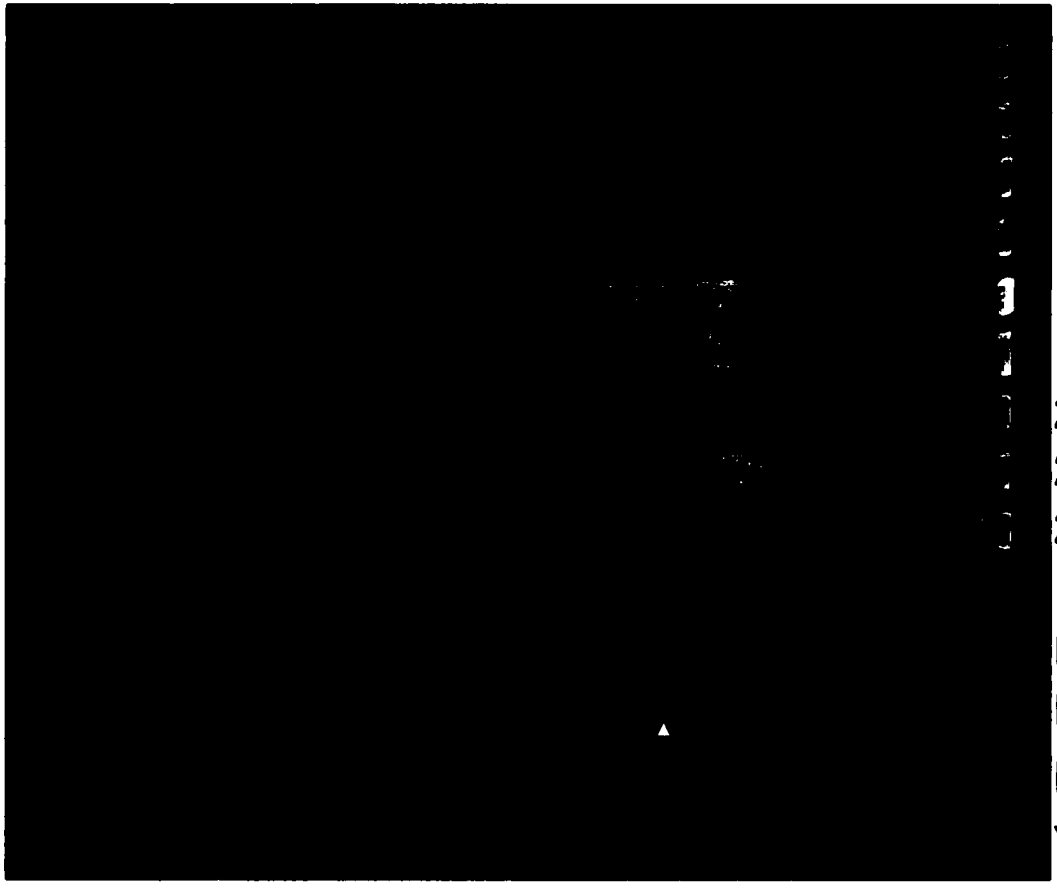

12 hr; Control
12 hr; 1 μM
12 hr; 4 μM
18 hr; Control
18 hr; 1 μM
18 hr; 4 μM
24 hr; Control
24 hr; 1 μM
24 hr; 4 μM
123 bp ladder
Lambda Hind III Digest
Low Range Marker
Lambda Ladder
Yeast Chromosome

D. DISCUSSION

It has been established that Mt-damage is a prominent feature of MeHg exposure (Sager *et al.*, 1983; Sager and Syversen, 1986; Brown *et al.*, 1988; Cadrin *et al.*, 1988; Wasteneys *et al.*, 1988). Studies using neuroblastoma cell lines (Sarafian *et al.*, 1994), cerebellar granule neurons (Sarafian *et al.*, 1989; Kunimoto and Suzuki, 1997) and T cell hybridomas (Aten *et al.*, 1995) have shown, that as well as Mt damage, another feature of MeHg exposure is apoptotic cell death.

D. 1 Reactive oxygen species as mediators of apoptosis

The mechanisms by which MeHg induces apoptosis are not clear. In a wide range of environmental toxicants, including MeHg, reactive oxygen species (ROS) have been implicated as the primary mediator of cellular toxicity (Sarafian and Bredesen, 1994). Many intracellular reactions, including respiration, reduce oxygen to superoxides or hydrogen peroxide. Although these molecules are only moderately reactive with other biological molecules, they can also form hydroxyl radicals which are highly reactive (Sarafian and Bredesen, 1994).

It was shown in studies using the hypothalamic neuronal cell line GT1-7 that MeHg treatment resulted in the formation of ROS (Sarafian *et al.*, 1994). The amount of oxidants created were measured using 2,7-dichlorofluorescein (DCF) which was oxidized to a fluorescent derivative by peroxides and free radicals (Sarafian *et al.*, 1994). The rate of DCF oxidation, in the presence of MeHg, increased in a dose-

dependent manner. 3 hr, 10 μM MeHg treatments increased the levels of ROS production 100-fold (Sarafian *et al.*, 1994). This increase in ROS was also associated with decreased levels of the reducing agent, glutathione (GSH), the major cellular antioxidant, and the loss of cell viability (Sarafian *et al.*, 1994). Wasteneys *et al.* (1988) showed that MeHg treatments of this duration and dose caused severe Mt damage. Therefore, as well as increases in ROS, loss of cell viability may also result from extensive Mt damage.

There is evidence which suggests that ROS may induce apoptosis due to oxidative damage to both mitochondrial membranes and DNA (Polyak *et* al., 1997). DNA damage was observed in studies where ROS was generated under experimental ischemic conditions. It was noted that double stranded DNA (dsDNA) breaks 10-50 kb in size, similar to the 50-300 kb fragments generated by apoptosis, were produced (Hou *et al.*,1997). As well, the presence of single stranded DNA (ssDNA) breaks and alkali-labile sites were observed. Alkali-labile sites have been previously characterized as abasic sites that can arise from oxidative damage (Barzilay and Hickson, 1995). It is possible, therefore, that ROS generated by MeHg treatments may cause extensive DNA damage, chemically, resulting in dsDNA breaks or in alkali-labile DNA. It is also likely that MeHg may be inducing an apoptotic process which results initially in either alkali-labile or ssDNA breaks (Tomei *et al.*, 1993). As a result of the apoptotic process, the number of ssDNA breaks become more frequent resulting in the formation of dsDNA fragments

D. 2 Comet assay detects MeHg-induced DNA fragmentation resulting from apoptosis

The alkaline comet assay detects ssDNA cleavage in individual cells making this a very sensitive method for detecting the early stages of apoptosis (Olive *et al.*, 1991; 1995). When both undifferentiated and neuronally differentiated P19 cells were treated with MeHg, it was observed by the comet assay that DNA fragmentation was induced in a time and dose- dependent manner (Fig. 22).

Tomei *et al.* (1993) demonstrated the presence of alkali-labile base modifications during apoptosis when DNA from apoptotic CH3T10$^{1}/_{2}$ cells was examined by gel electrophoresis. It was observed that under neutral conditions a banding pattern indicative of internucleosomal cleavage was not present. However, when DNA extracts from the same cells were examined by alkaline gel electrophoresis, extensive DNA laddering was observed. The comet assays of MeHg-treated P19 cells reported in this thesis were incubated under alkaline conditions (pH 13). It is possible, therefore, that MeHg treatments created alkali-labile sites in a time- and dose-dependent manner, which under alkaline conditions, resulted in extensive ssDNA breaks observed by the comet assay. Neutral gel electrophoresis of the same treatments should clarify this point.

The formation of alkali-labile base modifications as a result of oxidative DNA damage does not explain the observed differences in the incidence of comets between undifferentiated and differentiated cells under identical treatment conditions. For example, when neuronally differentiated P19 cells were treated with 4 μM MeHg for

12 hr less than 5% of the cells were apoptotic as assessed by comet, while with the same treatment 98% of undifferentiated cells were apoptotic. One would expect that if alkali-labile DNA was an effect of oxidative DNA damage, the same extent of damage would occur in both undifferentiated and differentiated cells. However, it is possible that since P19 neurons were more resistant to Mt damage they may also be more resistant to MeHg-induced, oxidative DNA damage.

D. 3 Gel electrophoresis detects HMW and LMW DNA fragments

The PFGE data indicate that, in contrast to the comet results, the majority of the cells loaded do not have extensively fragmented DNA. The presence of a bright band at the top of the gel near the wells indicated that most of the DNA was either intact or had infrequent ssDNA breaks following MeHg treatments of both undifferentiated and neuronally differentiated cells. The proportion of DNA which did enter the gel was HMW fragments released from a few double strand scissions, which were produced by more frequent ssDNA breaks (Walker *et al.*, 1997).

The patterns of HMW DNA fragmentation differed between the undifferentiated and differentiated cells, showing an obvious accumulation of fragments 50-100 kb in size in the differentiated cells (Fig. 28). In the undifferentiated cells there did not appear to be a distinct accumulation of specific sized DNA fragments, but rather a range of different sizes of fragments was observed in all the samples (Fig 27). By conventional agarose gel electrophoresis LMW DNA fragmentation was observed in undifferentiated cells (Fig. 26), but not in differentiated P19 cells (data not shown). It

is possible that there are different endonuclease activities in undifferentiated and differentiated P19 cells as has been reported for human myeloid cells which differentiate into granulocytes (Anzai *et al.*, 1995). The different cleavage patterns observed in P19 cells may also be a reflection of a difference in packing of the DNA in the undifferentiated and differentiated cells which might affect the accessibility of endonucleases.

D. 4 TUNEL and DNA morphology do not correspond with comet data

The comet assay indicated that most of the undifferentiated P19 cells were apoptotic following a 12 hr, 4 μM MeHg treatment. These data do not correspond with the results from other assays which showed with identical MeHg treatments that only 12-18% of cells were TUNEL positive and exhibited condensed DNA morphology. This discrepancy may be because the success of the TUNEL assay is dependent on the generation of 3'-OH ends. Endonucleases which generate 3'-P ends, instead of the typical 3' -OH ends, have been identified in certain cell types (reviewed by Walker *et al.*, 1997) and perhaps are present in P19 cells. However, these reasons do not explain why an equally low percentage of cells exhibit the condensed nuclear or DNA morphology characteristic of the late stages of apoptosis.

D. 5 MeHg induces apoptosis in P19 cells

Apoptosis is an active biochemical process which has been shown to require energy in the form of ATP. For example, both morphological changes such as

chromatin condensation and biochemical changes such as caspase activation, are ATP dependent processes (Kass *et al.*, 1996; Ferrari *et al.*, 1998). It has also been shown that the balance between death by the processes of apoptosis and necrosis appears to depend on the level of available intracellular ATP such that under ATP-depleting conditions apoptosis is aborted and necrosis occurs (Eguchi *et al.*, 1997; Renvoize *et al.*, 1998).

Studies using cerebellar granule neurons showed that ATP levels were reduced by MeHg in a dose and time dependent manner with a 3 hr, 5 μM treatment resulting in the decline of ATP to 50% of control levels and 3 hr, 20 μM treatments reducing ATP to >98% of control levels (Sarafian *et al.*, 1989). It is possible that ATP levels in P19 cells are significantly reduced such that the energy requirements for chromatin condensation and caspase activation cannot be met. Therefore, a decrease in ATP levels may explain why only a small percentage of P19 cells exhibit collapsed nuclear morphology following MeHg treatment.

The results of the comet assay show that essentially all of the undifferentiated cells suffer extensive DNA damage when exposed to MeHg. However, the PFGE experiments indicate that this damage is primarily due to ssDNA breaks. Therefore, it is likely that the comet assay detects either single stranded breaks or alkali-labile base modifications that are introduced into DNA at the earliest stages of apoptosis. Both single stranded breaks (Walker *et al.*, 1997) and alkali-labile base modifications (Tomei *et al.*, 1993) have been observed in DNA at the earliest stages of apoptosis. As apoptosis proceeds, enough closely spaced single strand breaks accumulate such that

double strand breaks predominate (Walker *et al.*, 1997). However, it appears that MeHg interferes with this normal progression resulting in cells that do not show the classical apoptotic markers. These markers include HMW DNA fragmentation of the entire cell population and collapsed nuclear morphology.

The data in this study indicate that MeHg is an effective inducer of apoptosis. Apoptosis appears to be initiated by MeHg, but with time, this death process may be aborted and the cells ultimately die by secondary necrosis.

SUMMARY

MeHg pollution was recognized as a serious environmental health problem when severe neurological effects such as visual and sensory disturbances were observed as a result of exposure. These severe neurological effects were classified as a disorder called Minimata Disease. Biochemical and morphological studies showed that the effects of MeHg were selective and that the developing nervous system was particularly vulnerable to this toxicant. Brain autopsies of fetuses exposed to MeHg *in utero* showed that regions of the brain were significantly underdeveloped due to lack of cell proliferation and cell migration. Both of these processes are dependent on the Mt component of the cytoskeleton. More recently it has been shown in studies using laboratory animals that MeHg may affect brain development by inducing apoptosis (Kunimoto *et al.*, 1997). Therefore, the inhibition of mitosis and the induction of apoptosis may both be responsible for the neurological damage observed following environmental MeHg exposure.

E. 1 Methylmercury-disassembles Mts and induces apoptosis

Earlier work established that MeHg disassembled Mts in undifferentiated and neuronally differentiated P19 cells, in a time- and dose-dependent manner (Cadrin *et al.*, 1988; Wasteneys *et al.*, 1988l; Graff and Reuhl, 1997). It was also established that there was a differential sensitivity to Mt-induced disassembly between undifferentiated and differentiated cells. Data in Chapter I of this thesis are consistent with these findings. A novel observation was also made in Chapter I which indicated

that MeHg treatments alter the way in which polymer Mt proteins are disassembled such that their extractability from the cell is affected.

Previous studies demonstrated that MeHg induced apoptosis in neuronal cell cultures and in T lymphocyte cell lines (Sarafian and Verity, 1991; Sarafian *et al.*, 1994; Aten *et al.*, 1996; Kunimoto and Suzuki, 1997). Consistent with these findings data in this study obtained by Comet assay, TUNEL, DNA morphology, and gel electrophoresis showed that MeHg is an effective inducer of apoptosis in undifferentiated cells. In both undifferentiated and differentiated cells the extent of MeHg-induced apoptosis was time- and dose- dependent and was correlated with the extent of Mt damage observed.

It is not clear how MeHg exposure induces apoptosis. There is evidence that reactive oxygen species (ROS) may be involved (discussed in D.1, Chapter II). It is also possible that MeHg-induced apoptosis may occur as a result of Mt damage by this toxicant in a manner similar to that of colchicine, vinblastine, and taxol..

E. 2 Mt-targeting drugs induce apoptosis

Mt-damage occurring in human breast cancer, leukemia, and prostate cancer cells from exposure to taxol, vincristine or colchicine induces apoptosis (Blagosklonny *et al.*, 1997, Srivastava *et al.*, 1998; Poruchynsky *et al.*, 1998; Torres and Horwitz, 1998). When these cell lines were examined following drug treatment it was observed in all cases that exposure to these Mt-targeting drugs resulted in both the

phosphorylation of bcl-2 and the activation of caspases (Blagosklonny *et al.*, 1997, Srivastava *et al.*, 1998; Poruchynsky *et al.*, 1998).

Bcl-2 is typically presented as an inhibitor of apoptosis. However, studies have shown that when phosphorylated its ability to interfere with apoptosis is inhibited (Haladar *et al.*, 1994; 1995). *In vivo* studies showed that when bcl-2 was transfected into bcl-2-negative lymphoid cells, the majority of bcl-2 was phosphorylated in the presence of okadaic acid (OA), a protein phosphatase inhibitor (Haladar *et al.*, 1995). When these cells were stained to detect changes in nuclear morphology, typical apoptotic nuclear morphology was observed.

The importance of bcl-2 phosphorylation in the apoptotic pathway was also demonstrated in studies in which human leukemia, breast cancer, and prostate cancer cells expressed a phosphorylated form of bcl-2 following exposure to taxol (Srivastava *et al.*, 1998). It was also observed in ovarian tumour and breast tumour cells that bcl-x_L, an anti-apoptotic bcl-2 relative, became phosphorylated following Mt-disruption with colchicine, vinblastine, nocodazole or taxol (Poruchynsky *et al.*, 1998). In both studies Mt disruption resulted in bcl-2/bcl-x_L phosphorylation and the induction of apoptosis (Srivastava *et al.*, 1998; Poruchynsky *et al.*, 1998).

The activation of *raf-1* kinase, a cytoplasmic kinase involved in the regulation of cell proliferation, transformation, differentiation, and apoptosis signal transduction (Lovric *et* al., 1998; Torres and Horwitz, 1998) has been implicated in the apoptotic process following Mt damage. Mt-damaging agents such as taxol, colchicine, and vinblastine activate *raf-1* kinase leading to bcl-2 phosphorylation and cell death

(Blagosklonny *et al.*, 1997; Poruchynsky *et al.*, 1998; Torres and Horwitz, 1998). In the presence of alkylating agents, DNA damaging compounds, or antimetabolites neither *raf-1* kinase activation or bcl-2 phosphorylation were observed, indicating that the initiation of the *raf-1* signaling cascade occurs specifically as a result of Mt disruption (Blagosklonny *et al.*, 1997; Srivastava *et al.*, 1998). These results provide evidence that the loss of Mt integrity by Mt-disrupting drugs triggers a signal transduction pathway leading to bcl-2 phosphorylation and ultimately to apoptotic cell death.

E. 3 MeHg-induced Mt damage is correlated with MeHg-induced apoptosis

In chapter I of this thesis the time- and dose-dependent effects of MeHg on Mt depolymerization were characterized. It was observed that the expression of MAP2c, in undifferentiated cells as well as neuronal differentiation offered considerable protection against MeHg-induced Mt damage. It has been hypothesized that mechanisms which promote Mt stability, such as tubulin isotype sorting, tubulin posttranslational modifications, and MAP expression confer resistance of Mts against the depolymerizing effects of colchicine and nocodazole as well as MeHg (Falconer *et al.*, 1992; Graff and Reuhl, 1997).

In chapter II of this thesis it was established by a variety of experiments that MeHg induced apoptosis in both undifferentiated and neuronally differentiated P19 cells. Although MeHg may be having a variety of toxic effects on the cell, such as damaging DNA or affecting membrane integrity, the effects of this toxicant on Mt

integrity were observed and correlated with the extent of DNA damage measured by the Comet assay. Several studies have shown that Mt damage activates signal transduction pathways leading to *raf-1* kinase activation and bcl-2 phosphorylation as a result of Mt damage (Blagosklonny *et al.*, 1997; Srivastava *et al.*, 1998; Poruchynsky *et al.*, 1998; Lovric *et al.*, 1998; Torres and Horwitz, 1998). It is possible that this is the mechanism by which MeHg-induced apoptosis occurs in both undifferentiated and neuronally differentiated P19 cells. Mechanisms which decrease Mt sensitivity to MeHg may also alter the sensitivity to MeHg-induced apoptosis. For example MAP expression may make Mts more resistant to drug-induced Mt-damage, preventing *raf-1* kinase activation and bcl-2 phosphorylation. Therefore, if the Mts are not significantly disrupted by MeHg, the signal transduction pathways which lead to apoptosis may not be triggered.

REFERENCES

Abe, T., Haga, T. and Kurokawa, M. 1975. Blockage of axoplasmic transport and depolymerization of reassembled microtubules by methylmercury. *Brain Res.* **86**: 504-508.

Addison, C.J. 1997. Microtubule-associated protein 2 (MAP2) expression in transiently and stably transfected P19 embryonal carcinoma cells. MSc Thesis. University of Ottawa, Ottawa.

Aitchison, W.A. and D.L. Brown. 1986. Duplication of the flagellar apparatus and cytoskeletal microtubule system in the alga *Polytomella*. *Cell Motil. Cytoskel.* **6**: 122-127.

Anzai, N., Kawabata, H., Hirama, T., Masutani, H., Ueda, Y., Yoshida, Y. and M. Okuma. 1995. Types of nuclear endonuclease activity capable of inducing internucleosomal DNA fragmentation are completely different between human $CD34^+$ cells and their granulocytic descendants. *Blood.* **3**: 917-923.

Arends, M.J., Morris, R.G. and A.H. Wyllie. Apoptosis: The Role of the Endonuclease. *Am. J. Path.* **136(3)**: 593-608.

Aten, J., Prigent, P., Poncet, P., Blanpied, C., Claessen, N., Druet, P. and F. Hirsch. 1995. Mercuric chloride-induced programmed cell death of a murine T cell hybridoma. *Cell. Immunol.* **161**: 98-106.

Audebert, S., Desbruyères, E., Gruszczynski, C., Koulakoff, A., Gros, F., Denoulet, P and B. Eddé. 1993. Reversible polyglutamylation of α- and β-tubulin and microtubule dynamics in mouse brain neurons. *Mol. Biol. Cell.* **4**: 615-626.

Baas, P. W., Pienkonski, T.P., Cimbalnik, K. A. Toyama, K., Bakalis, S., Ahmad, F.J. and K.S. Kosik. 1994. Tau confers drug-stability but not cold stability to microtubules in living cells. *J. Cell Sci.* **107**: 135-143.

Banerjee, S., Fallis, A. G. and D.L. Brown. 1997. Differential effects of taxol on two human cancer cell lines. *Oncology Res.* **9**: 237-248.

Barzilay, G. and I.D. Hickson. 1995. Structure and function of apurinic/apyrimidinic endonucleases. *Bioessays.* **17**: 713-718.

Bass, P. W., Black, M.M. and J.A. Banker. 1988. Polarity orientation of microtubules in hippocampal neurons: uniformity in the axon and nonuniformity in the dendrite. *Proc. Natl. Acad. Sci. U.S.A.* **85**: 8335-8339.

Black, M.M. and P.W. Baas. 1989. The basis of polarity in neurons. *Trends Neurosci.* **12**: 211-214.

Blagosklonny, M.V., Giannakakou, P, E. Deiry, W.S., Kingston, D.G.I., Higgs, P.I., Neckers, L. and T. Fojo. 1997. Raf-1/bcl-2 phosphorylation: A step from microtubule damage to cell death

Blose, S.H., Meltzer, D.I. and J.R. Feramisco. 1984. 10-nm filaments are induced to collapse in living cells microinjected with monoclonal and polyclonal antibodies against tubulin. *J. Cell Biol.* **98**:847-858.

Boucher, D., Larcher, J., Gros, F and P. Denoulet. 1994. Polyglutamylation of tubulin as a progressive regulator of *in vivo* interactions between the microtubule associated protein tau and tubulin. *Biochem.* **33**: 12471-12477.

Brown, D.L., Reuhl, K.R., Bormann, S. and J.E. Little. 1988. Effects of methylmercury on the microtubule system of mouse lymphocytes. *Toxicol and Appl. Pharm.* **94**: 66-75.

Bulinski, J.C. and G.G. Gundersen. 1991. Stabilization and posttranslational modification of microtubules during cellular morphogenesis. *Bioessays.*

Cadrin, M. , Wasteneys, G.O., Jones-Villeneuve, E.M.V., Brown, D.L. and K. R. Reuhl. 1988. Effects of methylmercury in retinoic acid-induced neuroectodermal derivatives of embryonal carcinoma cells. *Cell Biol.and Toxicol.* **4**: 61-80

Chaly, N., Bladon, T., Setterfield, G., Little, J.E., Kaplan, J.G. and D.L. Brown. 1984. Changes in distribution of nuclear matrix antigens during the mitotic cell cycle. *J. Cell Biol.* **99**: 661-671.

Chen, C. and H. Okayama. 1987. High-efficiency transformation of mammalian cells by plasmid DNA. *Mol. Cell Biol.* **7**: 2745-2752.

Choi, B.H., Lapham, L.W., Amin-Zaki, L. and Salem, T. 1978. Abnormal neuronal migration, degenerated cerebral cortical organization, and diffuse white matter astrocytosis of human fetal brain: a major effect of methylmercury poisoning *in utero. J.Neuropathol. Exp. Neurol.* **37**: 719-733.

Cohen, G.M., Sun, X. M. Fearnhead, H., MacFarlane, M., Brown, D.G., Snowden, R.T. and D. Dinsdale. 1994. Formation of large molecular weight fragments of DNA is a key committed step of apoptosis in thymocytes. *J. Immunol.* **153**: 507-516.

Cross, D., Dominguez, J., Maccioni, R.B. and J. Avila. 1991. MAP-1 and MAP-2 binding sites at the C-terminus of β-tubulin. Studies with synthetic tubulin peptides. *Biochem.* **30**: 4362-4366.

Cuvillier, O., Pirianov, G., Kleuser, B., Vanek, P.G., Coso, O.A.. Gutkind, J.S. and S. Spiegel. 1996. Suppression of ceremide-mediated programmed cell death by sphingosine-1-phosphate. *Nature.* **381**: 800-803.

Daum, G., Eisenmann-Tappe, I., Fries, H., Troppmair, J and U.R. Rapp. 1994. The ins and outs of Raf kinases. *Trends Biochem. Sci.* **19**: 474-479.

Debernardis, D., Siré, E.G., De Feudis, P., Vikhanskaya, F., Valenti, M., Russo, P., Parodi, S., D'Incalci, M. and M.Broggini. 1997. p53 status does not affect sensitivity of human ovarian cancer cell lines to paclitaxel. *Cancer Res.* **57**: 70-874.

Diaz-Nido, J., Serrano, L., López-Otin, C., Vandekerckhove and J. Avila. 1990. Phosphorylation of a neuron-specific β-tubulin isotype. *J. Biol. Chem.* **265**: 13949-13954.

Doll, T., Meichsner, M., Reiderer, B.M., Honegger, P. and A. Matus. 1993. An isoform of microtubule-associated protein 2 (MAP2) containing four repeats of the tubulin-binding motif. *J. Cell Sci.* **106**: 633-640.

Earnshaw, W.C. 1995. Nuclear changes in apoptosis. *Curr. Opin. Cell Biol.* **7**: 337-343.

Eguchi, Y., Shimizu, S and Y. Tsujimoto. 1997. Intracellular ATP levels determine cell death fate by apoptosis or necrosis. *Cancer Res.* **57**: 1835-1840.

Enari, M., Sakahira, H., Yokoyama, H., Okawa, K. Iwamatsu, A. and S. Nagata.1998. A caspase-activated DNase that degrades DNA during apoptosis, and its inhibitor, ICAD. *Nature* **391**: 43-50.

Escargueil, I., Nègre-Salvayre, A., Pieraggi, M. T. and R. Salvayre. 1992. Oxidized low-density lipoproteins elicit DNA fragmentation of cultured lymphoblastoid cells. *FEBS Lett.* **305**: 155-159.

Falconer, M.M., Echeverri, C.J. and D.L. Brown. 1992. Differential sorting of beta tubulin isotypes into colchicine-stable microtubules during neuronal and muscle differentiation of embryonal carcinoma cells. *Cell Mot.Cytoskel.* **21**: 313-325.

Falconer, M.M., Vaillant, A., Reuhl, K.R., Laferrière, N., and D.L. Brown. 1994. The molecular basis of microtubule stability in neurons. *Neurotoxicology*. **15**: 109-122.

Ferrari, D., Stepczynska, A., Los, M., Wesselborg, S.and K. Schulze-Osthoff, K. 1998. Differential regulation and ATP requirement for caspase-8 and caspase-3 activation during CD95- and anticancer drug-induced apoptosis. *J. Exp. Med.* **188**: 979-984.

Filipski, J., Leblanc, J., Youdale, T., Sikorska, M. and P.R. Walker. 1990. Periodicity of DNA folding in higher order chromatin structures. *EMBO J.* **9**: 1319-1327.

Fujita, S., Shimada, M. and Nakamura, T. 1966. H_3-thymidine autoradiographic studies of the cell proliferation and differentiation in the internal and external granular layers of the mouse cerebellum. *J. Comp. Neurol.* **128**: 191-208.

Gard, D.L. and M. Kirschner. 1985. A polymer-dependent increase in phosphorylation of β-tubulin accompanies differentiation of a mouse neuroblastoma cell line. *J. Cell Biol.* **100**: 764-774.

Gavrieli, Y., Y. Sherman and S.A. Ben-Sasson. 1992. Identification of programmed cell death *in situ* via specific labelling of nuclear DNA fragmentation. *J. Cell Biol.* **119**:493-501.

Graff, R.D. and K.R. Reuhl. 1996. Cytoskeleton toxicity of heavy metals. In- Toxicology of Metals. L. W. Chang, editor. Lewis Publishers. New York. USA. pp. 639-657.

Graff, R.D., Falconer, M.M., D.L. Brown and K.R. Reuhl. 1997. Altered sensitivity of posttranslationally modified microtubules to methylmercury in differentiating embryonal carcinoma-derived neurons. *Toxicol and Appl.Pharm.* **144**: 215-224.

Gundersen, G.G., M.H. Kalnoski and J.C. Bulinski. 1984. Distinct populations of microtubules: tyrosinated and nontyrosinated alpha-tubulin are distributed differently *in vivo*. *Cell.* **38**: 779-789.

Haladar, S. Jena, N. and C.M. Croce. 1994. Antiapoptosis potential of *bcl2* oncogene by dephosphorylation. *Biochem. Cell Biol.* **72**: 455-462.

Haladar, S., Jena, N. and C.M. Croce. 1995. Inactivation of Bcl-2 by phosphorylation. *Proc. Natl. Acad. Sci. USA.* **92**: 4507-4511.

Hockenberry, D.M. Oltavi, Z.N., Yin, X. M., Milliman, C.L., and S. J. Korsmeyer. 1993. *Bcl-2* functions in an antioxidant pathway to prevent apoptosis. *Cell.* **75**:241-251.

Hou, S. T., Tu, Y., Buchan, A. M., Huang, Z., Preston, E., Rasquinha, I., Robertson, G.S. and J.P. MacManus. 1997. Increases in DNA lesions and the DNA damage indicator Gadd45 following transient cerebral ischemia. *Biochem. Cell Biol.* **75**: 383-392.

Imura, N., K. Miura, Inokawa, M. and Nakada, S. 1980. Mechanism of methylmercury cytotoxicity: by biochemical and morphological experiments using cultured cells. *Toxicology.* **17**: 241-254.

Jacobson, M.D., Burnett, J.F., King, M.D., Miyashita, T., Reed, J.C. and M.C. Raff. 1993. Bcl-2 blocks apoptosis in cells lacking mitochondrial DNA. *Nature.* **361**: 365-369.

Jacobson, M.D and M.C. Raff. 1995. Programmed cell death and *bcl-2* protection in very low oxygen. *Nature.* **374**: 814-816.

Jacobson, M.D. 1996. Reactive oxygen species and programmed cell death. *Trends in Biochem. Sci.* **21**: 83-86

Johnson, E. M., Greenlund, L.L.S., Atkins, P.T. and C.Y. Hsu. 1995. Neuronal apoptosis: current understanding of molecular mechanisms and potential role in ischemic brain injury. *J. Neurotrauma.* **12**: 843-852.

Jones-Villeneuve, E.M.V., McBurney, M.W. Rogers, K.A. and V.L. Kalnins. 1982. Retinoic acid induces embryonal carcinoma cells to differentiate into neurons and glial cells. *J. Cell Biol.* **94**: 253-262.

Jordan, M.A., Wendell, K., Gardiner, S., Derry, W.B., Copp, H. and L. Wilson. 1996. Mitotic block induced in HeLa cells by low concentrations of paclitaxel (Taxol) results in abnormal mitotic exit and apoptotic cell death. *Cancer Res.***56**: 816-825.

Jordan, M.A. and L. Wilson. 1998. Microtubules and actin filaments: dynamic targets for cancer chemotherapy. *Current Opinion Cell Biol.* **10**: 123-130.

Joshi, H.C. and D.W. Cleveland. 1989. Differential utilization of β-tubulin isotypes in differentiating neurites. *J. Cell Biol.* **109**: 663-673.

Joshi, H.C. and D.W. Cleveland. 1990. Diversity among tubulin subunits: Toward what functional end ? *Cell Motil. Cytoskel.* **16**: 159-163.

Kane, M., Liu, Z. and E. Zandi. 1997. AP-1 function and regulation. *Curr. Opin. Cell Biol.* **9**: 240-246.

Kass, G.E., Eriksson, J.E., Weis, M., Orrenius, S. and S.C. Chow. 1996. Chromatin condensation during apoptosis requires ATP. *Biochem. J.* **318**: 749-752.

Keates, R. A. B. and Yott, B. 1983. Inhibition of microtubule polymerization by micromolar concentrations of mercury (II). *Can. J. Biochem. Cell Biol.* **62**: 814-818.

Kerr, J.F.R., Wyllie, A.H. and A.R. Currie. 1972. Apoptosis: a basic biological phenomenon with wide-ranging implications in tissue kinetics. *Br. J. Cancer.* **26**: 239-257.

Khan, I.A. and R.F. Ludueña. 1996. Phosphorylation of βIII-tubulin. *Biochem.* **35**: 3704-3711.

Khawaja, S., G.G. Gundersen and J.C. Bulinski. 1988. Enhanced stability of microtubules enriched in detyrosinated tubulin is not a direct function of detyrosination level. *J. Cell Biol.* **106**: 141-149.

Kindler, S., Schwanke, B., Schulz, B. and C.C. Garner. 1990b. Complete cDNA sequence encoding rat high and low molecular weight MAP2. *Nucleic Acids Res.* **18**: 2822.

Kluck, R.M., Bossy-Wetzel, E., Green, D.R. and D.D. Newmeyer. 1997. The release of cytochrome c from mitochondria: a primary site for Bcl-2 regulation of apoptosis *Science.* **275**: 1132-1136

Kung, A.L., Sherwood, S.W. and R.T. Schimke. 1990. Cell line-specific differences in the control of cell cycle progression in the absence of mitosis. *Proc. Natl. Acad. Sci. USA.* **87**: 9553-9557.

Kunimoto, M. and Suzuki. T. 1997. Migration of granule neurons in cerebellar organotypic cultures is impaired by methylmercury. *Neurosci. Lett.* **226**: 183-186.

Kuriyama, R. and Sakai, H. 1974. Role of tubulin -SH groups in polymerization to microtubules. *J. Biochem.* **76**: 651-654.

Laemmli, U.K. 1970. Cleavage of structural proteins during the assembly of the head of bacteriophage T4. *Nature.* **227**: 680-685.

Laferrière, N.B. and D.L. Brown. 1996. Expression and posttranslational modification of class III β-tubulin during neuronal differentiation of P19 carcinoma cells. *Cell Mot. Cytoskel.* **35(3)**: 188-199.

Laferrière, N.B., MacRae, T.H. and D.L. Brown. 1997. Tubulin synthesis and assembly in differentiating neurons. *Biochem. Cell Biol.* **75**: 7-21

LeClerc, N., K.S. Kosik, N. Cowan, T.P. Pienkowski and P.W. Bass. 1996. Juvenile and Mature MAP2 isoforms induce distinct patterns of process outgrowth. *Mol. Biol. Cell.* **7**: 443-455.

LeDizet, M. and G. Piperno. 1986. Cytoplasmic microtubules containing acetylated α-tubulin in *Chlamydomonas reinhardtii* spatial arrangement and properties. *J. Cell Biol.* **103**: 13-22.

Lee, G., Cowan, N. and M. Kirschner. 1988. The primary structure and heterogeneity of tau protein from mouse brain. *Science.* **239**: 285-288.

Lee, M.K., Rebhun. L.I. and A. Frankfurter. 1990. Posttranslational modifications of class III β-tubulin. *Proc. Natl. Acad. Sci. USA.* **87**: 7195-7199.

Lewis, S.A., Ivanov, I.E., Lee, G.H. and N. J. Cowan. 1989. Organization of microtubules in dendrites and axons is determined by a short hydrophobic zipper in microtubule-associated proteins MAP2 and tau. *Nature.* **342: 498-505.**

Li, Y. and M.M. Black. 1996. Microtubule assembly and turnover in growing axons. *J. Neurosci.* **16**: 531-544.

Littauer, U.Z., Giveon, D., Thierau, M., Ginzburg, I. and H. Ponstingl. 1986. Common and distinct tubulin binding sites for microtubule-associated proteins. *Proc. Natl. Acad. Sci. USA.* **83**: 7162-7166.

Long, B.H. and C.R. Fairchild. 1994. Paclitaxel inhibits progression of mitotic cells to G_1 phase by interference with spindle formation without affecting other microtubule functions during anaphase and telophase. *Cancer Res.* **54**: 4355-4361.

Lopata, M.A. and D.W. Cleveland. 1987. *In Vivo* microtubules are copolymers of available β-tubulin isotypes: Localization of each of six vertebrate β-tubulin isotypes using polyclonal antibodies elicited by synthetic peptide antigens. *J. Cell Biol.* **105**: 1707-1720.

Lovric, J., Dammeier, S., Kieser, A., H. Mischak, and W. Kolch. 1998. Activated Raf induces the hyperphosphorylation of stathmin and the reorganization of the microtubule network. *J. Biol. Chem.* **273**: 22848-22855.

MacPherson, P.A. and McBurney, M.W. 1995. P19 embryonal carcinoma cells: A source of cultured neurons amenable to genetic manipulation. *Methods: a companion to methods in enzymology.* 7:238-252.

Matus, A. 1988. Microtubule-associated proteins: Their potential role in determining neuronal morphology. *Ann. Rev. Neurosci.* **11**: 29-44.

Matus, A. 1990. Microtubule-associated proteins. *Current Opinions Cell Biol.* **2**: 10-14.

Matus, A. 1991. Microtubule-associated proteins and neuronal morphogenesis. *J. Cell Sci. Suppl.* **15**: 61-67.

Matus, A. 1994. MAPS. In: Microtubules. J.S. Hyams and C.W. Lloyd. Wiley-Liss, Inc. New York. USA. pp. 155-166.

McBurney, M.W. and B. J. Rogers. 1982. Isolation of male embryonal carcinoma cells and their chromosome replication patterns. *Dev. Biol.* **89**: 503-506.

Mitchison, T. and M. Kirschner. 1984a. Microtubule assembly nucleated by isolated centrosomes. *Nature.* **312**: 232-237.

Mitchison, T. and M. Kirschner. 1984b. Dynamic instability of microtubule growth. *Nature.* **321**: 237-242.

Miura, K., Nakada, S., Suzuki, K. and Nobumasa. I. 1979. Ultrastructural studies on the cytotoxic effects of mercuric chloride on mouse glioma. *Ecotoxicol. and Environ. Safety.* **3**: 352-361.

Miura, K., Inokawa, M. and Imura, N. 1984. Effects of methylmercury and some metal ions on microtubule networks in mouse glioma cells and *in vitro* tubulin polymerization. *Toxicol and Appl. Pharmacol.* **73**: 218-231.

Moritz, M., Braunfeld, M.B., Sedat, J.W., Alberts, B. and D.A. Agard. 1995. Microtubule nucleation by γ-tubulin-containing rings in the centrosome. *Nature.* **378**: 638-640.

Nicholson, D.W. and N.A. Thornberry. 1997. Caspases: Killer proteases. *Trends in Biochem. Sci.***22**: 299-306.

Nuñez, G. and M. F. Clarke. 1997. The Bcl-2 family of proteins: regulators of cell death and survival. *Trends in Cell Biol.* **4**: 399-403.

Oberhammer, F., Wilson, J.W., Dive, C., Morris, I.D., Hickman, J.A., Wakeling, A.E., Walker, P.R. and M. Sikorska. 1993. Apoptotic death in epithelial cells: cleavage of DNA to 300 and/or 50 kb fragments prior to or in the absence of internucleosomal fragmentation. *EMBO J.* **12**: 3679-3684.

Olesen, O. F. 1994. Expression of low molecular weight isoforms of microtubule-associated protein 2. *J. Biol. Chem.* **269**: 32904-32908.

Olive, P.L., Wolodek, D. and J. P. Bánath. 1991. DNA double strand breaks measured in individual cells subjected to gel electrophoresis. *Cancer Res.* **51**: 4671-4676.

Olive, P. L., Frazer, G. and J. P. Bánath. 1993. Radiation-induced apoptosis measured in TK6 human B lymphoblast cells using the comet assay. *Radiation Res.* **136**: 130-136.

Olive, P. L. and J. P. Bánath. 1995. Sizing highly fragmented DNA in individual apoptotic cells using the comet assay and a DNA crosslinking agent. *Exp. Cell Res.* **221**: 19-26.

Olive, P. L., Johnston, P. J., Bánath, J. P. and R. E. Durand. 1998. The comet assay: A new method to examine heterogeneity associated with solid tumors. *Nature Med.* **4**: 103-105

Osborne, B.A. and L. M. Schwartz. 1994. Essential genes that regulate apoptosis. *Trends in Cell Biol.* **4**: 394-398.

Ostling, O., and K. J. Johanson. 1984. Microelectrophilic study of radiation-induced DNA damages in individual mammalian cells. *Biochem. Biophys. Res. Commun.* **123**: 291-298.

Panda, D., Miller, H.P., Banerjee, A., Ludueña, R.F. and L. Wilson. 1994. Microtubule dynamics in vitro are regulated by the tubulin isotype composition. *Proc. Natl. Acad. Sci. USA.* **91**: 11358-11362

Peitsch, M.C., Muller, C. and J.T. Schopp. 1993. DNA fragmentation during apoptosis is caused by frequent single-stranded cuts. *Nucleic Acids Res.***21**: 4206-4209.

Piperno, G. and M.T. Fuller. 1985. Monoclonal antibodies specific for an acetylated form of α-tubulin recognize the antigen in cilia and flagella from a variety of organisms. *J. Cell Biol.* **101**: 2085-2094.

Piperno, G., M. LeDizet and X. Chang. 1987. Microtubules containing acetylated α-tubulin in mammalian cells in culture. *J. Cell Biol.* **104**: 289-302.

Pittman, S., Geyp, M., Fraser, M., Ellem, K., Peaston, A. and C. Ireland. 1997. Multiple centrosomal microtubule organizing centres and increased microtubule stability are early features of VP-16-induced apoptosis in CCRF-CEM Cells. *Leukemia Res.* **21**: 491-499.

Polyak, K., Xia, Y., Zweier, J.L., Kinzler, K. W. and B. Vogelstein. 1997. A model for p53-induced apoptosis. *Nature.* **389**. 300-305.

Poruchynsky, M. S., Wang, E.E., Rudin, C.M., Blagosklonny, M.V. and T. Fojo. 1998. Bcl-x_L is phosphorylated in malignant cells following microtubule disruption. *Cancer Res.* **58**: 3331-3338.

Prasad, K., Nobles, E. and Ramanujam. M. 1979. Differential sensitivites of glioma cells and neurobalstoma cells to methylmercury toxicity in cultures. *Environ. Res.* **19**: 189-201.

Rao, L. and E. White. 1997. Bcl-2 and the ICE family of apoptotic regulators: making a connection. *Curr. Opin. in Gen. Dev.* **7**: 52-58.

Ray, S., Ponnathpur, V., Huang, Y., Yang, C., Mahoney, M.E., and A.M. Ibrado. 1994. 1-β-D-arabinofuranosylcytosine-, mitoxantrone-, and paclitaxel-induced apoptosis in HL-60 cells: improved method for detection of internucleosomal DNA fragmentation. *Cancer Chemother.Pharmacol.* **34**: 365-371.

Renvoize, C., Biola, A., Pallardy, M. and J. Breard. 1998. Apoptosis: identification of dying cells. *Cell Biol Toxicol.* **14**: 111-120.

Rodier, P.M., Aschner, M. and Sager, P.R. 1984. Mitotic arrest in the developing CNS after prenatal exposure to methylmercury. *Neurobehav. Toxicol. and Teratol.* **6**: 379-385.

Rossé, T., Olivier, R., Monney, L., Rager, M., Conus, S., Fellay, I., Jansen, B and C. Borner. 1998. Bcl-2 prolongs cell survival after Bax-induced release of cytochrome c. *Nature.* **391**: 496-499.

Roy, C., Brown, D.L., Little, J.E., Valentine, B. K., Walker, P.R., Sikorska, M., Leblanc, J. and N. Chaly. 1992. The topoisomerase II inhibitor teniposide (VM-26) induces apoptosis in unstimulated mature murine lymphocytes. *Exp. Cell Res.* **200**: 416-424.

Rudner, A.D. and A.W. Murray. 1996. The spindle assembly checkpoint. *Current Opin.Cell Biol.* **8**: 773-780.

Sager, P.R., Doherty, R.A. and Rodier, P.M. 1982. Effects of methylmercury on developing mouse cerebellar cortex. *Exp. Neurol.* **85**:371-382.

Sager, P.R., Doherty, R.A. and J.B. Olmsted. 1983. Interaction of methylmercury with microtubules in cultured cells and in vitro. *Exp. Cell Res.* **146**: 127-137.

Sager, P.R. 1988. Selectivity of methyl mercury effects on cytoskeleton and mitotic progression in cultured cells. *Toxicol. and Applied Pharm.* **94**: 473-486.

Sager, P.R. and T.L.M. Syversen. 1986. Disruption of microtubules by methylmercury. In-The Cytoskeleton: A Target for Toxic Agents. T.W. Clarkson, P.R. Sager and T.L.W. Syversen, editors. Plenum Press. New York. USA. pp 97-116.

Sambrook, J., Fritsch, E.F. and T. Maniatis. 1989. Molecular Cloning: a laboratory manual, Vol. I. Cold Spring Harbor Laboratory Press, Cold Spring Harbor

Sarafian, T. Hagler, J., Vartavarian, L. and M.A. Verity. 1989. Rapid cell death induced by methyl mercury in suspension of cerebellar granule neurons. *J. Neuropath. Exp. Neurology.* **48**: 1-10.

Sarafian, T. and M. A. Verity. 1991. Oxidative mechanisms underlying methyl mercury neurotoxicity. *Int. J. Devl. Neuroscience.* **9**: 147-153.

Sarafian, T. A., Vartavarian, L., Kane, D.J., Bredesen, D.E. and M.A. Verity. 1994. bcl-2 expression decreases methyl mercury-induced free-radical generation and cell killing in a neural cell line. *Toxicology Letters.* **74**: 149-155.

Sarafian, T. A., Bredesen, D. E. and M. A. Verity. 1996. Cellular resistance to methylmercury. *Neurotoxicology.* **17**: 27-36.

Schoenfeld, T.A. and R.A. Obar. 1994. Diverse distribution and function of fibrous microtubule-associated proteins in the nervous system. *Internatl. Rev.Cytol.* **151**: 67-137.

Schulze, E. and M. Kirschner. 1987. Dynamic and stable populations of microtubules in cells. *J. Cell Biol.* **104**: 277-288.

Serrano, L., Montejo De Garcini, E., Hernández, M.A. and J. Avila. 1985. Localization of the tubulin binding site for tau protein. *Eur. J. Biochem.* **153**: 595-600.

Shelanski, M.L., Gaskin, F. and Cantor, C.R. 1973. Microtubule assembly in the absence of added nucleotides. *Proc. Nat. Acad. Sci. USA.* **70**: 765-768.

Skerfving, S., Hansson, K., Mags. C., Lindstern, J., and N. Ryman. 1974. Methylmercury-induced chromosome damage in man. *Environ. Res.* **7**: 83-98.

Srivastava, R. K., Srivastava, A. R., Korsmeyer, S.J., Nesterova, M., Cho-Chung, Y.S. and D.L. Longo. 1998. Involvement of microtubules in the regulation of bcl2 phosphorylation and apoptosis through cyclic AMP-dependent protein kinase. *Mol. Cell Biol.* **18**: 3509-3517.

Sullivan, K.F. and D.W. Cleveland. 1986. Identification of conserved isotype-defining variable region sequences for four vertebrate β-tubulin polypeptide classes. *Proc. Natl. Acad. Sci. USA.* **83**: 4327-4331.

Sullivan, K. F. 1988. Structure and utilization of tubulin isotypes. *Ann. Rev. Cell Biol.* **4**: 687-716.

Sun, X.M. and G. M. Cohen. 1994. Mg^{2+}- dependent cleavage of DNA into kilobase pair fragments is responsible for the initial degradation of DNA in apoptosis. *J. Biol. Chem.* **269**: 14857-14860.

Takemura, R., Okabe, S., Umeyama, T., Kanai, Y., Cowan, N.J. and N. Hirokawa. 1992. Increased microtubule stability and alpha tubulin acetylation in cells transfected with microtubule-associated proteins MAP1B, MAP2 or tau. *J. Cell Sci.* **103**: 953-964.

Tan, X. and J.Y.J. Wang. 1998. The caspase-RB connection in cell death. *Trends in Cell Biol.* **8**: 116-120.

Tang, C., Willingham, M.C., Reed, J.C., Miyashita, T., Ray, S., Ponnathpur, V., Huang, Y., Mahoney, M.E., Bullock, G., and K. Bhalla. 1994. High levels of p26Bcl-2 oncoprotein retard taxol-induced apoptosis in human pre-B leukemia cells. *Leukemia.* **8**: 1960-1969.

Thrower, D., Jordon, M.A. and L. Wilson. 1991. Quantitation of cellular tubulin in microtubules and tubulin pools by competitive ELISA. *J. Immunol. Meth.* **136**: 45-51.

Tomei, L. D., Shapiro, J. P. and F.O. Cope. 1993. Apoptosis in C3H/10T$^{1}/_{2}$ mouse embryonic cells: Evidence for internucleosomal DNA modifications in the absence of double-strand cleavage. *Proc. Natl. Acad. Sci. USA.* **90**: 853-857.

Torres, K. and S.B. Horwitz. Mechanisms of taxol-induced cell death are concentration dependent. *Cancer Res.* **58**: 3620-3626.

Towbin, H., Staehlin, T. and J. Gordon. 1979. Electrophoretic transfer of proteins from polyacrylamide gels to nitrocellulose sheets: procedure and some applications. *Proc. Natl. Acad. Sci. U.S.A.* **76**: 4350-4354.

Trielli, M.O., Andreassen, P.R., Lacroix, F.B. and R.L. Margolis. 1996. Differential taxol-dependent arrest of transformed and nontransformed cells in the G1 phase of the cell cycle, and specific-related mortality of transformed cells. *J.Cell Biol.* **135**: 689-700.

Tucker, R.P., L.I. Binder and A.I. Matus. 1988. Neuronal microtubule-associated proteins in the embryonic avian spinal cord. *J. Comp. Neurol.* **271**: 44-55.

Vaillant, A. 1997. Microtubule-associated protein 1a: Analysis of its microtubule binding domain and its function in differentiating P19 neurons. PhD Thesis. University of Ottawa, Ottawa.

Vale, R.D. 1990. Microtubule-based motor proteins. *Current Opinions Cell Biol.* **2**: 15-22.

Vale, R.D., Coppin, C.M., Malik, F., Kull, F.J. and R.A. Milligan. 1994. Tubulin GTP hydrolysis influences the structure, mechanical properties, and kinesin-driven transport of microtubules. *J. Biol.Chem.* **269**: 23769-23775.

Verschaeve, L., Kirsch-Volders, M., Hens, L., Susanne, C., Groetenbriel, C., Haustermans, R., LeComte, A., and D. Roossels. 1976. Genetic damage induced by occupationally low mercury exposure. *Environ. Res.* **12**: 306-316.

Vogel, D.G., Margolis, R. and N.K. Mottet. 1985. The effects of methyl mercury binding tto microtubules. *Toxicol. Appl. Pharmacol.* **80**: 473-486.

Walker, P.R., Smith, C. Youdale, T., Leblanc, J., Whitfield, J.F. and M. Sikorska. 1994. Endonuclease activities associated with high molecular weight and internucleosomal DNA fragmentation in apoptosis. *Exp. Cell Res.* **213**: 100-106.

Walker, P.R., Pandey, S. and M. Sikorska. 1995. Degradation of chromatin in apoptosis. *Cell Death Differ.* **2**: 97-104.

Walker, P.R. and M. Sikorska. 1997. New aspects of the mechanism of DNA fragmentation in apoptosis. *Biochem. Cell. Biol.* **75(4)**: 287-299.

Walker, P.R., LeBlanc, J. and M. Sikorska. 1997. Evidence that DNA fragmentation in apoptosis is initiated and propagated by single-strand breaks. *Cell Death and Diff.* **4**: 506-515.

Wallin, M., Larsson, H. and Edstrom, A. 1977. Tubulin sulfhydryl groups and polymerization *In Vitro*. *Exp. Cell Res.* **107**: 219-225.

Wang, T.H., Wang, H.S, Ichijo, H., Giannakakou, P, Foster, J.S., Fojo, T. and J. Wimalasena. 1998. Microtubule-interfering agents activate c-Jun N-terminal kinase/stress-activated protein kinases through both ras and apoptosis signal-regulating kinase pathways. *J. Biol. Chem.* **273(9)**: 4928-4936.

Wasteneys, G.O., Cadrin, M., Reuhl, K.R. and Brown, D.L. 1988. The effects of methylmercury on the cytoskeleton of murine embryonal carcinoma cells. *Cell Biol. and Toxicol.* **4**: 41-60.

Weaver, V.M., Lach, B., Walker, P.R. and M. Sikorska. 1993. Role of proteolysis in apoptosis: involvement of serine proteases in internucleosomal DNA fragmentation in immature thymocytes. *Biochem. Cell Biol.* **71**: 488-500.

Weaver, V.M., Carson, C.E., Walker, P.R., Chaly, N., Lach, B., Raymond, Y., Brown, D.L. and M. Sikorska. 1996. Degradation of nuclear matrix and DNA cleavage in apoptotic thymocytes. *J. Cell Sci.* **109**: 45-56.

Wertz, I.E. and M.R. Hanley. 1996. Diverse molecular provocation of programmed cell death. *Trends Biochem. Sci.* **21**: 359-364.

Wilson, L. 1986. Microtubules as targets for drug and toxic chemical action: The mechanisms of action of colchicine and vinblastine. In: The Cytoskeleton. T.W. Clarkson, P.R. Sager and T.L.M. Syversen. Plenum Press. New York. USA. pp. 37-52.

Wyllie, A.H. 1980. Glucocorticoid-induced thymocyte apoptosis is associated with endogenous endonuclease activation. *Nature*. **284**: 555-556

Wyllie, A.H., Kerr, J.F.R. and A.R. Currie. 1980. Cell death: the significance of apoptosis. *Int. Rev. Cyt.* **68**: 251-307.

Wyllie, A. 1997. Clues in the p53 murder mystery. *Nature*. **389**: 237-238

Yang, J., Lui, X., Bhalla, K., Kim, C. N., Ibrado, A.M, Chai, J., Peng, T., Jones, D.P. and X. Wang. 1997. Prevention of apoptosis by bcl2: Release of cytochrome c from mitochondria blocked. *Science*. **275**: 1129-1136.